



저작자표시-비영리-변경금지 2.0 대한민국

이용자는 아래의 조건을 따르는 경우에 한하여 자유롭게

- 이 저작물을 복제, 배포, 전송, 전시, 공연 및 방송할 수 있습니다.

다음과 같은 조건을 따라야 합니다:



저작자표시. 귀하는 원저작자를 표시하여야 합니다.



비영리. 귀하는 이 저작물을 영리 목적으로 이용할 수 없습니다.



변경금지. 귀하는 이 저작물을 개작, 변형 또는 가공할 수 없습니다.

- 귀하는, 이 저작물의 재이용이나 배포의 경우, 이 저작물에 적용된 이용허락조건을 명확하게 나타내어야 합니다.
- 저작권자로부터 별도의 허가를 받으면 이러한 조건들은 적용되지 않습니다.

저작권법에 따른 이용자의 권리는 위의 내용에 의하여 영향을 받지 않습니다.

이것은 [이용허락규약\(Legal Code\)](#)을 이해하기 쉽게 요약한 것입니다.

[Disclaimer](#)

CTCF-dependent 3D chromatin structure
controls STAT5-mediated transcription
in CD4⁺ T cells

Eun-Chong Lee

Department of Medicine
The Graduate School, Yonsei University

CTCF-dependent 3D chromatin structure controls STAT5-mediated transcription in CD4⁺ T cells

Directed by Professor Hyoung-Pyo Kim

The Doctoral Dissertation
submitted to the Department of Medicine,
the Graduate School of Yonsei University
in partial fulfillment of the requirements for the degree of
Doctor of Philosophy in Medical Science

Eun-Chong Lee

December 2023

This certifies that the Doctoral Dissertation
of Eun-Chong Lee is approved.

Thesis Supervisor: Hyoung-Pyo Kim

Thesis Committee Member#1: Hyun Seok Kim

Thesis Committee Member#2: Sang-Jun Ha

Thesis Committee Member#3: Ho-Keun Kwon

Thesis Committee Member#4: Kyung Hyun Yoo

The Graduate School
Yonsei University

December 2023

*“We Don't Make Mistakes,
We Just Have Happy Accidents”*

Bob Ross

ACKNOWLEDGEMENTS

From the first steps taken in 2017 to the fruition of this research, I sincerely thank everyone who have become a part of my journey.

Above all, I express my gratitude to God for providing the strength to reach this point.

I am deeply thankful for the invaluable guidance and advice of Professor Hyoung-Pyo Kim, my mentor, who charted the right direction and blueprint for me, fueling my passion for “Epigenetics”. I also extend my heartfelt thanks to the reviewing professors, Hyun Seok Kim, Sang-Jun Ha, Ho-Keun Kwon, and Kyung Hyun Yoo, for their careful examination of the paper during the evaluation process and their involvement in shaping it into a more desirable outcome. In addition, I would like to express my gratitude to Professor Yeun Kyu Jang and Hwan Young Lee, who have encouraged me until I took my first step into graduate school with an interest in epigenetics.

I would like to express my gratitude to the lab colleagues with whom I may have spent more time than with my family. The time spent with Tae-Gyun was a period of inspiration and learning. The analysis of the numerous results generated during this project would have been impossible without the unwavering determination of

Woong-Jae. Also, I want to thank Sugyung and Kyungwoo for their efforts until the completion of the research.

I cannot forget the time I spent with the lab seniors in the results of this research. Thanks to Min-Ji, I developed a flexible mindset that allows me to plan experiments confidently in any situation, and thanks to Yeeun, I was able to adapt well and grow in the unfamiliar environment of the lab. Although it was a short period, the advice from Sueun as she completed her degree became an opportunity to broaden my narrow perspective at the beginning of my degree. I express my gratitude to Bobae, spent most of the period, helping me reflect on and gain insights into my shortcomings. Mugu is a truly good influence among the people I've met, and Yong-Jin remains memorable for providing me with the joy of the research.

I want to express my gratitude to the family members I've shared joys and sorrows with until the completion of my degree. I thank Dr. Chul Min Yang for providing a perspective that allows me to revisit even the seemingly ordinary things. And especially to Mikyoung, with her thoughtful care during tough and tiring times, continues to be a source of inspiration as I write this. Above all, to Jung-Sik, I am extremely grateful for the invaluable connection that seems impossible to fill with a few simple words here. I look forward to the continued support and growth of Heon-Woo, Jieun, and Chang Hoon

as key members of our lab in the future.

As I conclude, I want to express my sincere gratitude to my ever-respected father and my unwaveringly supportive mother, who has always stood by me with unconditional love. I owe my ability to take firm steps towards my goals to both of you, as you provided steadfast support. I also extend my thanks to my precious younger brother.

The journey through the academic program feels like a series of countless failures, especially during the pursuit of a Ph.D., where failure seems more abundant. Reaching this point signifies overcoming many setbacks, and I intend to cherish each moment without taking the time for granted. They say effort is about carving away, sacrificing the pleasures of eating, playing, sleeping, relationships, and everything else in one's life. Despite any shortcomings in the process of creating this thesis, the experience of carving out a piece of life has been a valuable lesson in my life.

My journey is not over yet, and I believe the connections made here will continue to bring happiness amid future challenges. To all those I may not have mentioned but who supported and watched over me with love, I sincerely thank you.

With sincere thoughts in the winter of 2023,

Eun-Chong Lee

TABLE OF CONTENTS

ABSTRACT	viii
I. INTRODUCTION	1
1. Characteristics and impactful role of CD4 ⁺ T cells	1
2. Epigenetic research for understanding 3D genome in CD4 ⁺ T cells	3
3. CTCF as a coordinator of 3D chromatin structure organization	5
II. MATERIALS AND METHODS	7
1. Mice and Cell culture	7
2. Flow cytometry	7
3. RNA extraction and quantitative real-time polymerase chain reaction (qRT-PCR)	8
4. Western blotting	9
5. RNA sequencing	9
6. Precision nuclear run-on sequencing (PRO-seq)	10
7. Assay for Transposase-Accessible Chromatin using sequencing (ATAC- seq)	10
8. Cell fixation	11
9. Chromatin Immunoprecipitation Sequencing (ChIP-seq)	11
10. <i>in situ</i> Hi-C	12
11. HiChIP	13
12. CRISPR/RNP nucleofection	14
13. T7E1 mismatch detection assay	15
14. Cloning and sequencing for check mutation rate	15

15. RNA-Seq data processing	16
16. ChIP-Seq data processing	17
17. ATAC-seq data processing	17
18. PRO-seq data processing	18
19. <i>in situ</i> Hi-C data analysis	19
20. HiChIP data analysis	19
21. Aggregated Peak Analysis (APA)	20
22. Definition of regulatory elements for annotating HiChIP loop anchors	20
23. Motif enrichment Locus Overlap analysis	21
24. Quantification and statistical analysis	21
25. Data visualization	21
III. RESULTS	22
1. Conditional CTCF knockout was induced in CD4 ⁺ T cells, leading to an effective reduction of CTCF levels.	22
2. Compartment organization does not rely on CTCF, yet CTCF is crucial for insulating Topologically Associating Domains (TADs).	27
3. CTCF and transcriptional activity play a crucial role in facilitating the formation of enhancer loops.	31
4. Super loop is engaged to super-enhancer and cell-identity related genes.	37
5. Super loops have a low pausing index and regulate cell-specific genes.	40
6. Super-loops are closely associated with the influence of epigenetic regulators.	46
7. STAT5 is a transcription factor that represents the super-loop and super-	

enhancer in CD4 ⁺ T cells.	49
8. The proper expression of cell identity genes relies on CTCF, which governs the formation of enhancer loops.	54
9. The rewiring of the STAT5 enhancer network resulting from CTCF depletion alters the response to the JAK inhibitor.	61
10. CTCF functions both as an enhancer blocker and facilitator, overseeing the precise targeting of STAT5.	61
IV. DISCUSSION	75
V. CONCLUSION	84
REFERENCES	85
ABSTRACT(IN KOREAN)	98
PUBLICATION LIST	100

LIST OF FIGURES

Figure 1. CD4 ⁺ T cells were subjected to a conditional knockout of CTCF, resulting in an efficient depletion of CTCF	24
Figure 2. Disrupted occupancies of CTCF and SMC1 due to CTCF depletion	26
Figure 3. CTCF is dispensable for compartment organization	28
Figure 4. CTCF is essential for TAD insulation	30
Figure 5. CTCF plays a significant role in the formation of loops	34
Figure 6. Positive correlation between loop strength and the presence of CTCF and active transcription markers	36
Figure 7. As the loop strength increases, the involvement of the super-enhancer also increases	38
Figure 8. As the intensity of the loop increases, the pausing index decreases	42
Figure 9. Robust enhancer loop formation is coupled to release of RNA Pol II pausing	44
Figure 10. The establishment of robust enhancer loops is linked to the alleviation of RNA Polymerase II pausing	45
Figure 11. Loop formation determines the regulation of RNA Polymerase II pause-release	48

Figure 12. STAT5 is the most prominently identified transcription factor in both super-loops and super-enhancers of CD4⁺ T cells51

Figure 13. Promoter-promoter interaction and STAT5 are involved in gene regulation of super-loops53

Figure 14. Differential loop analyses using H3K27ac HiChIP revealed genome-wide changes in enhancer loop strength following CTCF depletion57

Figure 15. The significant role of CTCF in the maintenance of enhancer loop formation58

Figure 16. The rewiring of super-loops resulting from CTCF depletion is associated with alterations in both gene expression and the pausing of RNA Pol II59

Figure 17. Inhibiting the phosphorylation of STAT5 induced by tofacitinib experiment reveals STAT5 target genes63

Figure 18. The modified STAT5 enhancer network resulting from CTCF depletion brings about changes in the efficacy of a JAK inhibitor64

Figure 19. Established chromatin interaction between the super-enhancer bound by STAT5 and the *Dexi* promoter following CTCF depletion69

Figure 20. The chromatin interaction between the super-enhancer bound by STAT5 and the *Igfbp4* promoter is disturbed following

CTCF depletion	71
Figure 21. The chromatin interaction between the super-enhancer bound by STAT5 and the <i>Batf3</i> promoter is perturbed following CTCF depletion	73
Figure 22. Super-loop oversees the influence of enhancer activity to the promoter and the regulation of Pol II pause-release	82

LIST OF TABLES

Table 1. Primer sequences used for RT-qPCR	8
Table 2. sgRNA sequences used for CRISPR/RNP Nucleofection ...	14
Table 3. Primer sequence for amplification of CRISPR KO target region	15
Table 4. Sequencing primer for reading DNA sequence after cloning	16

ABSTRACT

CTCF-dependent 3D chromatin structure controls STAT5-mediated transcription in CD4⁺ T cells

Eun-Chong Lee

*Department of Medicine
The Graduate School, Yonsei University*

(Directed by Professor Hyoung-Pyo Kim)

To ensure proper gene expression in cellular processes, the role of enhancers influencing gene expression through long-range interactions is crucial, in addition to proteins acting at the promoter. CTCF is known as a protein that plays a key role in the 3D chromatin structure. However, the mechanism by which CTCF regulates gene expression remains controversial. Here, I demonstrate that CTCF has the ability to regulate the transcription of targets through enhancer-promoter interactions in CD4⁺ T cells. Remarkably, the CTCF depletion in CD4⁺ T cells unveils the functional significance of the critical master regulator, STAT5. STAT5-bound super-enhancers contribute to maintaining enhancer loops robustly in a CTCF-independent manner. Additionally, the deep involvement of enhancer loop formation in the pause-release of RNA pol II is observed. In

contrast, the altered enhancer loop structure orchestrated by CTCF has an impact on the accurate expression of genes defining cellular identity. CTCF influences the strength of enhancer loops and, furthermore, is a crucial factor in regulating the Pol II pausing mechanism in the transcription process of target promoters. In a nutshell, my study provides mechanistic insights into how the JAK/STAT signaling pathway remains intact during CD4⁺ T cell activation, and even in such conditions, the impact CTCF can have on cell identity genes through rewiring the enhancer network. This finding offers a comprehensive perspective on the intricate functions of CTCF in promoting appropriate gene expression in immune cells.

Key words : CD4⁺ T cell, CTCF, STAT5, Pol II Pausing, 3D chromatin structure

CTCF-dependent 3D chromatin structure controls STAT5-mediated transcription in CD4⁺ T cells

Eun-Chong Lee

*Department of Medicine
The Graduate School, Yonsei University*

(Directed by Professor Hyoung-Pyo Kim)

I. INTRODUCTION

1. Characteristics and impactful role of CD4⁺ T cells

Cellular functions are carried out by clusters of interacting proteins. Unraveling the fundamental aspects of how these spatially and temporally organized interactions contribute to biological processes is crucial for advancing the understanding of cellular mechanisms¹. Regulating gene expression is an indispensable process, ranging from the basic metabolism of cells to determining cell identity². Immunity is complementarily achieved by the innate and adaptive immune systems. It is crucial for the adaptive immunity to function properly as it develops an efficient immune response against antigens that have been encountered before. The T helper cells, also known as CD4⁺ T cells, are a type of T cell that play a crucial role in regulating the various immune cells involved in adaptive immunity. When an antigen-presenting cell (APC) expresses an antigen on MHC class II, CD4⁺ T cells recognize it through T cell receptors (TCRs) and

assist the activity of other immune cells by releasing various cytokines. These cells help to activate or suppress immune responses and are crucial for B cell antibody class switching, the activation of cytotoxic T cells, and the enhancement of phagocyte killing activity.

Given that CD4⁺ T cells play diverse roles in the immune system, it is not surprising that they can influence the immune response against diseases. The immune system must maintain a balance of sensitivity to respond to non-self-antigens without reacting to self-antigens. When CD4⁺ T cells produce an undesirable reaction to routine antigens, a hypersensitivity response that causes allergies and autoimmune diseases can occur. Specifically, regulating JAK-STAT5 signaling is considered important in the treatment of melanoma and leukemia^{3,4}.

As CD4⁺ T cells play a crucial role in immunity, numerous studies have been actively conducted until recently. Most of the research on CD4⁺ T cells is related to hematopoiesis, T cell differentiation^{5,6} and T cell receptor^{7,8}. From a deeper perspective, the classification of multiple subsets of T cells is an important topic in the study of CD4⁺ T cells. In addition to the classical model of differentiation of Type 1 helper T (Th1) and Th2 cells, unexpected increases in the numbers of CD4⁺ T cell subsets, including Th17, Th9, follicular helper T (Tfh) and regulatory T (Treg) cells, have been recognized^{9,10}.

Approaches to therapy have been taken from both a genetic perspective and an epigenetic perspective¹¹, such as histone modification, non-coding RNA, and 3D chromatin structures¹²⁻¹⁴. However, among them, how changes in 3D genome structure can affect the mechanisms of T cell-related diseases still has yet to be fully discovered.

2. Epigenetic research for understanding 3D genome in CD4⁺ T cells

Nucleosome packaging of DNA creates a physical obstacle to transcription initiation. When DNA is tightly bound to histones and forms closed chromatin, the RNA polymerase complex is unable to bind to the transcription start site proximal to the coding region, and transcription factors are obstructed from interacting with their binding sites in gene regulatory regions. A nucleosome can adopt an open configuration in response to enzymatic modification of specific histone residues¹⁵.

Histone acetylation is directly linked to transcription activation, and several general transcription factors and coactivator proteins such as CBP and p300 function as histone acetyltransferases (HATs)¹⁶⁻¹⁸. Enhancers, which are defined by H3K27ac signal, exist at a distance from their target genes and assist transcription by interacting with target promoters^{19,20}. Enhancers are comprised of short DNA sequences acting as binding sites for transcription factors (TFs)²¹. These TFs recruit various epigenetic cofactors, influencing the transcriptional structure of adjacent chromatin. Consequently, TFs generate specific transcriptional responses to external cues, leading to changes in transcription activation and translation. Numerous transcription factors play crucial roles in genome organization, influencing the fate and functions of immune cells. Super-enhancers are large clusters of enhancers that control essential genes, have densely occupied transcription factors, and greater capacity to activate gene expression than typical enhancers^{22,23}.

The effects of lysine methylation of histones on gene transcription are more complex and depend on both the lysine residue involved and the number of methyl groups. Methylated histones can correspond to both transcriptional activation and repression, depending on the number and location of the methyl group. In addition to acetylation and methylation, numerous other post-translational histone modifications have been discovered, including phosphorylation and ubiquitination^{24,25}. Histone modification's importance in various diseases such as systemic sclerosis (SSc)²⁶, Systemic Lupus

Erythematosus (SLE)²⁷, and Type 1 Diabetes (T1D)²⁸ is drawing attention in CD4⁺ T cells²⁹.

Chromatin is efficiently organized in the nucleus, enabling proper expression machinery³⁰. The understanding of enhancer function and 3D genome organization has significantly improved in recent years, aided by several technological advances. These include high-resolution genome-wide mapping of enhancer-promoter contacts in various human and mouse cell types. Chromosome conformation capture (3C) quantifies the number of physical interactions between distant genomic regions in 3D space and is based on ligation proximity³¹. Molecular approaches, such as Hi-C, can be used to map all interactions between distant loci in the genome and provide a view of 3D genomic organization representing an individual cell's identity^{32,33}.

Gene expression programs are associated with hierarchies in genome organization. In mammalian cells, genetic ablation or acute protein depletion of key players in 3D genome architecture, such as CTCF, Yin Yang 1 (YY1), and the Cohesin complex, have provided insights into how the genome is spatially organized into different functional layers³⁴. The latest research is being done on 4D nucleome network to develop and apply approaches to map the structure and dynamics in space and time into how the nucleus is organized and functions³⁵.

3. CTCF as a coordinator of 3D chromatin structure organization

As previously noticed, chromatin, the material forming chromosomes, is organized within a three-dimensional (3D) space inside the cell nucleus³⁰. This organization efficiently packages the genome, facilitating gene expression and replication³⁶. Higher-order 3D chromatin structures involve various regulatory interactions, including enhancer-promoter interactions and repressive interactions mediated by elements such as CCCTC-binding factor (CTCF) and cohesin. CCCTC-binding factor (CTCF) is a highly conserved zinc finger protein among eukaryotic species³⁷ that binds to the consensus sequence defined by 11 zinc finger motifs in its structure³⁸. CTCF is a multivalent protein that can regulate gene expression through various mechanisms^{39,40}. CpG methylation of DNA can disrupt CTCF's binding⁴¹ and CTCF can bind to multiple sequences through combinations of its zinc fingers. Initially identified as a transcriptional repressor of the chicken c-Myc proto-oncogene, CTCF encodes a nuclear phosphoprotein that plays a role in cell cycle progression, apoptosis, and cellular transformation⁴². CTCF localizes between the promoter and enhancer to interfere with enhancer function and inhibit target gene expression.

CTCF's early discovery revealed its specialized ability to function as an "Enhancer blocker". However, CTCF can also bring the promoter into contact with the distal enhancer, increasing gene expression, which is called "Enhancer facilitator" Recently, the loop extrusion model has been established, which contributes to topologically associating domain (TAD) formation. CTCF, Cohesin, and their cofactors drive this model, where Cohesin extrudes chromatin outwards until it meets chromatin barriers anchored by CTCF⁴³. The chromatin looping structure made by CTCF can also be under developmental control. For example, at the mouse *Hoxa* cluster, CTCF sites delimit the boundary between two distal interaction domains in motor neuron cells⁴⁴.

Previous studies suggest that CTCF is involved in cell differentiation and development, and CTCF knockout mice exhibit embryonic lethality. Mutations in CTCF and its

binding sites have been implicated in diverse human diseases such as cancer⁴⁵⁻⁴⁷. In addition to its function as insulators, CTCF plays roles in gene activation, alternative splicing, and immunoglobulin class switching^{42,48,49}. There are reports that CTCF binding at gene promoters can promote enhancer-promoter interactions⁵⁰⁻⁵². A recent study has shown that the establishment of enhancer-promoter interactions in cells involves CTCF, cohesin, and other architectural factors⁵³. However, these factors do not play a significant role in maintaining these interactions. Instead, once established, molecular mechanisms such as histone modifications, chromatin remodeling, DNA modification, and long non-coding RNAs can serve as a memory system to sustain enhancer-promoter interactions and gene expression.

In this context, this study explores the intricacies of 3D chromatin organization, with a focus on the role of CTCF and related factors in shaping genome conformation and regulating gene expression in CD4⁺ T cells. Through a detailed analysis of these mechanisms and their implications on cell identity and function, my research aims to provide a comprehensive understanding of the relationship between genome organization and transcriptional regulation. This work emphasizes the significance of considering the 3D structure of DNA in the study of immune cell function.

II. MATERIALS AND METHODS

1. Mice and Cell culture

Mice carrying a conditional *Ctcf* allele (*Ctcf^{f/f}*) were crossed with Rosa26-CreER (CreER) mice to generate a tamoxifen-inducible CTCF conditional knockout strain (CreER;*Ctcf^{f/f}*) as described in the previous study. Age- and sex-matched CreER littermate mice were used as wild-type (WT) controls throughout the study. All mouse experimental procedures were approved by the Department of Laboratory Animal Resources Committee of Yonsei University College of Medicine. CD4⁺ T cells were isolated from mouse spleen by positive selection with MagniSort™ Mouse CD4 Positive Selection Kit (Thermo Fisher Scientific). Post-sort purities of >85% were assessed by flow cytometry. CD4⁺ T cells were maintained in RPMI supplemented with 10% heat-inactivated fetal bovine serum and 100 U/ml penicillin/streptomycin. CD4⁺ T cells were stimulated with coated α CD3 (2 μ g/ml, Biolegend) and α CD28 (1 μ g/ml, Biolegend) in the presence of IL-2 (100 U/ml, Roche) for 6 days. The medium was changed every 2 days. For the deletion of the *Ctcf* allele in vitro, 4-OH-tamoxifen (Sigma) dissolved in 100% ethanol was added on the first day of culture (final 0.5 μ M).

2. Flow cytometry

Fluorochrome-conjugated anti-mouse CD4 were obtained from eBioscience. Cell death and apoptosis were analyzed using an Annexin V/Propidium iodide (PI) staining kit (eBioscience). Cell proliferation was determined using CFSE staining according to manufacturer's protocol. Suspension cells are stained with the antibodies described above at the appropriate dilutions using FACS buffer (phosphate-buffered saline supplemented with 1% bovine serum albumin). Stained samples were analyzed by multicolor flow cytometry immediately after the end of the incubation period. Suspension cells stained with antibodies are acquired by the FACSVerser flow cytometer

(BD Biosciences). All flow cytometry data were analyzed with the FlowJo software (Treestar). Two biological replicates were performed for each condition.

3. RNA extraction and quantitative real-time polymerase chain reaction (qRT-PCR)

Total RNA is isolated from CD4⁺ T cells using Hybrid-R Total RNA purification kit (GeneAll Biotechnology) following manufacturer's instructions. 1µg of total RNA are used for cDNA synthesis with the PrimeScript™ RT Master Mix (Takara Bio). SYBR Green-based qRT-PCR are performed using the QuantiNova SYBR Green PCR kit (Qiagen). qRT-PCR is achieved with the QuantStudio 3 Real-time PCR System (Applied Biosystems). The PCR process is started at 95 °C for 2 minutes, followed by 40 cycles of 95 °C for 5 seconds and 60 °C for 10 seconds, and ended after melting curve stage. Gene expressions are normalized to *Rpl7* mRNA. The primer sequences are listed in **Table 1**. Four biological replicates were performed for each condition.

Table 1. Primer sequences used for RT-qPCR

Genes	Forward (5'-3')	Reverse (5'-3')
<i>Rpl7</i>	ATGTGCCCCGAGAACCAA	GACGAAGGAGCTGCAGAACCT
<i>Ctcf</i>	GAATTTGCCGTGAGTGGAGT	TGCTGGATGAGAGCATATCG
<i>Dexi</i>	GCTTGACGTCTTCGATGGAT	CCGAGTCCTCATTTCTCCTG
<i>Socs1</i>	ACCTTCTTGGTGCGCGAC	GGGCCCCGAAGCCATCTT
<i>Usp7</i>	GTGTCCGGGACCTGTTAGAA	TTGTGGAAATGTGCCACTGT
<i>Top2a</i>	GAACACCACAGACGAGGAGAAG	CATACAGGAGGCAGAGCACGAA
<i>Igfbp4</i>	CGTCCCGTAGACAAAATGGT	GAATTTGCCGTGAGTGGAGT
<i>Tns4</i>	CAAGCGAGAAGTGAAGGTTGCC	GCTACCCACAAAATTCTGCGCC
<i>Ccr7</i>	CGGAGCAAGATGAAGATCGTGG	GATGAAGAGGTCTTCGTGGGTAC

<i>Tatdn3</i>	GGTGCCTTTGTCATCAGGGACA	GACGGATAAGGTCACTGCTGTC
<i>Nsl1</i>	AGAGGCTCAAGACCATGACGGA	TCCAGGACTTGGCTTCGCTGTA
<i>Batf3</i>	AAATGTGCACTCACGCTCAG	CAGAGGCAGCTGTTTCACAA
<i>Fam71a</i>	CAACCAAACGGAGGCAGTAT	CATGGCCTCACTCATTTCCT
<i>Atf3</i>	AGAAGGCTGACAAGCTCCACGA	CATCTTCTCGTGCTCCTTCAGC

4. Western blotting

Protein extracts are isolated from CD4⁺ T cells using T-PER™ Tissue Protein Extraction Reagent (Thermo Fisher Scientific). For inhibition of phosphatases' activity, Protease Inhibitor Cocktail (Sigma) are added to all buffers. The concentration of protein was determined by Protein Assay Dye Reagent (Bio-Rad). Proteins were separated using sodium dodecyl sulfate-polyacrylamide gel electrophoresis and transferred onto polyvinylidene fluoride membrane. After blocking with 5% skim milk, the membrane was incubated with primary antibodies: α -tubulin from Santa Cruz; CTCF, p-STAT5, STAT5 from Cell Signaling Technology, followed by incubation with horseradish peroxidase-conjugated secondary antibody at 1:2000 dilution: HPR-linked anti-Mouse IgG from Cell Signaling Technology. The target proteins were visualized using Pierce Western Blotting Substrate (Thermo Fisher Scientific) and Image Quant LAS 4000 (GE Healthcare). Three biological replicates were performed for each condition.

5. RNA sequencing

Total RNA is isolated from CD4⁺ T cells in the same way when preparing them for qRT-PCR. The total RNA-seq library is prepared using the TruSeq Stranded Total RNA with Ribo-Zero Gold (Illumina). Messenger RNA was isolated by NEBNext® Poly(A) mRNA Magnetic Isolation Module (New England Biolabs). Strand-specific libraries were generated using NEBNext® Ultra™ RNA Library Prep Kit for Illumina® (New

England Biolabs) according to the manufacturer's protocol. Barcoded libraries were pooled and sequenced on the Illumina HiSeq 2500, generating 100 bp paired-end reads. Four biological replicates were performed for total RNA-seq and three biological replicates were performed for mRNA-seq for each condition.

6. Precision nuclear run-on sequencing (PRO-seq)

PRO-seq was performed as previously described⁵⁴. Briefly, chromatin samples prepared using the appropriate number of live cells (2 million to 2.5 million cells) were permeabilized with sucrose buffer. Biotin-NTPs (combinations of biotin-CTP with unlabeled CTP, UTP, ATP and GTP) were used as the nuclear run-on substrates. Total RNA was extracted with Trizol LS(Ambion) and further fragmented with 0.2N NaOH on ice for 10 min. Then biotin labelled RNA fragments were enriched by streptavidin beads M-270(Invitrogen). The 3' adaptor was added to RNAs with T4 RNA ligase I and 5' adaptor was also ligated to RNA after RppH and T4 PNK treatment at 37 °C for 1 hour each. The RNA fragments with adapters on both sides were reverse transcribed by Superscript III RT enzyme into cDNA and amplified by KAPA HiFi master mix(Roche). Libraries were purified using dual (0.5x–1.8x) SPRI Ampure XP beads and paired-end sequenced (100 bp) on the Illumina HiSeq 2500 platform. Four biological replicates were performed under the WT condition, and three biological replicates were performed under the KO condition.

7. Assay for Transposase-Accessible Chromatin using sequencing (ATAC-seq)

ATAC-seq was performed as previously described⁵⁵. Briefly, 50,000 cells are pelleted, resuspended in Lysis buffer (10mM Tris, pH 7.4, 10mM NaCl, 3mM MgCl₂, 0.1% NP-40, 0.1% Tween-20, 0.01% Digitonin) for 10 minutes on ice, and washed with Lysis buffer without NP-40 and Digitonin. Then, the tagmentation reaction is processed using Nextera DNA Library Prep Kit (Illumina) with 1% Tween-20 and 0.1% Digitonin at 37 °C

for 30 minutes. Transposed DNA is purified with the MinElute PCR Purification kit (Qiagen). qPCR reaction is run with part of the DNA and SYBR green to estimate cycle number from exponential amplification. Two-sided size selection is applied to amplified library DNA from a size range of 100–1,000bps with AMPure XP beads (Beckman Coulter). paired-end sequenced (100 bp) on the Illumina HiSeq 2500 platform. Two biological replicates were performed for each condition. Four biological replicates were performed for each condition.

8. Cell fixation

Sorted CD4⁺ T cells are pelleted and resuspended in fresh 1% formaldehyde (Sigma). Cells are incubated at room temperature for 10 minutes with shaking. Glycine (Duchefa Biochemie) are added at a final concentration of 125mM to quench the formaldehyde, and cells are incubated at room temperature for 5 minutes with rotation. Finally, cells are pelleted and washed with PBS three times, pelleted again, and stored at -80 °C deep freezer. These fixed sample are taken into ChIP-seq, *in situ* Hi-C and HiChIP protocol.

9. Chromatin Immunoprecipitation Sequencing (ChIP-seq)

ChIP-seq was performed as previously described⁵⁶. ChIPmentation is a method that combines ChIP-seq library preparation by Tn5 transposase. The chromatin samples prepared using the appropriate number of fixed cells (5×10^5 for H3K27ac, H3K4me1, H3K4me3, H3K27me3 and 1×10^7 for CTCF, SMC1A, STAT5, Pol II phosphorylated on CTD Serine 5) are lysed in Buffer A (5mM PIPES, pH 8.0, 85mM KCl, 0.5% NP-40) for 10 minutes on ice and then washed once with buffer A without NP-40. Subsequently, cells are resuspended in buffer B (10mM Tris pH 8.0, 2mM EDTA, 0.2% SDS, 5mM PMSF) and incubated for 10 minutes on ice. Cells in buffer B are sonicated as many as 8 set by BMS Bioruptor (High power, 30 seconds ‘ON’, 30 seconds ‘OFF’; 5 cycle per 1 set). Sonicated chromatin is spun down at 14,000rpm 4°C to remove cell

debris. After shearing, the chromatin diluted with 280mM RIPA Buffer and precleared with Dynabeads A/G (Thermo Fisher Scientific) is subsequently immunoprecipitated with each antibody recognizing 1 μ g of H3K27ac (Abcam), H3K4me1 (Abcam), H3K4me3 (Millipore) H3K27me3 (Abcam) or 5 μ g of CTCF (Cell Signaling Technology), SMC1A (Bethyl Lab), STAT5 (Cell Signaling Technology), Pol II phosphorylated on CTD Serine 5 (Cell Signaling Technology). The chromatin–antibody complex is captured with Dynabeads A/G for 2 hours, and subsequently washed with RIPA buffer, LiCl buffer and 10mM Tris, pH 8.0. Then, the tagmentation reaction is processed using Nextera DNA Library Prep Kit (Illumina) at 37 $^{\circ}$ C for 10 minutes. After the tagmentation, each sample is washed sequentially with 140mM RIPA buffer twice, and TE buffer (10mM Tris pH 8.0, 1mM EDTA) twice. Reverse-crosslinking and elution are done by resuspending the beads with ChIP elution buffer (10mM Tris pH 8.0, 1% Triton X-100, 300mM NaCl, 0.4% SDS) and Proteinase K (New England Biolabs) at 55 $^{\circ}$ C for 1 hour and 65 $^{\circ}$ C overnight. DNA is purified by AMPure XP beads (Beckman Coulter). qPCR reaction is run with part of the DNA and SYBR green to estimate cycle number from exponential amplification. Two-sided size selection is applied to amplified library DNA from a size range of 200-400bps with AMPure XP beads (Beckman Coulter) and paired-end sequenced (100 bp) on the Illumina HiSeq 2500 platform. Two biological replicates were performed for each condition.

10. *in situ* Hi-C

In situ Hi-C was performed as previously described³³. Approximately 2 million cells 1% fixed are used per replicate in Hi-C. The crosslinked cells are lysed in Cell lysis buffer (10 mM Tris-HCl, pH 7.5, 10 mM NaCl, 0.2% NP-40) for 10 minutes on ice and then washed once with lysis buffer without NP-40. Subsequently, cells are resuspended in 0.5% SDS and incubated for 10 minutes at 62 $^{\circ}$ C then quenched by 3% Triton X-100 for 15 minutes at 37 $^{\circ}$ C. Then, 10X NEBuffer 2 and MboI (New England Biolabs) are

added to digest chromatin at 37°C with shaking overnight. Enzymes are inactivated by heating for 20 minutes at 62°C. Digested fragments are biotin-labeled and ligated by T4 DNA ligase buffer (New England Biolabs) at 16°C overnight. Subsequently, cells are resuspended in buffer B and incubated for 10 minutes on ice. Cells in buffer B are sonicated as many as 6 set by BMS Bioruptor. After shearing, reverse-crosslinking and elution are done with Proteinase K (New England Biolabs) at 55°C for 1 hour and 65°C overnight. The DNA fragment is purified Phenol-Chloroform extraction and Ethanol precipitation. Ligation junctions are enriched by Dynabeads™ MyOne™ Streptavidin C1 (Thermo Fisher Scientific). Then, the tagmentation reaction is processed using Nextera DNA Library Prep Kit (Illumina) at 55°C for 10 minutes. After the tagmentation, each sample is washed sequentially with 50mM EDTA, and Tween wash buffer (5mM Tris pH 7.5, 0.5mM EDTA, 1M NaCl, 0.05% Tween-20), 10mM Tris, pH 8.0. DNA is purified by AMPure XP beads (Beckman Coulter). Final libraries are directly PCR amplified from Streptavidin beads, size selected with AMPure XP beads (Beckman Coulter). Each library was paired-end sequenced (100 bp) on Illumina HiSeq 2500 platform. Two biological replicates were performed for each condition.

11. HiChIP

HiChIP was performed as previously described⁵⁷, using antibodies against 3μg of H3K27ac (Abcam). HiChIP libraries are prepared in the same protocol as *in situ* Hi-C that progresses to get biotin-labeled and ligated DNA. After shearing, ChIP is processed as described in ChIP-seq. Post-ChIP DNA are enriched by Dynabeads™ MyOne™ Streptavidin C1 and subsequently processed to tagmentation reaction. Finally, Libraries are prepared as described in Hi-C. Each library was paired-end sequenced (100 bp) on Illumina HiSeq 2500 platform. Two biological replicates were performed for each condition.

12. CRISPR/RNP nucleofection

Cells were isolated as described above and cultured for 2 days before transfection. To prepare the duplex, each Alt-R crRNA and Alt-R tracrRNA (IDT) was reconstituted to 100 μ M with Nuclease-Free Duplex Buffer (IDT). The primer sequences are listed in **Table 2**. Oligos were mixed at equimolar concentration in a sterile microcentrifuge tube. Oligos were annealed by heating at 95 $^{\circ}$ C for 5 min in thermocycler and the mix was cooled to room temperature slowly. In a microcentrifuge tube, two crRNA-tracrRNA duplexes (3 μ l equal to 150pmol each) and 5 μ g TrueCut Cas9 Protein v2 (ThermoFisher scientific) were mix gently and incubated at room temperature for 10 min. 200 μ l complete T cell media per well of a 96-well plate was prewarmed. 1.5 million T cells were resuspended in 20 μ l primary cell nucleofection solution (P4 primary Cell 4D-Nucleofector X kit S, Lonza). T cells were mixed and incubated with 15 μ l RNP-complex at room temperature for 2 min in microcentrifuge tubes. The cell/RNP mix was transferred to Nucleofection cuvette strips (4D-Nucleofector X kit S; Lonza). Cells were electroporated using a 4D nucleofector (4D-Nucleofector Core Unit; Lonza, 4D-Nucleofector X Unit; Lonza). Pulses CM137 for activated CD4⁺ T cells. After nucleofection, prewarmed T cell media was used to transfer transfected cells in 96-well plates. T cells were cultured at 1.5 million per well in 200 μ l complete T cell media for 2 days

Table 2. gRNA sequences used for CRISPR/RNP Nucleofection

Index	gRNA Sequence
Control	GCGAGGTATTCGGCTCCGCG
GAS1	CAACAAGCGTTATCGCTTCC
GAS2	GGCACAACCGGTCTTCTTCG
GAS3	TAAACTTATGAGTCGTTTCC

GAS4	TGAGTCGTTTCCTGGAACAT
CTCF1	TGTCCGCCGGTAGCCACCAG
CTCF2	TTGTCCGCCGGTAGCCACCA

13. T7E1 mismatch detection assay

T7 Endonuclease I (T7E1) was purchased from New England Biolabs and assayed according to manufacturer's protocol. Briefly, genomic DNA was extracted from cells that underwent CRISPR KO experiment, and the target region was amplified by PCR. The primer sequences are listed in **Table 3**. The amplified products were purified using AMPure XP beads (Beckman Coulter). The obtained DNA was quantified, and 200ng of DNA was denatured at 95°C. Annealing was induced by lowering the temperature from 95°C to 85°C at a rate of 2°C per second, and then gradually reducing the temperature from 85°C to 25°C at a rate of 0.1°C per second. The recombined dsDNA was then subjected to mismatch digestion using T7 endonuclease at 37°C for 20 minutes, and the fragments were confirmed by agarose gel electrophoresis.

Table 3. Primer sequence for amplification of CRISPR KO target region

Target site	Forward primer (5'-3')	Reverse primer (5'-3')
<i>Dexi</i> enhancer	GGTATCGATGGCACTCCTGT	TCTCACGGGGTACAGAGGAG
<i>Igfbp4</i> enhancer	CCACCTCAGAGCTCCACACT	AGTTCCCTTTCCCAACATCC
<i>Batf3</i> enhancer	GCCTTGTGGCAGAGTTTCTT	AGAGGCCACGACTCACAAAC

14. Cloning and sequencing for check mutation rate

Genomic DNA was extracted from cells that underwent CRISPR KO experiment, and the target region was amplified by PCR using the same method as the T7E1 assay. The amplified DNA was electrophoresed on agarose gel to purify the target sequence DNA

of appropriate size using the Gel SV kit (GeneAll). The purified DNA bait was inserted into the TA cloning vector (Takara), and transformation was carried out using DH5 alpha (Enzynomics) according to the manufacturer's instructions. The resulting colonies were prep using the plasmid SV kit (GeneAll), and sanger sequencing was performed using universal primers in **Table 4**.

Table 4. Sequencing primer for reading DNA sequence after cloning

index	Primer sequence
M13F-pUC	GTTTTCCCAGTCACGAC
M13R-pUC	CAGGAAACAGCTATGAC

15. RNA-Seq data processing

Paired end sequencing reads were trimmed using Trim Galore (version 0.6.4) with the command-line settings “trim_galore --paired”. The trimmed reads were then aligned to the mouse mm10 genome assembly using STAR (version 2.6.0a)⁵⁸ with the parametrs -chimSegmentMin 20 --twopassMode Basic --quantMode TranscriptomeSAM. Gene expression levels were measured using RSEM (version 1.3.1)⁵⁹ with the parameters --paired-end --estimated-rspd. Differentially expressed protein-coding genes were identified using the DEseq2 R package (version 1.34.0)⁶⁰ with an adjusted p-value threshold of 0.05 and a fold-change threshold of 2. For biological process gene ontology enrichment analysis of the differentially expressed gene symbols, the enrichGO function from the ClusterProfiler R package (version 3.14.3)⁶¹ was applied with a q-value threshold of 0.05. Strand-specific reads were chosen using SAMtools (version 1.9)⁶², and normalized using bamCoverage function from deepTools (version 3.3.0)⁶³ with the parameter “--normalizeUsing CPM” to generate strand-specific RNA-seq genome track signals.

16. ChIP-Seq data processing

Paired-end sequencing reads were trimmed using trim galore with the same parameters as in RNA-seq analysis, and subsequently aligned to the mouse mm10 genome assembly using bwa (version 0.7.12)⁶⁴ with default parameter settings. Low quality reads were extracted using SAMtools with parameters -1 30 -F 1804 -f 2, and duplicate reads were tagged using Picard tools (version 2.18.23) with default parameters. Mitochondrial reads and duplicate reads were further eliminated using SAMtools with the same parameters as before. Uniquely mapped reads were normalized using bamCoverage function from deepTools with command-line options “--normalizeUsing CPM” to generate ChIP-seq genome tracks. ChIP-seq heatmap signals were evaluated with computeMatrix function from deepTools with the command-line options “reference-point --referencePoint center --missingDataAsZero” and additional range information to present normalized read counts near peak center. Peaks were determined for each sample and biological replicate using MACS2 (version 2.1.2)⁶⁵ with command line options “macs2 callpeak -g mm -f BAMPE --nomodel” and input reference data, and additional command line options “-q 0.001” for H3K27ac ChIP-seq and “--broad” for H3K4me1 and H3K4me3 ChIP-seq. For H3K27ac ChIP-seq analysis, raw sequencing reads of replicates were merged and re-processed as combined results for further analysis. DESeq2 R package was used to define differential peaks of ChIP-seq data using read counts from each sample, with customized size factors assessed based on the proportion of uniquely mapped reads between samples, adjusted p-value threshold of 0.05, and a fold-change threshold of 2.

17. ATAC-seq data processing

Paired-end sequencing reads were trimmed using trim galore with the same parameters as in RNA-seq analysis. Trimmed reads were mapped to the mouse mm10 reference genome using bowtie2 (version 2.3.2)⁶⁶ with the parameters --end-to-end --very-

sensitive --maxins 2000. Reads with low mapping quality, duplicated reads, and mitochondrial reads were labeled and filtered using SAMtools and picard tools as in ChIP-seq analysis. Nucleosome-free regions were chosen, and Tn5 transposase-induced adaptor insertion sites were shifted using alignmentSieve function from deepTools with the command line-options "--maxFragmentLength 100 -ATACshift." Nucleosome-free region reads were normalized using deepTools as in ChIP-seq analysis to generate ATAC-seq genome tracks. ATAC-seq peak calling was performed using MACS2 with the same parameters as in ChIP-seq analysis without using input reference data. DESeq2 R package was applied to determine differentially accessible regions in the ATAC-seq data using read counts of each sample and customized size factors calculated based on the proportion of nucleosome free region reads between samples, an adjusted p-value threshold of 0.05, and a fold-change threshold of 2.

18. PRO-seq data processing

Paired-end sequencing reads were trimmed using trim galore with the same parameters as in RNA-seq analysis. Trimmed reads were mapped to the mouse mm10 reference genome using bwa mem as in ChIP-seq analysis. Reads with low mapping quality, duplicated reads, and mitochondrial reads were marked and filtered using SAMtools and picard tools as in ChIP-seq and ATAC-seq analysis. Uniquely mapped reads were normalized using deepTools as in ChIP-seq. Strand-specific reads were selected using SAMtools, and normalized using deepTools as in RNA-seq to generate strand-specific PRO-seq genome track signals. *De novo* transcript identification was performed using HOMER function findPeaks⁶⁷ with "--style groseq" option for each and merged samples. Enhancer RNAs were identified from PRO-seq data by detecting bidirectional *de novo* transcripts that displayed overlaps with Pol2S5P ChIP-seq peaks, H3K27ac ChIP-seq peaks, and ATAC-seq peaks, while ensuring they did not overlap with ± 2.5 kb from the transcription start site of all genes or the gene body of any coding genes.

19. *in situ* Hi-C data analysis

Paired-end read files were processed using HiC-Pro (version 2.11.4)⁶⁸. Default settings were used to align reads to the mouse mm10 genome, remove duplicate reads, assign reads to Dpn II restriction fragments, filter for valid interactions, and generate binned interaction matrices. After confirmation of good reproducibility between biological replicates using hic-spector⁶⁹, the replicate data were merged for re-processing as combined results. The validated contact pairs were transformed to Juicer .hic files by hicpro2juicebox function from HiC-Pro with the default parameter settings. To segregate A and B compartments, eigenvector for each chromosome of each sample were generated from the Hi-C data using Juicer tools function eigenvector (version 1.22.01) with KR normalization at 100kb resolution⁷⁰. The Juicer .hic files were converted to .cool files using hic2cool with default parameter options. Compartmentalization strength for KR-normalized Hi-C data at 100kb resolution was calculated using cooltools (version 0.3.2)⁷¹, defined as the ratio of $(A-A + B-B)/(A-B + B-A)$ interactions. Insulation score was computed using an algorithm that aggregated the number of interactions that occurred across chromosome bins and dividing it by the mean number of interactions for the whole chromosome, followed by logarithmization⁷². Topological domain (TAD) boundaries were decided using an insulation square analysis algorithm through matrix2insulation.pl function with parameters -b 500000 -ids 200000 -im mean -bmoe 3 -nt 0.1. Intra-TAD DNA interactions, represented as TAD strengths, were calculated using FAN-C (version 0.9.14)⁷³ with the command-line options “fanc aggregate --tads --expected-norm -log.”

20. HiChIP data analysis

Paired-end read files of separated and merged samples were processed using HiC-Pro, following the same steps as in *in situ* Hi-C analysis. H3K27ac HiChIP loops were called

using FitHiChIP (version 9.0)⁷⁴ with 10 kb bin sizes, bias correction by coverage, false discovery rate $<10^{-5}$, a minimum genomic distance of 20 kb, and a maximum genomic distance of 2 Mb. For identification of loops with differential strength of chromatin interaction, all H3K27ac HiChIP loops with $q < 10^{-5}$ in at least one of the two conditions were compared by applying DESeq2 (version 1.24.0) for the contact counts of each replicate. Gained and lost H3K27ac HiChIP loops were selected using a $p < 0.05$ and $\log[\text{FC}] > 1$ and $\log[\text{FC}] < -1$, respectively. The cutoff for super-loops was set to the elbow of the curve, and a tangent line at the cutoff was demonstrated in the graph. Loops below the elbow point of the curve were defined as typical-loops. Super-loops and Typical-loops were equally divided as S1, S2, T1, and T2 subgroups based on loop strength.

21. Aggregated Peak Analysis (APA)

To aggregate genome-wide interaction density near selected loops, the merged HiC and HiChIP matrix dataset were processed using the Juicer tools function `apa` (version 1.19.02) with command line options “-r 10000 -k KR -n 30 -w 10.” Genome-wide normalized APA results were applied for plotting and calculating Peak to Lower Left (P2LL) value.

22. Definition of regulatory elements for annotating HiChIP loop anchors

Promoters were defined as ± 2.5 kb from the transcription start site (TSS) of each protein-coding gene. Enhancers were identified as regions with an H3K27ac peak as determined by ChIP-seq. Super-enhancers were determined by utilizing the ROSE algorithm to H3K27ac peaks with the default stitching size of 12.5 kb²³. The presence of one or more promoter was considered a promoter HiChIP anchor. The absence of any promoter or enhancer was considered as a none HiChIP anchor.

23. Motif enrichment Locus Overlap analysis

The enrichment of transcription factor motifs within ATAC-seq peaks that overlapped with anchors from each group of HiChIP loops was obtained by BEDTools (version 2.29.2)⁷⁵ and analyzed using the "findMotifsGenome.pl" function from HOMER, employing total ATAC-seq peak regions as a background position. For Locus Overlap Analysis (LOLA), ATAC-seq peaks within region of interest were analyzed using LOLAweb (version 1.4.0)⁷⁶ with total ATAC-seq peak regions as a background regions and background universe, and compared against the LOLACore region databases for mm10 to identify enrichment of experimentally-derived transcription factor binding locations.

24. Quantification and statistical analysis

The statistical significance of differences between measurements was determined by Wilcoxon rank sum using the R package and GraphPad Prism 5, unless otherwise stated. Statistical details of experiments can be found in the figure legends.

25. Data visualization

All HiC and HiChIP matrix data were plotted by HiCExplorer (version 3.7.2)⁷⁷. All ChIP-seq and PRO-seq heatmap, saddle plot, and aggregate plot were generated by seaborn (version 0.10.1) and matplotlib (version 3.2.1) python packages. All RNA-seq, ChIP-seq, ATAC-seq, and PRO-seq genome tracks were generated by pyGenomeTracks (version 3.7)⁷⁸.

III. RESULTS

1. Conditional CTCF knockout was induced in CD4⁺ T cells, leading to an effective reduction of CTCF levels.

In order to investigate CTCF knockout cells, a bypass approach was necessary as CTCF knockout is embryonic lethal at E4.5-E5.5⁷⁹. The Cre recombinase with a tamoxifen inducible estrogen receptor (ER) fusion protein was deemed suitable for this purpose^{80,81}. Tamoxifen-treated CreER translocates to the nucleus and removes flanking loxP sites by site-specific recombination, allowing for the creation of CTCF knockout CD4⁺ T cells.

I utilized the CreER/LoxP system to obtain CTCF knockout CD4⁺ T cells (KO). Initially, CD4⁺ T cells were isolated from the mice spleen using magnetic activated cell sorting (MACS) and subsequently cultured with tamoxifen to acquire activated CD4⁺ T cells with CTCF KO, while wild-type CD4⁺ T cells (WT) were obtained in the absence of LoxP site (**Figure 1A**). The CD4⁺ marker of the T cells after MACS was confirmed by flow cytometry, and it was affirmed that CD4⁺ T cells with high purity of 90% or more were obtained (**Figure 1B**). Furthermore, while steadily inducing the activation of T cells with IL-2, the expression of CTCF mRNA was monitored, and it was discovered that CTCF completely disappeared after day 2 (**Figure 1C**). Ultimately, it was validated that the CTCF mRNA expression and CTCF protein of the activated T cells used in the experiment were entirely removed by day 6 (**Figure 1D, E**).

Previous studies have reported that when CTCF is knocked out in cells past the development stage, cell death slightly increases⁸². This experimental design also demonstrated that when apoptosis was measured in CD4⁺ T cells in CTCF KO, the cell death was slightly increased in KO compared to WT, but not significantly (**Figure 1F**). Additionally, it was found that the division rates of CTCF wild-type (WT) and KO were not significantly different in the case of cell proliferation (**Figure 1G**).

Meanwhile, Cohesin is known to play a pivotal role in forming a loop⁸³, ChIP-seq experiment was conducted to confirm the binding of CTCF and the change of SMC1A, the subunit of the Cohesin complex, binding pattern accordingly. It was verified that when CTCF is eliminated, a considerable amount of Cohesin disappears similarly to CTCF (**Figure 2A**). Notably, even after CTCF is knocked out, some Cohesin remained (**Figure 2B, C**)⁸⁴. This suggests that Cohesin is not entirely dependent on CTCF. After CTCF KO, differential RNA expression analysis revealed 1,074 deregulated protein coding genes (660 upregulated and 414 downregulated) with an adjusted p-value < 0.05, fold change > 2 (**Figure 2D; left**). The gene ontology analysis revealed that the genes upregulated by CTCF KO were mainly enriched for DNA replication and repair, whereas the downregulated genes were primarily associated with cell-cell adhesion and response to granulocytes (**Figure 2D; right**).

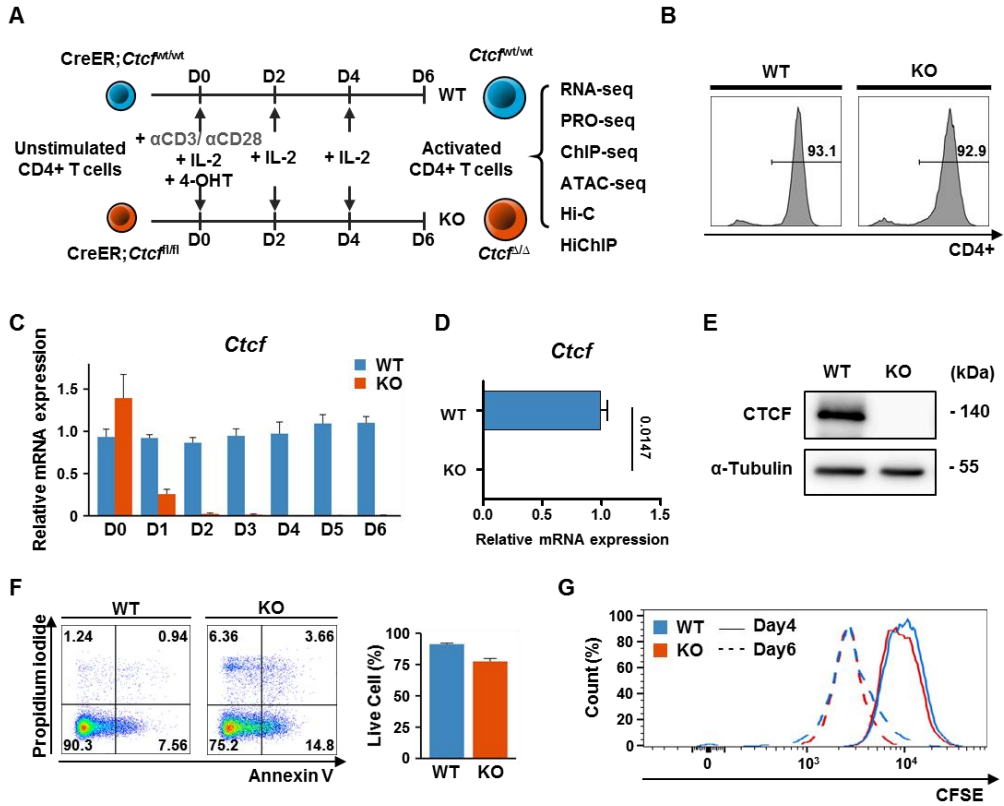


Figure 1. CD4⁺ T cells were subjected to a conditional knockout of CTCF, resulting in an efficient depletion of CTCF

(A) The experimental design scheme depicting the experimental approach employed in this study. (B) CD4⁺ T cell population after magnetic activated cell sorting (MACS). (C) Kinetics of CTCF mRNA expression with CTCF deletion by tamoxifen treatment. Error bars represent mean \pm standard error of the mean (s.e.m). n=2 biologically independent samples. (D and E) Validation of efficient CTCF deletion by tamoxifen treatment at day 6 in terms of RNA levels (D) and protein levels (E). Significance was calculated using one-sided Mann–Whitney U test. (F) Flow cytometric diagrams illustrating the live cell frequency with or without CTCF (left), accompanied by a summarized bar graph indicating the percentage of viable CD4⁺ T cells (right). Error bars represent mean \pm standard error of the mean (s.e.m). n=2 biologically independent samples (G) Day4-CFSE-labeled CD4⁺ T cells exhibiting proliferation-induced CFSE dilution were examined using flow cytometry, with analysis performed both on day 4 and day 6.

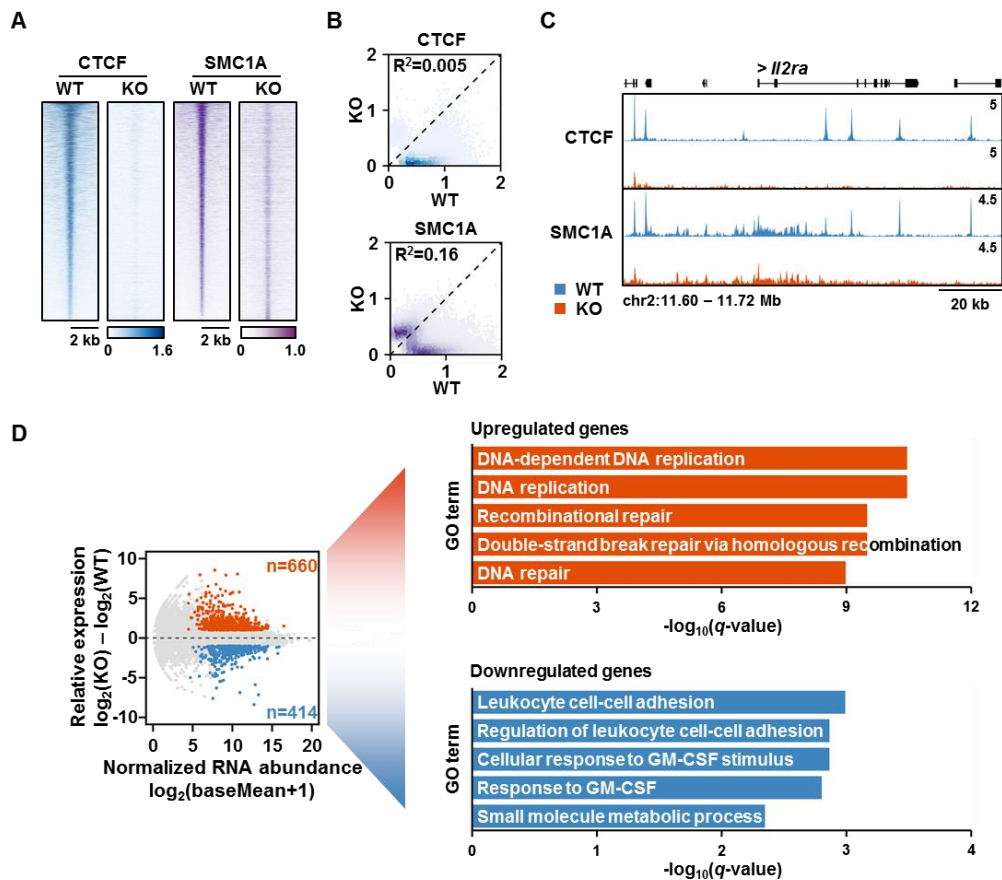


Figure 2. Disrupted occupancies of CTCF and SMC1 due to CTCF depletion

(A) Heatmaps of ChIP-Seq signals called for CTCF (left) and SMC1A (right). (B) Scatterplot of ChIP-Seq signals called for CTCF (up) and SMC1A (down). (C) Snapshot of signal tracks for CTCF ChIP-seq, SMC1A ChIP-seq in the representative genomic region. (D) RNA-seq MA plot (left) of WT versus KO. The number of protein coding genes exhibiting >2-fold increases in WT (blue) or KO (red) with an adjusted p-value <0.05 are indicated. Bar plot (right) of $-\log_{10}(q\text{-value})$ showing enrichment of gene ontology terms (biological process) associated with genes whose expressions were upregulated or downregulated by CTCF KO.

2. Compartment organization does not rely on CTCF, yet CTCF is crucial for insulating Topologically Associating Domains (TADs).

Since CTCF is known as an insulator, it is meaningful to check how genome organization changes when CTCF disappears. To investigate the effect of CTCF KO on 3D chromatin structure, *in situ* Hi-C was performed to quantify compartments and TADs³³. Contact maps (**Figure 3A**) and compartment signals (**Figure 3B, C, D**) indicated that the segregation of active and inactive chromosome regions into A and B compartments was not significantly affected by CTCF KO (WT vs KO; $r^2 = 0.96$), with only a 4% difference observed in compartments between WT and KO (**Figure 3E**). As previously described⁸⁵, each compartment is classified based on transcriptional activity, and genes where compartment changes occurred tended to have significantly altered expression (**Figure 3F**). These findings suggest that while CTCF may not be necessary for higher-order chromatin compartmentalization⁸², some regions have the potential to be affected (**Figure 3G**).

At the TAD level, defined by using insulation scores, KO CD4 T cells showed a decreased number of TADs compared with WT (**Figure 4A**). Based on WT boundaries, insulation scores showed that boundary strength noticeably weakened following CTCF deletion (**Figure 4B**). In this context, TAD boundaries, which prevent inter-TAD interactions, were significantly reduced by KO (**Figure 4C**). Consistent with previous reports in other cell models⁸², *in situ* Hi-C analysis revealed that CTCF depletion largely preserves compartment organization but interferes with TAD insulation in CD4⁺ T cells. (**Figure 4D**).

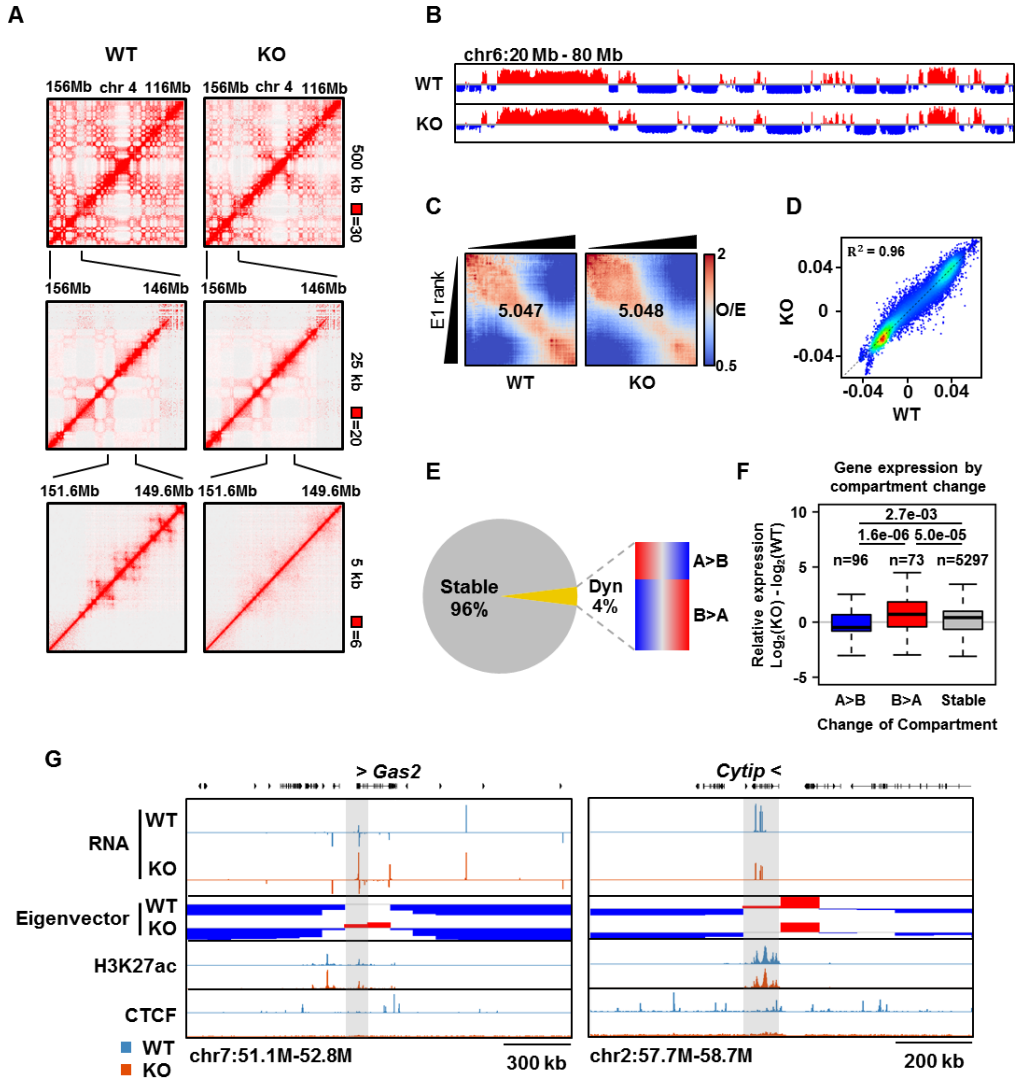


Figure 3. CTCF is dispensable for compartment organization

(A) Hi-C contact maps generated by Juicebox at 500 kb, 25 kb, and 5 kb resolutions. (B) Distributions of the first eigenvector values across the entirety of chromosome 6. Red color represents A compartments and blue color represents B compartments. (C) Saddle plots of compartmentalization strength in WT and KO by genome-wide 0.05 - 0.95 quantile range. (D) Comparison of cis Eigenvector 1 values between WT and KO. (E and F) The distribution plots (E) and corresponding protein coding gene expression (adjusted p-value <0.05) from compartment change between A and B in KO are indicated. (G) Snapshot of signal tracks for RNA-seq, Eigenvectors, H3K27ac, and CTCF ChIP-seq is presented in the representative genomic region where changes occurred from A to B and B to A.

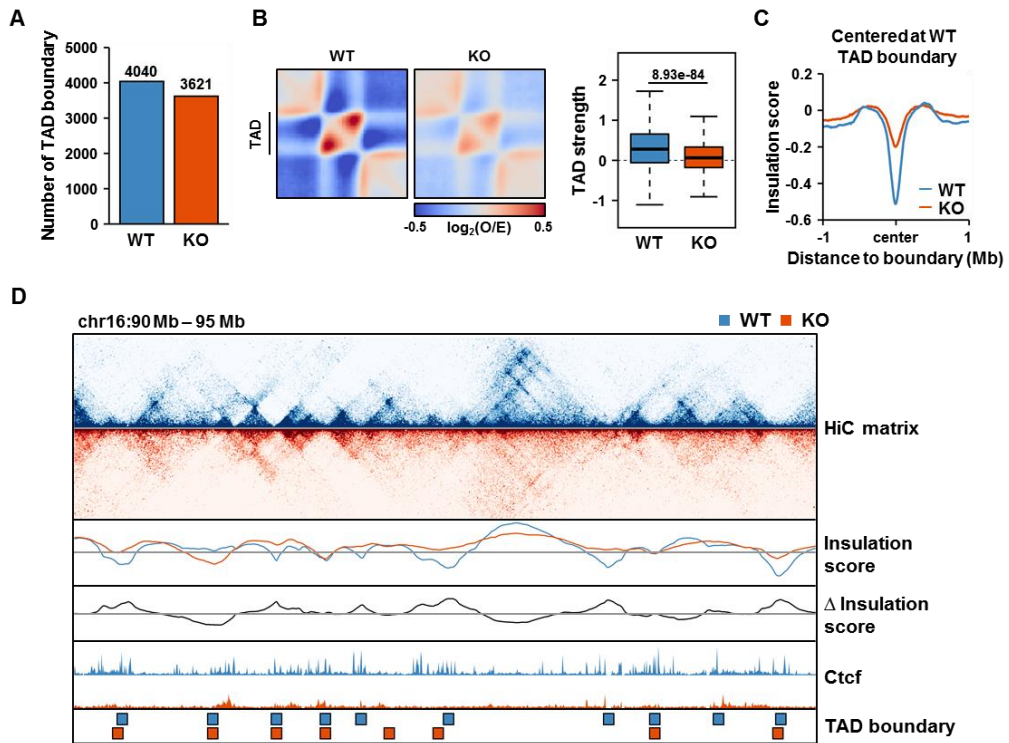


Figure 4. CTCF is essential for TAD insulation

(A) Number of TAD boundaries determined using Hi-C data in WT and KO. (B) Heatmaps(left) display the average observed/expected Hi-C interactions in the TAD regions regions, and boxplot(right) shows TAD strength between WT and KO. (C) Genome-wide averaged insulation scores plotted against distance around insulation center at TAD boundaries of WT CD4⁺ T cells. (D) Snapshot displaying Hi-C contact map, insulation score, CTCF ChIP-seq signal tracks and TAD boundary. The blue color represents WT, and the red color represents KO.

3. CTCF and transcriptional activity play a crucial role in facilitating the formation of enhancer loops.

In order to further investigate the substructure of TADs, high-resolution contact maps of interactions between active enhancers and target genes in CD4 T cells were generated using H3K27Ac HiChIP. Previous reports have indicated that CTCF depletion significantly decreases the number of loops⁸⁶. I observed a substantial decrease in the number of HiChIP loops due to CTCF depletion (75,845 in WT and 42,839 in KO) (**Figure 5A**). Interestingly, it was noteworthy that about half of the loops still remained.

Each loop is composed of two anchors, and the loops can be classified by me according to the presence or absence of CTCF in each anchor to determine the extent of CTCF involvement in loop formation (**Figure 5B**). Most of HiChIP loops in WT cells enriched CTCF at least at one of the loop anchors (**Figure 5C**). This indicates that CTCF plays a crucial role in mediating enhancer-promoter interactions. Remarkably, when the results were classified according to the presence or absence of CTCF in the anchor, it was found that about half of the anchors were not bound by CTCF (**Figure 5D**). This suggests that factors other than CTCF also play a role in maintaining enhancer-promoter loops.

To gain a deeper understanding of the properties of the loops, the loops were classified according to their intensity using ranking of super enhancer (ROSE) algorithm, which is generally used for super-enhancer analysis⁸⁷. In 3D chromatin studies involving CTCF, it has been suggested that there is a positive correlation between loop strength, enhancer-promoter interactions, and transcription levels^{53,88}. The loop strength was weighted using q values, which indicate the statistically significant level, and super-loops were defined as regions past the point where the slope is 1 (**Figure 5E**). According to this criterion, loops with $-\log_{10} q$ value exceeding 35.6 in WT and 28.7 in KO were defined as super-loops. Furthermore, based on these values, super loops and typical loops were distinguished, and the loops belonging to each region were divided equally into S1 and S2, T1 and T2 (**Figure 5E**).

To verify that this definition method was not biased by loops limited to H3K27ac ChIP and that the statistical significance and contact count of the interaction were compatible criteria, the H3K27ac HiChIP analysis results for loop distribution were cross-validated with Hi-C data (**Figure 5F**). Strong loops had a higher contact count and a lower q value, indicating that the intensity of the loops could be expressed by the contact count and statistical significance. In addition, higher loop strength of super-loops compared to typical loops were verified by examining *in situ* Hi-C and HiChIP contact counts through Aggregate Peak Analysis (APA) (**Figure 5G, H**).

To investigate the correlation between loop strength and transcription factor binding, ChIP-seq experiments were conducted on factors that are important for the formation of 3D chromatin structures and are related to transcription activity, as well as experiments that represent gene expression. First, the signal enrichment of each marker was tracked in WT and KO as the loop strength increased in the order of T1, T2, S1, and S2 (**Figure 6A**). CTCF and Cohesin showed more enrichment as the loop strength increased, indicating that stronger loops involve stronger binding of CTCF and Cohesin in proportion (**Figure 6A; top left**). When examining DNA accessibility and H3K27ac, which are activation markers, it was found that accessibility and transcription activity also increased as loop strength increased (**Figure 6A, bottom left**)⁸⁹. The enhancer marker H3K4me1 and promoter marker H3K4me3 showed the same tendency, while the inactive chromatin marker H3K27me3 showed lower signal enrichment in stronger loops (**Figure 6A, middle right**)⁹⁰.

Comparing WT and KO in each graph, it can be seen that the signal is almost absent in the KO sample for CTCF, which was knocked out, while relatively higher enrichment is observed in KO than in WT for the other activation markers. To determine whether the cause of these results was an increase in the expression of the markers themselves in the absence of CTCF, or whether the original high signal was revealed by the disappearance of CTCF, the analysis was performed on anchors of WT CD4⁺ T cells

divided according to the presence or absence of CTCF (**Figure 6B**). Although there was some difference, it was interesting to note that the anchor without CTCF showed higher active marker enrichment than the anchor with CTCF. Taken together, these results imply a crucial function for CTCF in preserving chromatin interactions centered around enhancers, and indicate that potent transcriptional activity can promote the formation of robust enhancer loops independently of CTCF.

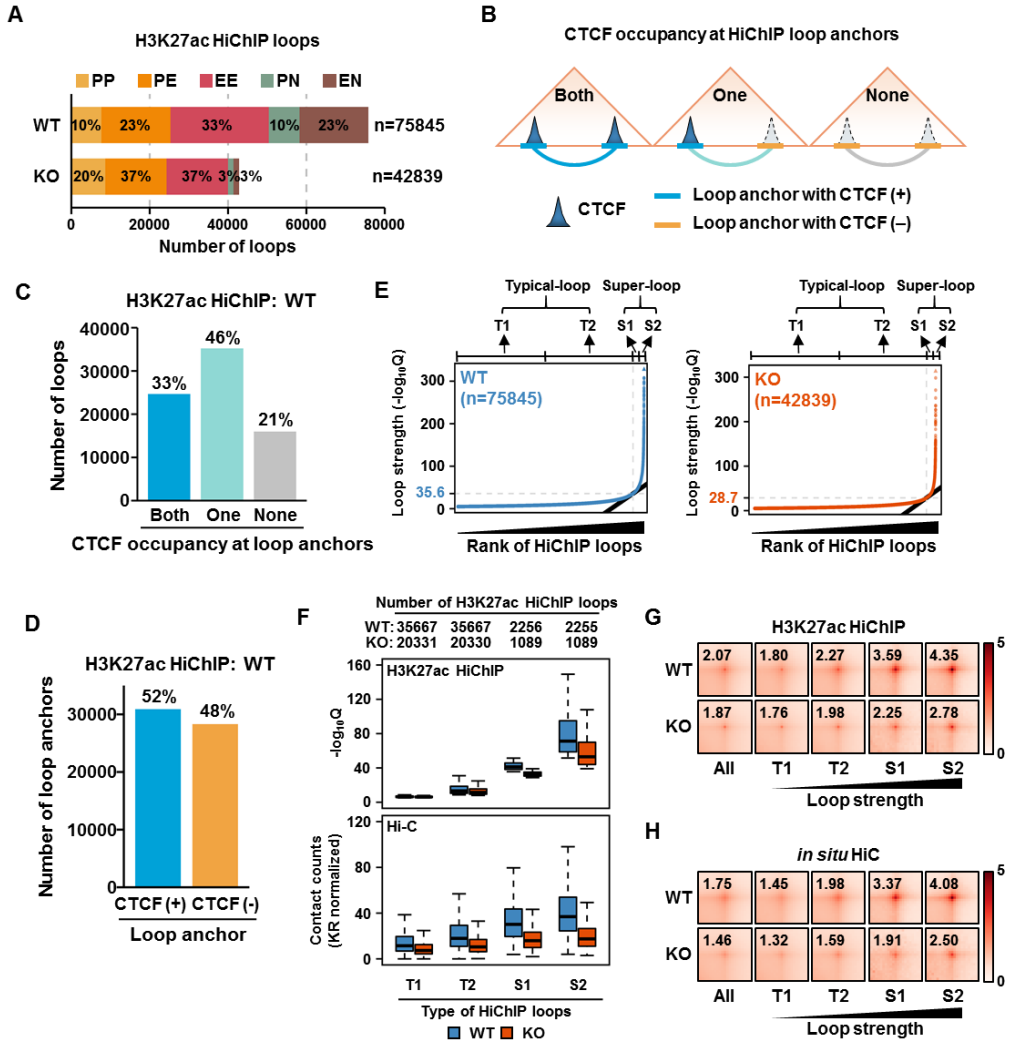


Figure 5. CTCF plays a significant role in the formation of loops

(A) Distribution of regulatory elements at the anchors of H3K27ac HiChIP loops in WT and KO. (B) Categorization of H3K27ac HiChIP loops into three distinct types based on the presence of CTCF occupancy at the loop anchors. (C) Quantity of HiChIP loops originating from wild-type CD4⁺ T cells, classified according to the description in (B). (D) Boxplot distribution showing the number of WT loop anchors with or without CTCF classified as described in (B). (E) H3K27ac HiChIP loop signal enrichment (as defined by the ROSE algorithm) representing, for each loop strength, calculated by $-\log_{10}(\text{q value})$. Both super-loops and typical-loops were further divided evenly based on their loop strength. (F) Boxplot showing $-\log_{10}(\text{q value})$ aspects from HiChIP data and contact counts from Hi-C data identified as loop strength increases. (G and H) Aggregate Peak Analysis (APA) was conducted on each set of HiChIP loops from WT (top) and KO (bottom) CD4⁺ T cells, involving the examination of *in situ* HiChIP (G) and Hi-C (H) contact counts.

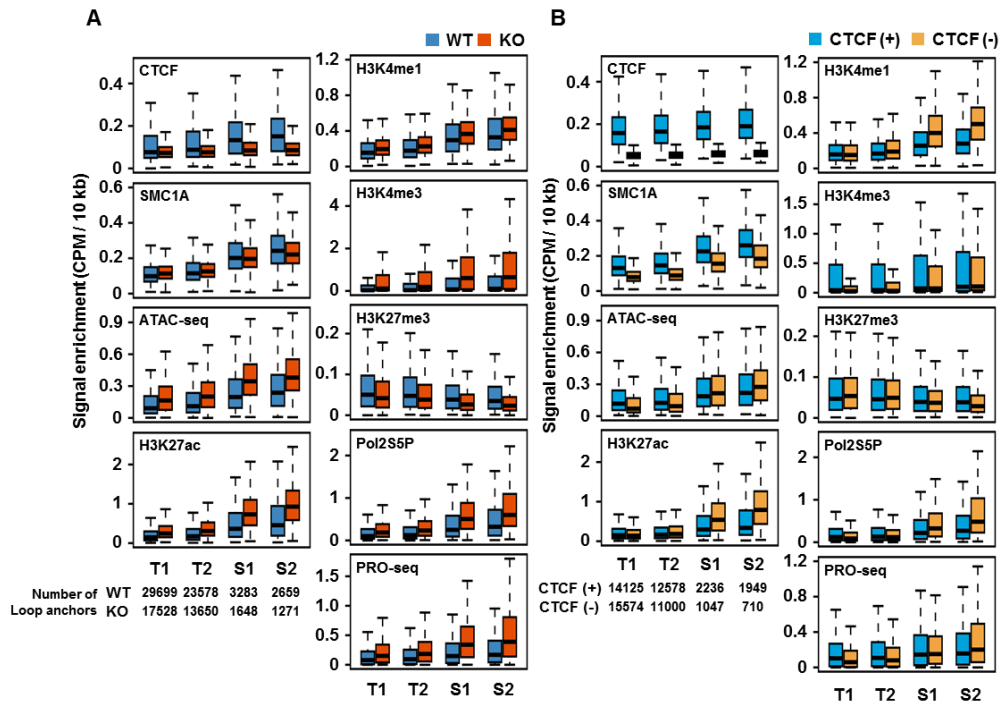


Figure 6. Positive correlation between loop strength and the presence of CTCF and active transcription markers

(A and B) HiChIP loop anchors were analyzed in CD4⁺ T cells from both WT and KO conditions, assessing the enrichment of ChIP-seq, PRO-seq, and ATAC-seq signals. Additionally, HiChIP loop anchors from WT CD4⁺ T cells, categorized by the presence (left) or absence (right) of CTCF occupancy, were investigated for the enrichment of ChIP-seq, PRO-seq, and ATAC-seq signals. The quantity of anchors in each group of HiChIP loops was indicated in the figures.

4. Super loop is engaged to super-enhancer and cell-identity related genes.

As previously described^{22,23}, super-enhancers are known to involve many active transcription factors and regulate the expression of genes that reflect cell identity. I was curious about the extent to which the 3D chromatin structure altered by CTCF could influence the cellular functions. In order to determine how the absence of CTCF affects the activity of super-enhancers, H3K27ac ChIP-seq and ROSE analysis were performed (**Figure 7A**). The WT super-enhancers yielded 619, while the KO super-enhancers yielded 629. Comparing the H3K27ac signal enrichment between the two groups, there was almost no significant difference (**Figure 7B**). Similar to the analysis of epigenome profiles based on loop strength, a bar graph was used to represent the involvement of super-enhancers and typical enhancers according to loop intensity (**Figure 7C**). This result indicates that super-loops contain more super-enhancers than typical loops, suggesting a high correlation between super-loop activity and super-enhancer activity. When the target genes regulated by WT and KO super-enhancers were linked using loop data, 1,801 and 2,427 genes were identified, respectively (**Figure 7D**). Gene ontology analysis of the target genes revealed terminologies that included genes important for CD4⁺ T cell functions, such as T cell activation and lymphocyte differentiation (**Figure 7E**). As expected, super-enhancers were found to regulate genes related to cell identity, and the depletion of CTCF had a minimal impact on the target genes of super-enhancers.

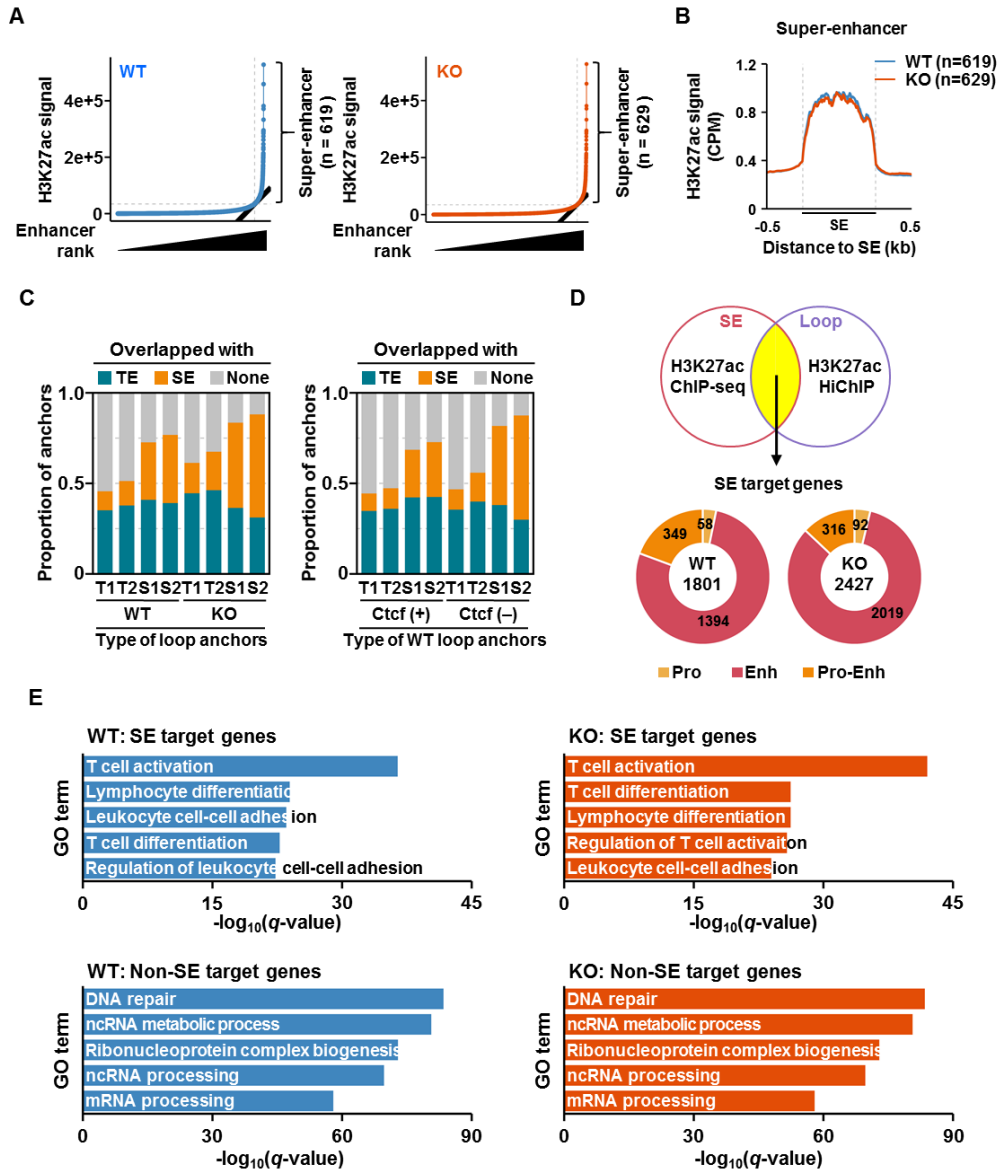


Figure 7. As the loop strength increases, the involvement of the super-enhancer also increases

(A) H3K27ac ChIP-seq signal enrichment (as defined by the ROSE algorithm) depicting ranking of enhancer regions in WT and KO. (B) Line plot showing normalized counts in H3K27ac signal enrichment of super-enhancer (SE) between CTCF WT and KO. The number of loops exhibiting >2-fold increases in WT (blue) or KO (red) with adjusted p value < 0.05 has been indicated. (C) Distribution of enhancer types at the anchors according to loop strength categorized by the presence or absence of CTCF (left), and divided into loops with and without CTCF in WT CD4⁺ T cells (right). (D) Super-enhancer target genes were pinpointed through a combined analysis of H3K27ac ChIP-seq and H3K27ac HiChIP, and their classification was based on the positioning of the super-enhancers either at promoters, distal enhancers, or both. (E) Bar plot of -log₁₀ q-value showing enrichment of gene ontology terms (biological process) associated with genes whose expressions targeted by super-enhancers of WT (left) or KO (right). Over representation analysis (ORA) applied using hypergeometric distribution.

5. Super loops have a low pausing index and regulate cell-specific genes.

Recent studies propose that super-enhancers facilitate elevated gene expression by expediting the swift release of transcriptional pausing⁹¹⁻⁹³. The pausing index is a measure of the efficiency of transcription elongation and is defined as the ratio of Pol II density at the promoter-proximal region where transcriptional pausing occurs to the gene body where elongation occurs⁹⁴. Pol II that binds to the promoter undergoes initiation, elongation, and termination while being phosphorylated on its C-terminal domain (CTD)⁹⁵. Pol II phosphorylated on CTD Serine 5 (Pol2S5P) is a modification that is found in both initiating and elongating Pol II. Therefore, to investigate how the Pol2S5P ChIP-seq signal changes with loop strength, genes were selected that do not have any connected loops, genes with typical loops, and genes with super-loops (**Figure 8A**). The ratio of promoter-proximal peak density to gene body density was calculated for each of these genes, and the pausing index was determined. The results showed that as loop strength increased from no loop to S2 loop, the gene body's ChIP-seq signal gradually increased. The pausing index, calculated as the ratio of these two densities, decreased as the loop strength increased (**Figure 8B**). The purpose of the pausing index is to measure how long Pol II lingers at the transcription start site, and it can also be calculated using PRO-seq, which tracks nascent RNA transcription⁹⁶. When PRO-seq data from the promoter and gene body of target genes connected by loops were analyzed, it showed the same pattern as the Pol II data (**Figure 8C**), with the pausing index decreasing as loop strength increased (**Figure 8D**).

When target genes were classified according to the strength of the connected loops and the average signal landscape of the promoter and gene body was examined, the highest enrichment was seen at the transcription start site (TSS), with the signal decreasing as the gene body progressed. Super-loops showed higher signal enrichment than typical loops and no loops, both at the TSS and gene body regions (**Figure 8E and 8F**). Super-loop connected genes have higher levels of Pol II binding and PRO-seq

signal (**Figure 6A; bottom right**)⁵³, and it suggests that the formation of super-loops may contribute to the recruitment and stabilization of Pol II at the TSS, leading to higher levels of transcription initiation and therefore a higher level of nascent RNA synthesis. Although the high signal at the TSS may contribute to a high pausing index, the gene body's enrichment in target genes connected by super-loops was sufficiently high to offset this effect, resulting in a low pausing index.

Remarkably, the analysis of the pausing index, based on PRO-seq signals, demonstrated that genes associated with super-enhancers exhibited decreased levels of transcriptional pausing when compared to those not associated with super-enhancers (**Figure 9A; bottom**)⁹⁷. I analyzed target genes to investigate the relationship between loop strength, pausing index, and RNA profiles, and found that as the strength of the loop increased, the RNA expression of the connected genes also tended to increase, as expected from PRO-seq and Pol II signals (**Figure 9B, C; Figure 8B, D**). Furthermore, When analyzing the biological processes associated with corresponding genes, I classified target genes of super-loops with low pausing indexes into T cell-specific gene ontologies, such as T cell activation and leukocyte cell-cell adhesion. On the other hand, genes with no loops or typical loops, which showed relatively high pausing indexes, were associated with general cell cycle regulation groups, such as ribosome biogenesis and mRNA processing (**Figure 10**). These results suggest that even in the absence of CTCF, super-enhancers and super-loops do not change significantly, and the expression of cell-specific target genes regulated by these factors is maintained quite robustly. This is consistent with previous reports that acute CTCF, Cohesin, and WAPL depletion minimally affect gene expression and enhancer-promoter interactions⁵³.

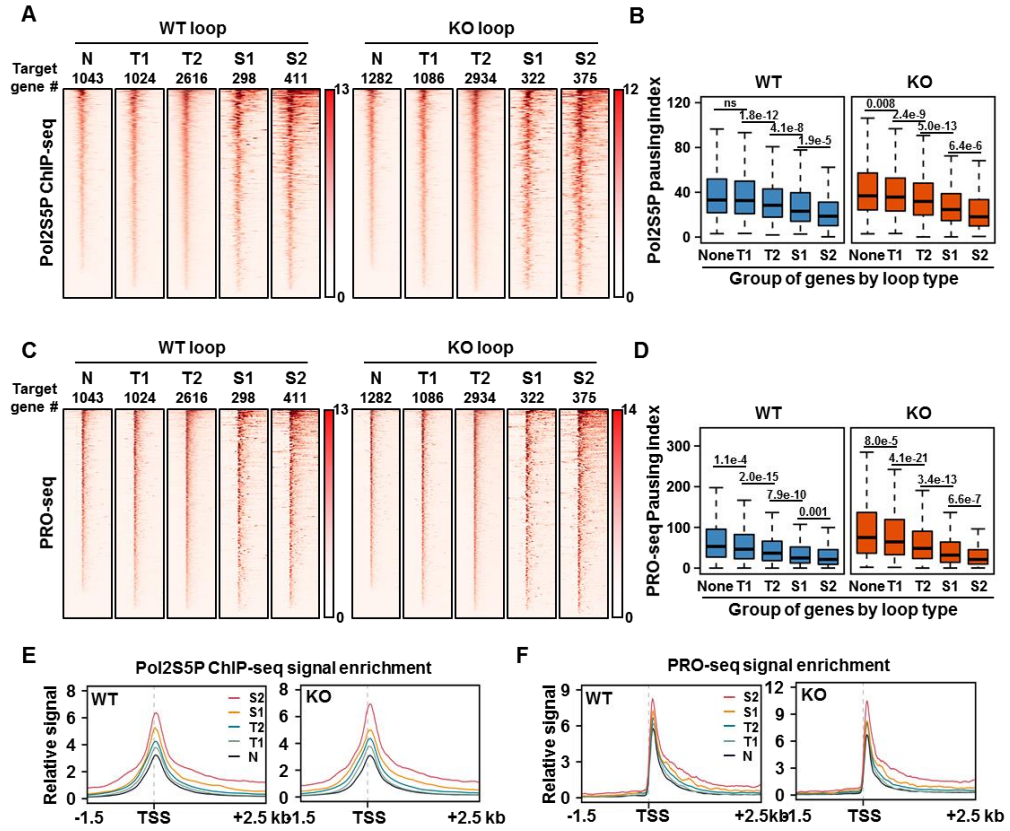


Figure 8. As the intensity of the loop increases, the pausing index decreases

(A) Heat map of ChIP-seq signals of Pol II (phosphorylated on CTD Serine 5) around the TSS regions based on loop strength, categorized by the presence or absence of CTCF. (B) Boxplot is utilized to display pausing index based on loop strength, categorized by the presence or absence of CTCF. Pausing index calculated by the signal enrichment of Pol II (phosphorylated on CTD Serine 5). (C) Heat map of PRO-seq signals (sense strand) around the TSS regions based on loop strength, categorized by the presence or absence of CTCF. (D) Boxplot is utilized to display pausing index based on loop strength, categorized by the presence or absence of CTCF. Pausing index calculated by the signal enrichment of PRO-seq. (E) Pol II phosphorylated on CTD Serine 5 (Pol2S5P) signal distribution profiles surrounding promoters in WT and KO according to each type of loops. (F) PRO-seq signal distribution profiles surrounding promoters in WT and KO according to each type of loops.

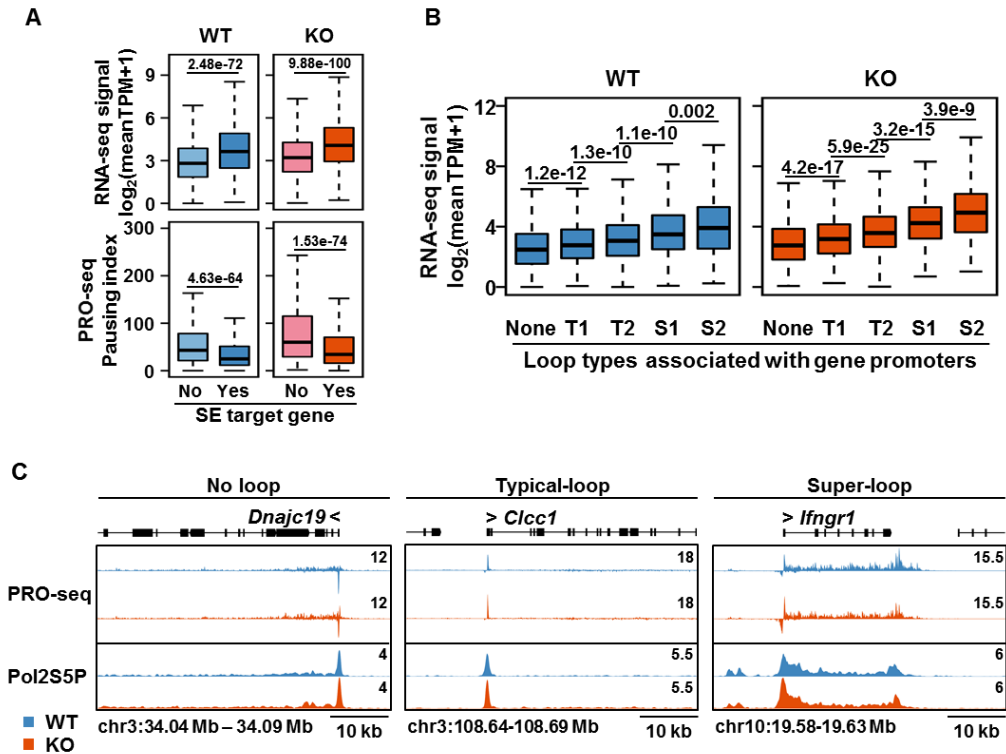


Figure 9. Robust enhancer loop formation is coupled to release of RNA Pol II pausing

(A) Protein coding genes, categorized by their association with super-enhancers, were scrutinized for both RNA expression (top) and pausing index (bottom). (B) Protein coding genes, categorized by the types of loops linked to gene promoters, were analyzed for both RNA expression (top) and pausing index (bottom). (C) Snapshot of signal tracks for PRO-seq, Pol II phosphorylated on CTD Serine 5 (Pol2S5P) is presented representative regions of genes that have no loop connected to their promoter, genes that have a typical loop connected to their promoter, and genes that have a super-loop.

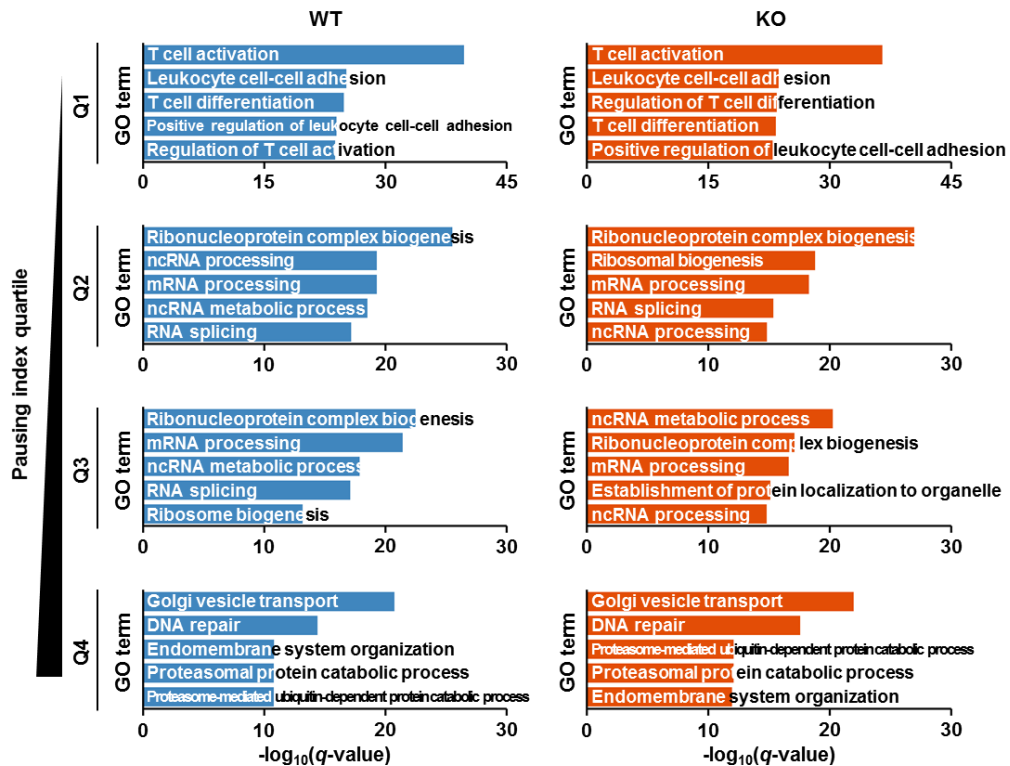


Figure 10. The establishment of robust enhancer loops is linked to the alleviation of RNA Polymerase II pausing

Protein coding genes, categorized into quartiles based on the pausing index in WT (left) and KO (right) CD4⁺ T cells, were scrutinized for the enrichment of gene ontology terms related to biological processes.

6. Super-loops are closely associated with the influence of epigenetic regulators.

CTCF, Cohesin, and architectural factors are involved in creating enhancer-promoter interactions, but their presence is not necessary to maintain these interactions. Once formed, various factors such as histone modifications, chromatin remodeling, DNA modification, and long non-coding RNAs may provide a "molecular memory" that is sufficient to sustain enhancer-promoter interactions and gene expression⁵³.

Enhancer RNAs (eRNAs), long non-coding RNAs originating from enhancers, are known to promote Pol II pause release⁹⁸. In line with these findings, the target genes were classified based on the strength of the loops they were connected to, and the regulatory sequences that corresponded to these genes were investigated (**Figure 11A**). While it is noteworthy that the number of genes influenced by super-enhancers increases when CTCF is absent, it suggests that a significant number of genes are still regulated by loops that do not include super-enhancers, indicating that super-enhancers may not fully explain this phenomenon. Notably, the majority of protein-coding genes featuring enhancer loops were linked to other genes through chromatin interactions between their promoters (**Figure 11A; bottom**).

Apart from enhancer interactions, another important consideration is the presence of promoter-promoter interactions. When considering all genes without taking into account the strength of loops, it was observed that more than 80% of genes possess promoter-promoter interactions (**Figure 11A; bottom**). This suggests that promoter-promoter interactions have significant explanatory power for gene regulation mechanisms. Furthermore, genes connected to typical loops have the highest portion of typical loops, while those connected to super-loops have the highest portion of super-loops, and promoter-promoter loops are proportional to the strength of the loops⁸⁸. When expression levels of genes connected by promoter-promoter loops in each anchor group, grouped by loop strength, were represented by PRO-seq signals, it was observed that strong loops also have high PRO-seq signals for both promoters (**Figure 11B**).

These findings indicate that active transcription events at distant enhancers, whether contributing to eRNA or protein-coding gene expression, can result in the swift alleviation of transcriptional pausing facilitated by robust enhancer loop formation.

Recent studies indicate that H3K4me3, associated with transcriptional start sites, regulates RNA Polymerase II (RNAPII) promoter-proximal pausing. Acute loss of H3K4me3 has been shown to increase RNAPII pausing⁹⁹. Consistent with these findings, all protein-coding genes in both WT and KO cells exhibited a negative correlation between H3K4me3 signals in promoter regions and the pausing index (**Figure 11C; left**). Remarkably, this negative correlation was most evident when genes were linked by strong enhancer loops (S2), in contrast to weaker loops (T1) or no connections (**Figure 11C**), emphasizing the pivotal role of enhancer loop strength in modulating the release of RNA Pol II pausing for the expression of cell identity genes in CD4⁺ T cells.

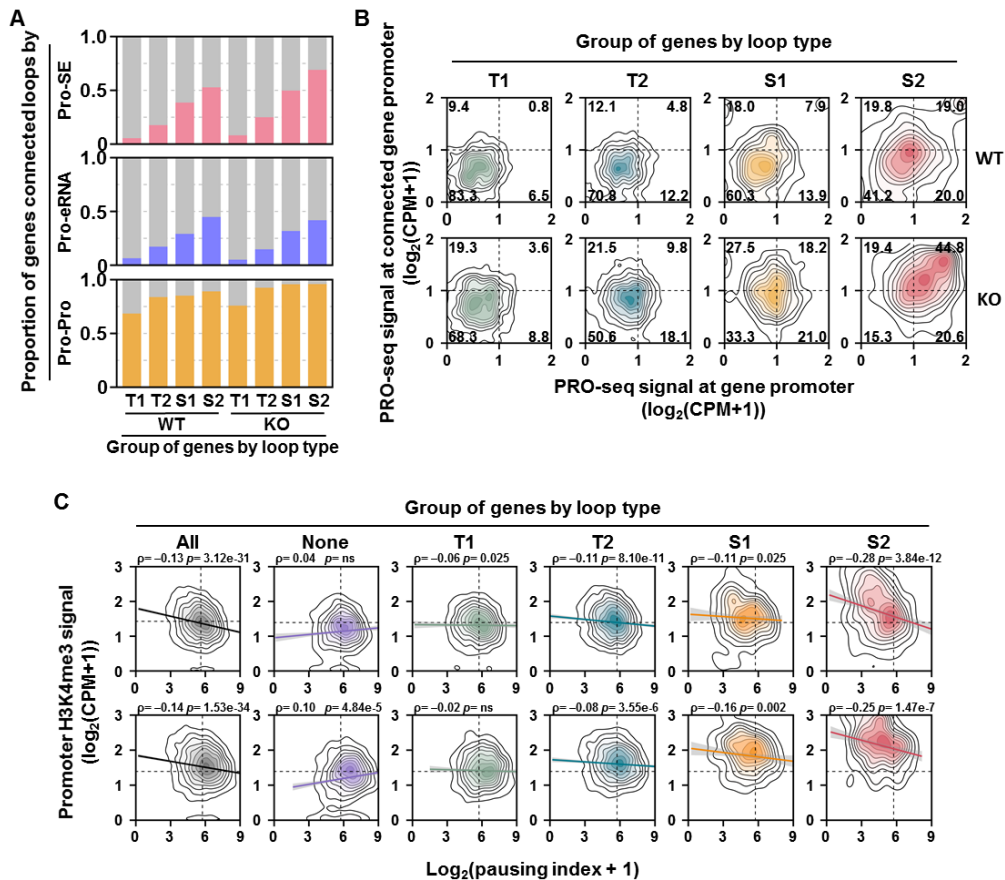


Figure 11. Loop formation determines the regulation of RNA Polymerase II pause-release

(A) Percentage of genes in each gene group with their promoters linked to super-enhancers (top), enhancer RNAs (middle), and promoters of other genes (bottom). (B) Contour plot representing the PRO-seq signal, converted to $\log_2(\text{CPM}+1)$, of the promoter of each gene present in each anchor of Pro-Pro loops. (C) Contour plots showing the correlations between pausing indices and H3K4me3 levels at the promoter regions of each gene group.

7. STAT5 is a transcription factor that represents the super-loop and super-enhancer in CD4⁺ T cells.

In DNA-to-DNA interactions, the presence of proteins to bind the two strands is inevitable. Therefore, to identify the transcription factor that can maintain the looping structure for consistent activation of CTCF-independent transcription, motif search analysis was conducted. I analyzed ATAC-seq peaks at the anchors of enhancer loops to explore transcription factor binding associated with enhancer loop formation. In WT cells, the CTCF motif exhibited the most substantial enrichment at all loop anchors, irrespective of loop strength, emphasizing its essential role in the creation of enhancer loops (**Figure 12A; left**). In KO CD4⁺ T cells, I noted an increase in transcription factors associated with immune cells, including NF- κ B and ETV4, at the anchors of typical loops (**Figure 12A**). Particularly noteworthy was the highest level of enrichment of the STAT5 motif at the anchors of stronger super-loops (S2) in KO cells (**Figure 12A; top right**). Furthermore, by comparing the accessible regions of the anchor with and without CTCF in the WT Super-loop, it was found that STAT5 motifs were also present in the anchor without CTCF (**Figure 12B**).

STAT5 is well known as a key transcription factor that regulates T cell immune responses as a master regulator of CD4⁺ T cells¹⁰⁰. The absence of CTCF and the presence of STAT5 in the anchor without CTCF suggest that cell type-specific regulators can perform an important role as auxiliary factors in maintaining the looping structure. This was also confirmed in motif search analysis of super-enhancer regions in WT and KO, where STAT5 motifs were consistently present, indicating the importance of STAT5 in regulating the cell type-specific function of super-enhancers in CD4⁺ T cells (**Figure 12C**). The activity of the STAT5 signaling pathway seemed to persist after CTCF depletion, as indicated by comparable levels of STAT5 phosphorylation and genome-wide STAT5 occupancy in KO CD4⁺ T cells (**Figure 12D**). Subsequently, the presence of STAT5 peaks in super-enhancers was confirmed

in WT and KO, and it was experimentally validated that STAT5 binds to almost all super-enhancers in CD4⁺ T cells (**Figure 12E**).

Significantly, I observed an augmented convergence of loop anchors with super-enhancers as the strength of the loops increased, with a more pronounced effect in KO cells compared to their WT counterparts. These results collectively demonstrate a strong correlation between STAT5-bound super-enhancers and the establishment of robust enhancer loops, especially in the absence of CTCF. This association is exemplified in the *Il4ra* and *Cish* loci (**Figure 13**).

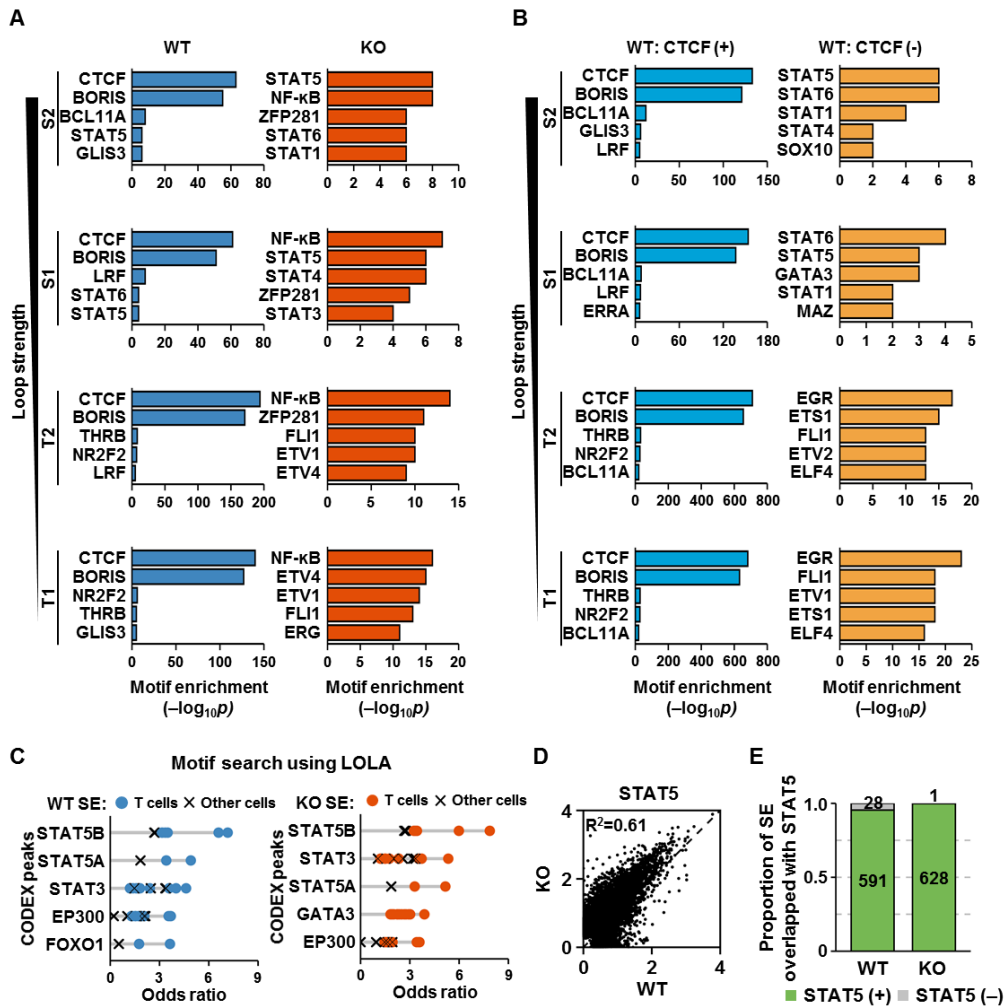


Figure 12. STAT5 is the most prominently identified transcription factor in both super-loops and super-enhancers of CD4⁺ T cells

(A and B) Transcription factor motif identification from ATAC-seq peaks in each group of loop anchors. (A) presents the results analyzed from WT and KO anchors in order of $-\log_{10}$ p-value, and (B) shows the results analyzed by dividing them based on the presence or absence of CTCF in the anchor in WT CD4⁺ T cells. (C) Graph representing the results of Locus Overlap Analysis (LOLA) on the accessible regions of super-enhancers in WT and KO, displayed by odds ratio. (D) Scatter plots of STAT5 ChIP-Seq signals from WT and KO CD4⁺ T cells. (E) Distribution showing the proportion of super-enhancers in WT and KO that contain STAT5 among all super-enhancers in WT and KO.

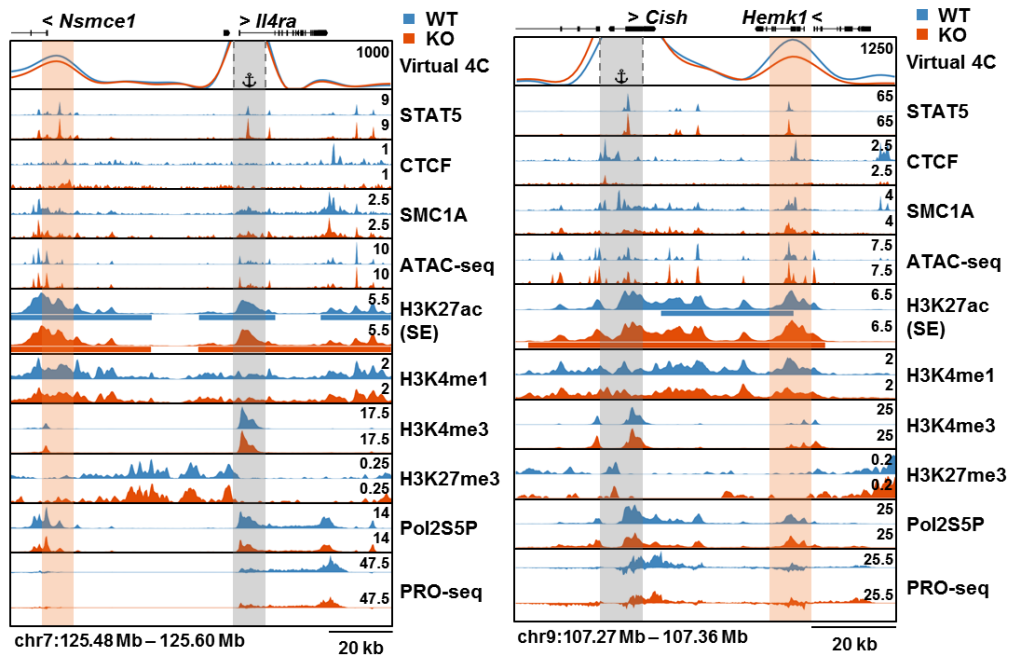


Figure 13. Promoter-promoter interaction and STAT5 are involved in gene regulation of super-loops

Snapshot is presented that displays various types of signals at representative regions, including virtual 4C plot, ChIP-seq, ATAC-seq, and PRO-seq signal tracks. The colors blue and red represent WT and KO, respectively, while the gray and orange vertical bar highlights the location of the promoter used as viewpoints. The ChIP-seq signal tracks show various factors such as STAT5, CTCF, SMC1A, Pol II phosphorylated on CTD Serine (Pol2S5P), H3K27ac, H3K4me1, H3K4me3, and H3K27me3. The snapshot also includes information on ATAC-seq, PRO-seq, and super-enhancer regions.

8. The proper expression of cell identity genes relies on CTCF, which governs the formation of enhancer loops.

So far, I have learned that CTCF is an important factor in forming loops, but at the same time, I have also looked into what factors can maintain the expression of important genes related to cell characteristics even in the absence of CTCF. At first glance, it may seem that CTCF does not have much influence on regulating gene expression in cells, but when focusing on changes in loops when CTCF is depleted, it becomes clear that this is not the case. Calculation of the differential loops reveals that a significant number of loops are created and disappear, with 10,233 loops newly formed and 8,870 loops disappearing (**Figure 14A**).

The physical proximity between distal enhancers and their target genes has been suggested to play a crucial role in controlling appropriate gene expression, as many enhancers are located quite far from the genes they regulate¹³. When the strength of the TAD boundary becomes weaker in KO, it is possible that the enhancer-promoter interaction, which was blocked by a strong TAD boundary in WT, could be newly established.

From this perspective, gained loops include more inter-TAD loops, which are formed beyond the existing TADs in WT, than lost loops (**Figure 14B**). Motif search results in lost and gained loops show that CTCF and STAT5 have the highest odds ratios in lost and gained loops, respectively (**Figure 14C**). This means that CTCF and STAT5 play a critical role not only in regulating loop strength and transcriptional activity, as confirmed in the super-loop analysis, but also in regulating newly formed and disappearing loops. When I examine the proportion of CTCF and STAT5 ChIP-seq data for loops at each condition's loop anchor, I can see that CTCF has a higher proportion in lost loops, and STAT5 has a higher proportion in gained loops compared to the opposite condition (**Figure 14D**). Depletion of CTCF had a more significant effect on super-loops than on typical-loops. In wild-type cells, over 40% of super-loops exhibited

decreased chromatin interactions, whereas in knockout cells, around one-third of super-loops were newly formed as a result of increased loop strength (**Figure 14E**). This indicates that loops that disappear when CTCF is depleted are mostly loops where CTCF was present at the anchor, and newly obtained loops are where STAT5 is present.

Many newly formed loops extend beyond the existing TADs, and considering that CTCF designs TAD boundaries, it is possible to predict that CTCF is present at TAD boundaries and observe the disappearance of the signal in CTCF KO (**Figure 15A**). The extent of the weakening of TAD boundaries can be expressed by subtracting the insulation score of WT from that of KO, the Δ insulation score (**Figure 15B**). To investigate whether CTCF can play a significant role in creating *de novo* loops, the number of CTCF peaks included in each loop was examined. Compared to other loops such as lost and constant loops, relatively more CTCF peaks were present within gained loops (**Figure 15C**). Based on these results, it can be concluded that the *de novo* loops formed in the CTCF KO are a result of the absence of CTCF, which would have served as a blocker according to the WT standard. Furthermore, the fact that the gained loop region has a high Δ insulation score, given that it represents a collapsed boundary, reinforces the conclusion that newly formed loops extend beyond the boundaries that existed in WT (**Figure 15D**). Through this series of results, it can be confirmed once again that CTCF is present in many TAD boundaries and that depletion of CTCF leads to merge TAD and show higher Δ insulation scores in these boundaries, emphasizing the importance of CTCF as a blocker in inhibiting interactions between TADs (**Figure 15E**).

These results collectively highlight the dual role of CTCF in the 3D enhancer network. CTCF preserves the strength of enhancer loops when located at loop anchors and, at the same time, prevents abnormal chromatin interactions by providing insulation when positioned between them.

In addition, the depletion of CTCF had a notable impact on the association between super-loops and their target genes: roughly half of the genes linked to super-loops in WT cells lost their connections (disrupted genes), while approximately half of the genes linked to super-loops in KO cells formed new connections following CTCF depletion (acquired genes) (**Figure 16A**). The genes that maintained their connections with super-loops, even in the absence of CTCF (preserved genes), might be facilitated by robust transcriptional activity at their loop anchors. Importantly, genes connected by super-loops in WT cells, whether these connections were preserved or disrupted due to CTCF depletion (preserved and disrupted genes, respectively), were predominantly associated with immune-related pathways (**Figure 16B; upper**). Conversely, genes in WT cells lacking connections to super-loops (acquired and unlinked genes) demonstrated a distinct inclination toward pathways linked to fundamental housekeeping functions, such as RNA metabolism (**Figure 16B; lower**). Interestingly, genes that established connections with super-loops due to CTCF depletion (acquired genes) were primarily linked to housekeeping functions rather than immune-related pathways (**Figure 16B; lower**).

These results imply that robust enhancer loops facilitate the connection between super-enhancers and cell identity genes. CTCF plays a pivotal role in this process by either preserving enhancer loop formation or hindering abnormal chromatin interactions to ensure the accurate pairing of super-enhancers with their target genes. Additionally, genes losing their super-loop connections due to CTCF depletion showed a significant decrease in RNA expression accompanied by an increase in transcriptional pausing (**Figure 16C, D**). In contrast, genes acquiring super-loop connections in CTCF-deficient cells exhibited elevated RNA expression and a decrease in transcriptional pausing (**Figure 16C, D**). This intricate interaction among super-loops, CTCF, and the control of transcriptional pausing highlights the essential role of 3D chromatin architecture in dictating gene expression patterns in CD4⁺ T cells.

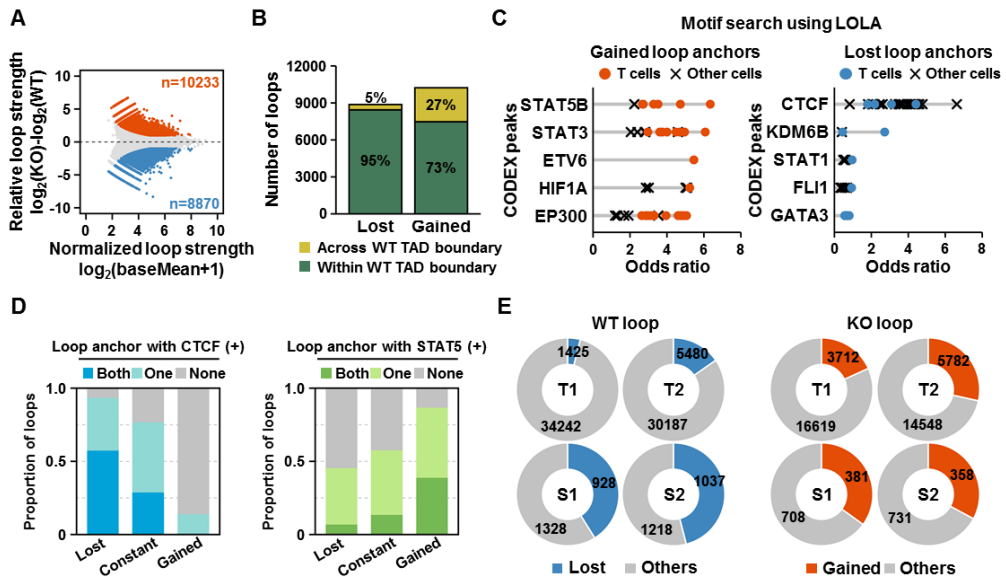


Figure 14. Differential loop analyses using H3K27ac HiChIP revealed genome-wide changes in enhancer loop strength following CTCF depletion

(A) MA plot showing significant changes in H3K27ac HiChIP loop strength. The number of loops exhibiting >2 -fold increases in CTCF WT (blue) or CTCF KO (red) CD4^+ T cells with an adjusted p -value <0.05 has been indicated. (B) Distribution showing the ratio of inter-TAD and intra-TAD loops among gained and lost loops in KO compared to WT. (C). Graph representing the results of Locus Overlap Analysis (LOLA) on the accessible regions among gained and lost loops in KO compared to WT, displayed by odds ratio. (D) Distribution that classifies the presence of CTCF (left) and STAT5 (right) on each anchor in gained loop, constant loop, and lost loop. The cases where both anchors have TF are classified as "both", the cases where only one side has them are classified as "One", and the cases where neither anchor has them are classified as "None". (E) Proportion of lost (left) or gained (right) loops within each loop type.

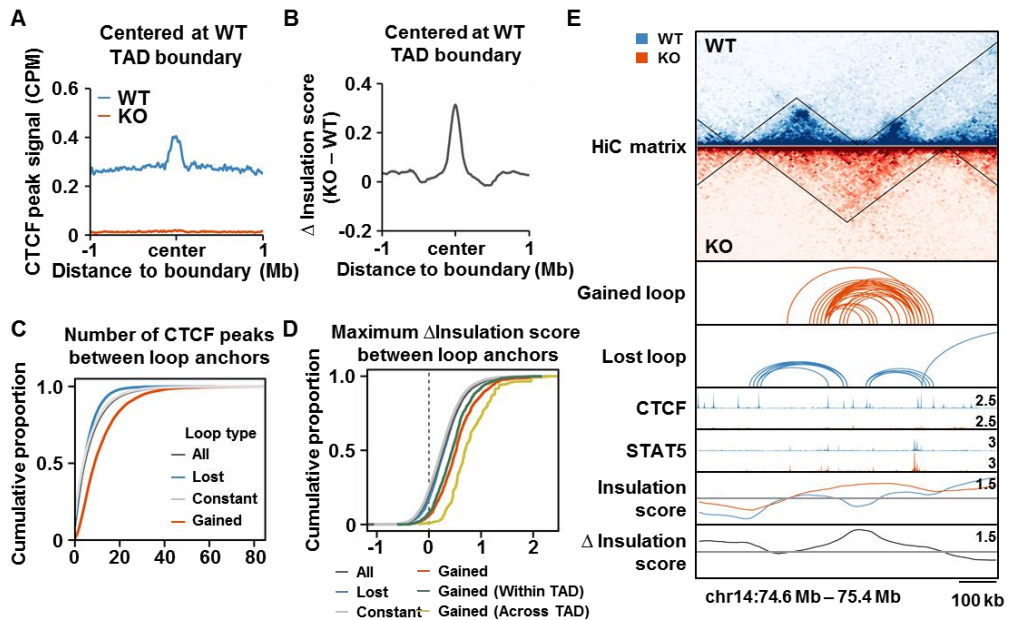


Figure 15. The significant role of CTCF in the maintenance of enhancer loop formation

(A) Line plot showing the comparison of CTCF peak signal between WT and KO based on WT TAD boundary. (B) Line graph depicting the variation in insulation score between WT and KO with reference to the TAD boundary of the WT. (C) cumulative plot shown the distribution of loops based on the number of CTCF peaks within the range of each loop type. (D) Cumulative proportion of the number of CTCF peaks between loop anchors within each loop type. (E) Snapshot displaying Hi-C contact map, arcs showing gained or lost H3K27ac loops, ChIP-seq signal tracks for CTCF and STAT5, insulation score, difference in insulation score between WT and KO (from top to bottom). The blue color represents WT and the red color represents KO.

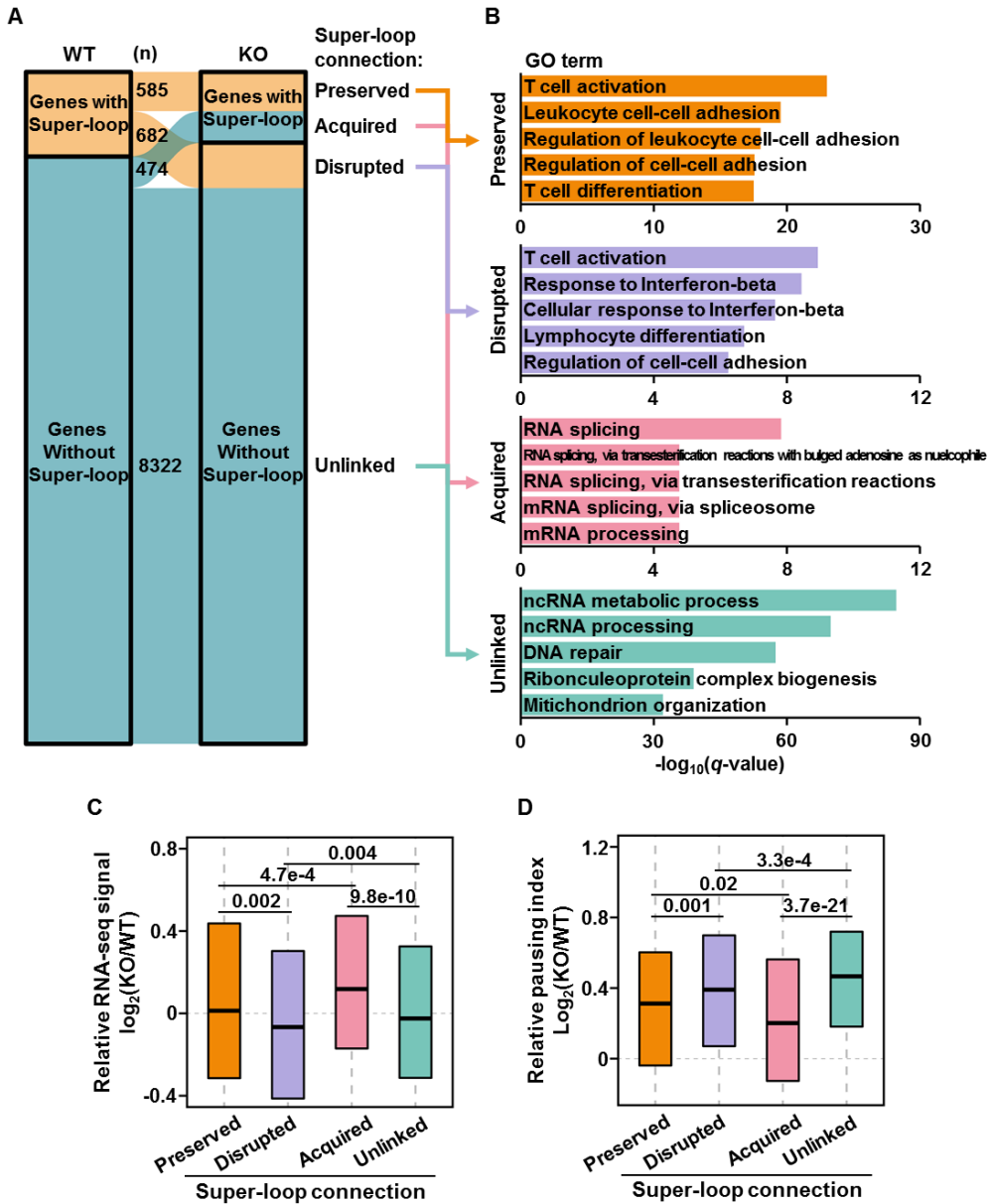


Figure 16. The rewiring of super-loops resulting from CTCF depletion is associated with alterations in both gene expression and the pausing of RNA Pol II

(A to D) Protein coding genes, categorized based on alterations in the connection of super-loops to their promoters (A), were analyzed for the enrichment of gene ontology terms related to biological processes (B), as well as for RNA expression (C) and pausing index (D).

9. The rewiring of the STAT5 enhancer network resulting from CTCF depletion alters the response to the JAK inhibitor.

If CTCF depletion contributes to the formation of gained and lost loops, changes in gene expression resulting from such changes in the 3D structure are likely to be mediated by transcription factors present in the enhancer. Based on the results of a series of analyses, STAT5 is expected to be a regulator that plays such a role (**Figure 12C, 14C**). Therefore, to verify the potential impact of STAT5 on gene expression in CTCF KO CD4⁺ T cells, an inhibitor experiment was conducted using tofacitinib, an oral Janus kinase inhibitor used for the treatment of psoriatic arthritis¹⁰¹, rheumatoid arthritis¹⁰², and ulcerative colitis¹⁰³. Tofacitinib results in a decrease of phosphorylation required for STAT5 activity by inhibiting the phosphorylation of JAK kinase^{4,104}. While maintaining the overall experimental design, tofacitinib and IL-2 were treated four hours prior to obtaining the sample (**Figure 17A**). Western blot analysis confirmed the significant decrease in STAT5 phosphorylation caused by tofacitinib (**Figure 17B**). As STAT5 target genes are expected to be affected when STAT5 activity decreases, RNA-seq and STAT5 ChIP-seq, as well as H3K27ac HiChIP data that reveal enhancer-promoter interactions, were used to finally identify STAT5 target genes in CD4⁺ T cells (**Figure 17C**). The resulting target genes included 669 in WT and 1,147 in KO, and it was confirmed that CD4⁺ T cell gene expression is regulated in various ways, such as cases where STAT5 is present only in the promoter, only in the enhancer, or in both (**Figure 17D**).

To investigate this, I examined changes in the RNA expression of STAT5 target genes after CTCF depletion (**Figure 18A**) and their correlation with modifications in chromatin interactions with STAT5-bound distal enhancers (**Figure 18B**). Following CTCF depletion, 67 STAT5 target genes showed upregulation, among which 51 displayed STAT5 loop gain (**Figure 18C; upper right**), while 69 STAT5 target genes

exhibited downregulation, with 15 of them experiencing STAT5 loop loss (**Figure 18C; lower right**).

Remarkably, modifications in the RNA expression of STAT5 target genes following CTCF depletion were noted in conjunction with adjustments in transcriptional pausing (**Figure 18D**). However, this correlation was most prominent when changes in loop strength occurred between STAT5-bound distal enhancers and promoters (**Figure 18D**). Then, two potential regulatory mechanisms are proposed by which CTCF depletion affects gene expression by disrupting 3D chromatin structure: (i) the absence of insulator CTCF initiates the formation of chromatin interactions connecting STAT5-bound distal enhancers to target genes, thereby enhancing their expression (**Figure 18E; left**); and (ii) the depletion of enhancer facilitator CTCF disrupts chromatin interactions between STAT5-bound distal enhancers and target genes, consequently reducing their expression (**Figure 18E; right**).

These findings demonstrate that the impact of CTCF depletion on the sensitivity of CD4⁺ T cells to JAK inhibitors is mediated through the rewiring of the STAT5 enhancer network, rather than by modifying the JAK/STAT signaling pathways.

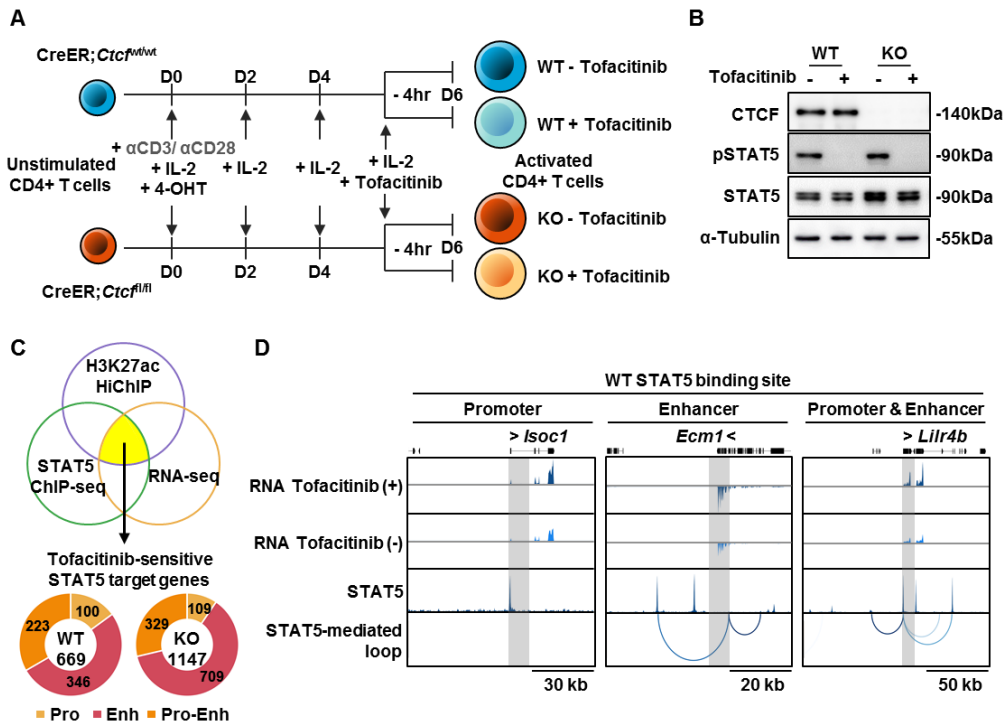
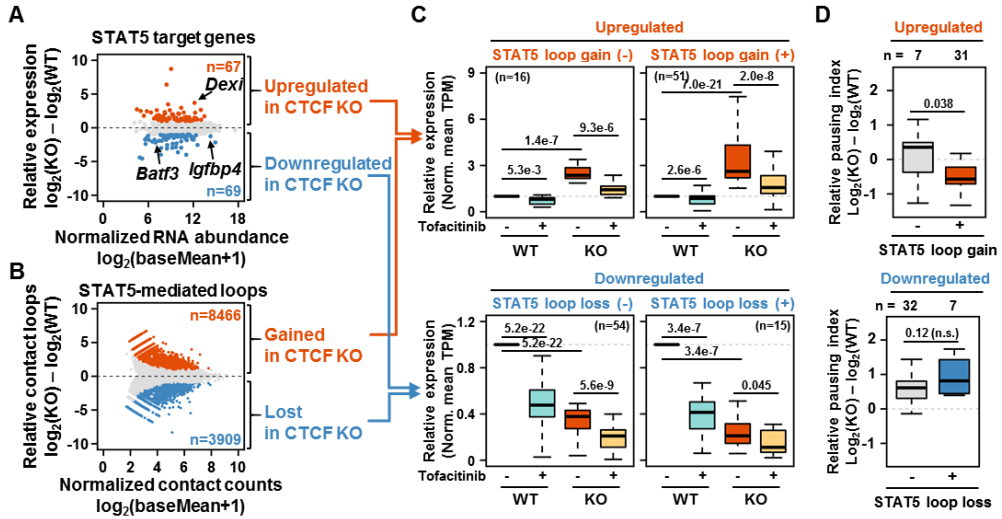


Figure 17. Inhibiting the phosphorylation of STAT5 induced by tofacitinib experiment reveals STAT5 target genes

(A) Scheme illustrating an experiment designed to reduce STAT5 activity by treating with tofacitinib. (B) The validation of the effectiveness of tofacitinib in inhibiting phospho STAT5 through measurement of protein levels. (C and D) Strategies (C) for discovering genuine STAT5 target genes in CD4⁺ T cells and representative genome tracks (D) of genes based on the type of connection, including RNA-seq, STAT5 ChIP-seq, and STAT5-mediated loops.



E

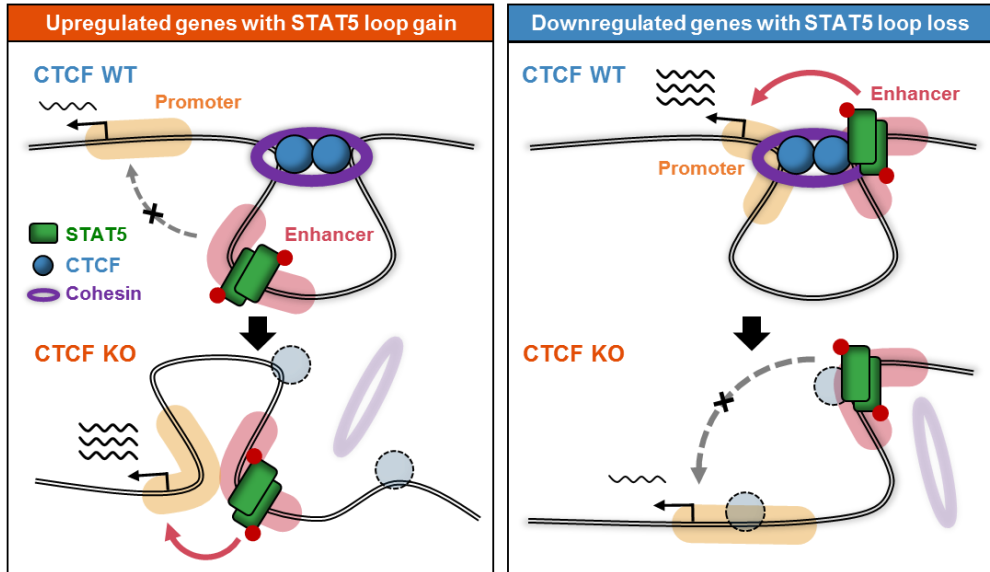


Figure 18. The modified STAT5 enhancer network resulting from CTCF depletion brings about changes in the efficacy of a JAK inhibitor

(A and B) MA plot represents the gene expression profile of STAT5 target genes (A) and STAT5-mediated loops (B) that are influenced by CTCF KO. The number of genes with >2-fold increase in wild-type (blue) or knockout (red) with an adjusted p-value <0.05 is shown. (C) Box plot (top right) representing the normalized transcripts per million (TPM) of target genes with increased gene expression linked to gained in CTCF knockout and box plot (bottom right) representing the normalized TPM of target genes with decreased gene expression linked to disappeared loops in CTCF knockout. The left bar graph illustrates the results tracking changes in loop-independent STAT5 target genes. (D) STAT5 target genes, whether exhibiting upregulation (top) or downregulation (bottom), were categorized according to the acquisition or loss of STAT5 loops, and subsequently assessed for changes in the pausing index. (E) Diagram depicting the function of CTCF in inhibiting (left) or promoting (right) chromatin interactions between promoters and distant enhancers bound by STAT5.

10. CTCF functions both as an enhancer blocker and facilitator, overseeing the precise targeting of STAT5.

Next, an experiment was devised to remove STAT5 binding in the enhancer using the CRISPR system (**Figure 19A**), to verify whether STAT5 in the enhancer of the looping structure that changes depending on the presence or absence of CTCF can actually have a significant impact. As CTCF acts as an insulator, the chromatin landscape surrounding *Dexi* among the 56 newly identified target genes of STAT5 was examined when CTCF was depleted. The *Dexi* gene encodes a dexamethasone-induced protein and has implications in the pathogenesis of type 1 diabetes mellitus and other autoimmune diseases¹⁰⁵⁻¹⁰⁷. It was found that there is a super-enhancer that controls the *Socs1* gene (**Figure 19B**). The super-enhancer of *Socs1* contains multiple STAT5 binding sites, and when a virtual 4C graph was created based on *Dexi*, it was confirmed that the interaction signal with the STAT5 binding site immediately upstream of the *Socs1* promoter increased significantly in CTCF KO. On the other hand, when a virtual 4C profile was created based on the STAT5 binding site, it was observed that the interaction with *Dexi* increased while the interaction with CTCF between them decreased in CTCF KO. From this, it can be inferred that the increase in *Dexi* in CTCF KO is due to the super-enhancer of *Socs1*, especially a specific STAT5 binding playing an important role. The gamma interferon activation site (GAS) element is well known as a motif of STAT proteins¹⁰⁸, so I used CRISPR to target two GAS motifs in that STAT5 binding site.

The T7E1 mismatch detection assay is commonly used to evaluate the effectiveness of site-specific nucleases¹⁰⁹. If a CRISPR-induced mismatch occurs at the intended site, a fragmented product smaller than the normal size is observed, and the assay results indicate that deletion of the STAT5 binding site has been effectively applied (**Figure 19C**). Furthermore, cloning and Sanger sequencing of the genome region induced with STAT5 binding deletion were performed to confirm that the mutation occurred properly. I obtained STAT5 binding site deletion samples with an average efficiency of about 70%

(**Figure 19D**). I noticed a significant alteration in transcriptional pausing at the *Dexi* promoter due to the establishment of a super-loop connecting the STAT5-bound super-enhancer, which differed from the minimal impact on enhancer looping observed at the *Socs1* and *Usp1* promoters following CTCF depletion (**Figure 19E**). The STAT5 target gene *Socs1* in WT CD4⁺ T cells decreased in response to tofacitinib regardless of the presence or absence of CTCF, but *Dexi* did not show any influence in WT CD4⁺ T cells as it was not a target of STAT5. However, when CTCF was depleted, the increased expression of *Dexi* was observed to be suppressed by tofacitinib (**Figure 19F**), indicating that *Dexi*, which was originally not affected by STAT5, became affected in CTCF KO. This suggests that STAT5 plays an important role in regulating the target gene through the enhancer in CD4⁺ T cells. The same results were obtained in the qRT-PCR experiment conducted after removing the STAT5 binding site in the enhancer (**Figure 19G**).

After the previous experiment confirmed role of STAT5 in new looping structures resulting from the loss of CTCF's function as an insulator, I aimed to investigate the role of STAT5 in cases where CTCF directly facilitates interaction between enhancers and promoters. Among 15 candidate genes that were STAT5 target genes in WT CD4⁺ T cells but lost interaction with STAT5 due to CTCF deletion, *Igfbp4* was selected as a candidate (**Figure 18C; lower right**). Examination of the surrounding region of the *Igfbp4* gene revealed an anchor where CTCF and STAT5 coexist in a distal super-enhancer region and strongly interact with the *Igfbp4* promoter (**Figure 20A**). Furthermore, when CTCF was depleted, there was little change in interaction with other nearby genes, but a significant decrease in interaction with *Igfbp4* was confirmed. Therefore, this case appears to be a situation where CTCF directly connects distal enhancer STAT5 to gene promoters to regulate expression, and I induced deletion of the GAS motif in the STAT5 binding site in the enhancer. T7E1 assay and Sanger sequencing are conducted as in the previous experiment, and sufficient mutation is

confirmed in the GAS motif (**Figure 20B and 19C**). The targeted disruption of the super-loop linking the *Igfbp4* gene and super-enhancer, induced by CTCF depletion, led to a heightened pausing index and reduced RNA expression specifically for the *Igfbp4* gene, while the pausing index and RNA expression for the *Top2a* and *Ccr7* genes showed less pronounced effects (**Figure 20D**). As seen in the RNA-seq results treated with tofacitinib, *Igfbp4* is affected by STAT5 inhibition, and it is significantly decreased compared to other nearby genes that are not significantly affected by CTCF KO (**Figure 20E**). The qRT-PCR results after the STAT5 binding mutation also showed that while other genes did not show a statistically significant difference, the expression of *Igfbp4* was significantly decreased (**Figure 20F**). The fact that the expression of the target gene decreased means that STAT5 plays a crucial role in the enhancer-promoter regulation mechanism of CD4⁺ T cells.

Then, I focused on the enhancer of *Batf3* to see if I could obtain the same conclusion by only removing the loop connected to the promoter while maintaining STAT5 in place (**Figure 21A**). When *Batf3* enhancer was analyzed using virtual 4C, it was found that the STAT5-mediated enhancer connected by CTCF was targeting *Batf3* more selectively than the surrounding genes, and a significant decrease in interaction with *Batf3* was observed when CTCF was depleted.

CTCF deletion was induced using two guide RNAs targeting the motif. As in previous experiments, the KO efficiency was confirmed, and a mutation rate of over 80% was observed (**Figure 21B and 20C**). When examining the RNA-seq results of surrounding genes, including *Batf3*, treated with tofacitinib, it was observed that *Batf3* and *Atf3* were affected by tofacitinib (**Figure 21D**). By specifically targeting the CTCF binding site of the enhancer and inducing specific deletion, only *Batf3* showed a significant decrease in expression, as seen in the qRT-PCR results (**Figure 21E**). This suggests that CTCF present on the enhancer in CD4⁺ T cells plays a role in helping to apply STAT5 activity to target genes, and it is precisely arranged to avoid affecting genes other than the target.

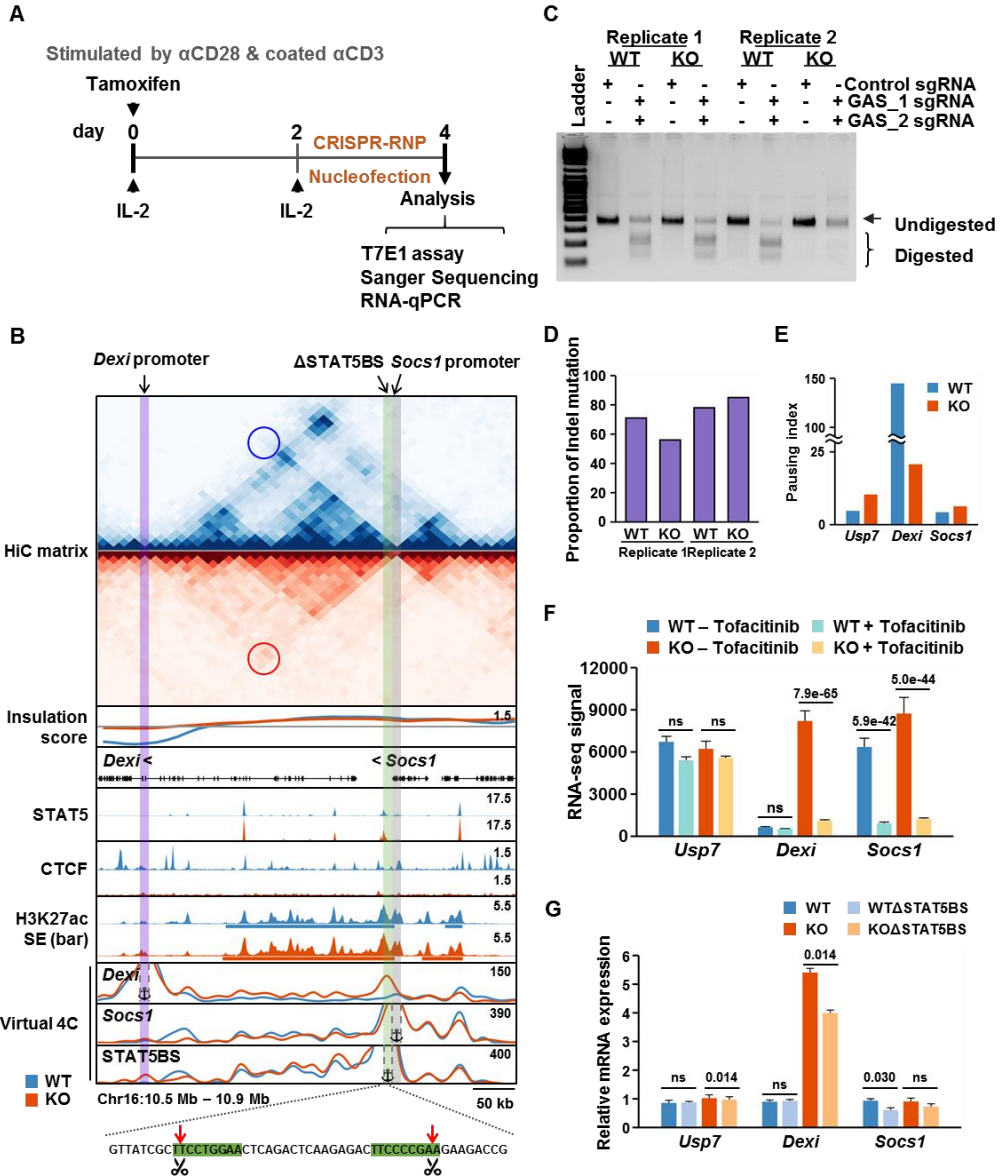


Figure 19. Established chromatin interaction between the super-enhancer bound by STAT5 and the *Dexi* promoter following CTCF depletion

(A) Scheme of the experimental design for editing TF binding sites through CRISPR/RNP nucleofection. (B) Snapshot showing Hi-C contact map, insulation scores, ChIP-seq signal tracks and virtual 4C plot (from top to bottom) at the *Dexi* locus. Blue color represents WT and red color represents KO. ChIP-seq signal tracks show STAT5, CTCF, H3K27Ac, and super-enhancer region information. Purple vertical bar highlights the location of *Dexi* promoter, green vertical bar highlights the location of STAT5 binding site of enhancer, and gray vertical bar highlights the location of *Socs1* used as viewpoints. (C) Results of the T7E1 mismatch detection assay for the CRISPR experiment targeting the STAT5 binding site of the enhancer connected to *Dexi*. (D) Distribution plot that summarizes the level of mutation in the target site from the results of the CRISPR experiment, based on sequencing results from at least 17 samples or more. (E) Changes in pausing indices for the indicated genes upon CTCF depletion. (F) Graph showing the expression of *Dexi* and surrounding genes in DESeq2 normalized count, based on RNA-seq data treated with tofacitinib. The statistical significance of differences between measurements was determined by two-side Wald test by the `nbinomWaldTest` function in DESeq2. (G) qRT-PCR results were obtained with the target STAT5 binding site edited in both WT and KO. The statistical significance of differences between measurements was determined by a one-sided Wilcoxon rank-sum test.

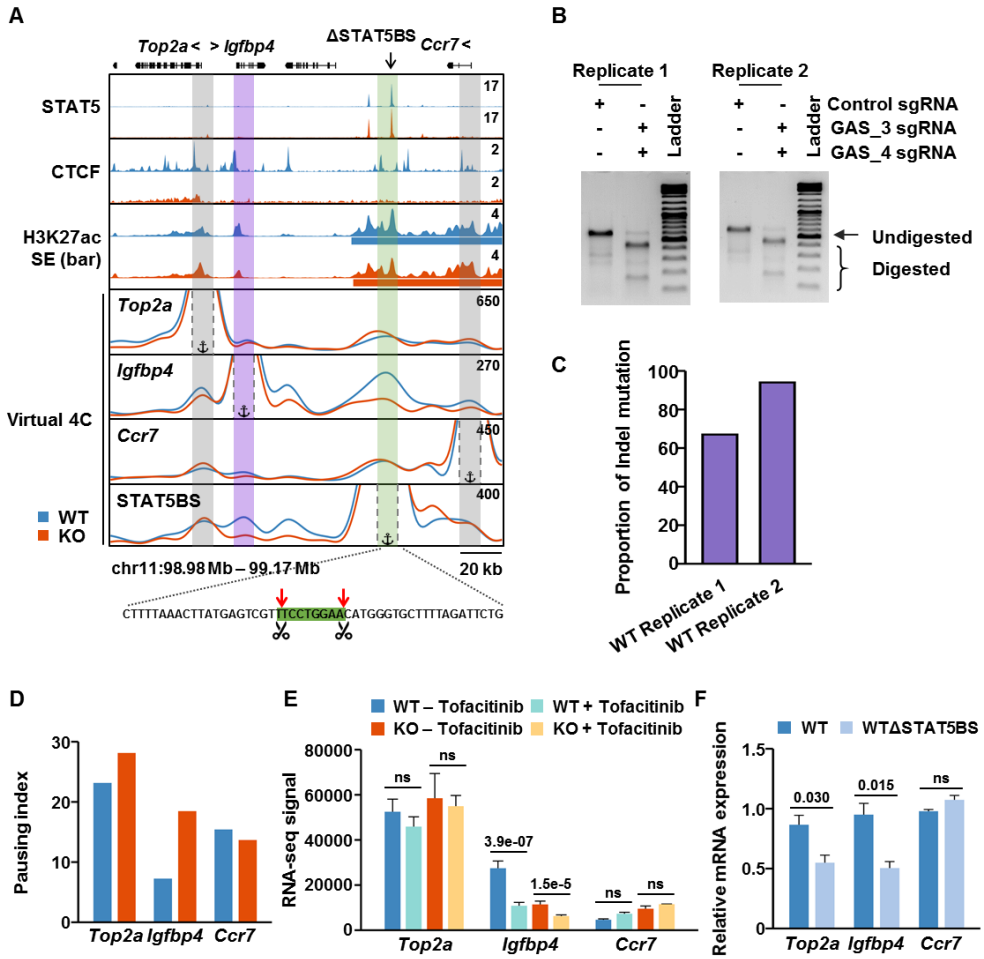


Figure 20. The chromatin interaction between the super-enhancer bound by STAT5 and the *Igfbp4* promoter is disturbed following CTCF depletion

(A) Snapshot showing ChIP-seq signal tracks and virtual 4C plot at the *Igfbp4* locus. Blue color represents WT and red color represents KO. ChIP-seq signal tracks show STAT5, CTCF, H3K27Ac, and super-enhancer region information. Purple vertical bar highlights the location of *Igfbp4* promoter, green vertical bar highlights the location of STAT5 binding site of enhancer, and gray vertical bar highlights the location of other genes' promoter used as viewpoints. (B) Results of the T7E1 mismatch detection assay for the CRISPR experiment targeting the STAT5 binding site of the enhancer connected to *Igfbp4*. (C) Distribution plot that summarizes the level of mutation in the target site from the results of the CRISPR experiment, based on sequencing results from at least 16 samples or more. (D) Changes in pausing indices for the indicated genes upon CTCF depletion. (E) Graph showing the expression of *Igfbp4* and surrounding genes in DESeq2 normalized count, based on RNA-seq data treated with tofacitinib. The statistical significance of differences between measurements was determined by two-side Wald test by the `nbinomWaldTest` function in DESeq2. (F) qRT-PCR results were obtained with the target STAT5 binding site edited in both WT and KO. The statistical significance of differences between measurements was determined by a one-sided Wilcoxon rank-sum test.

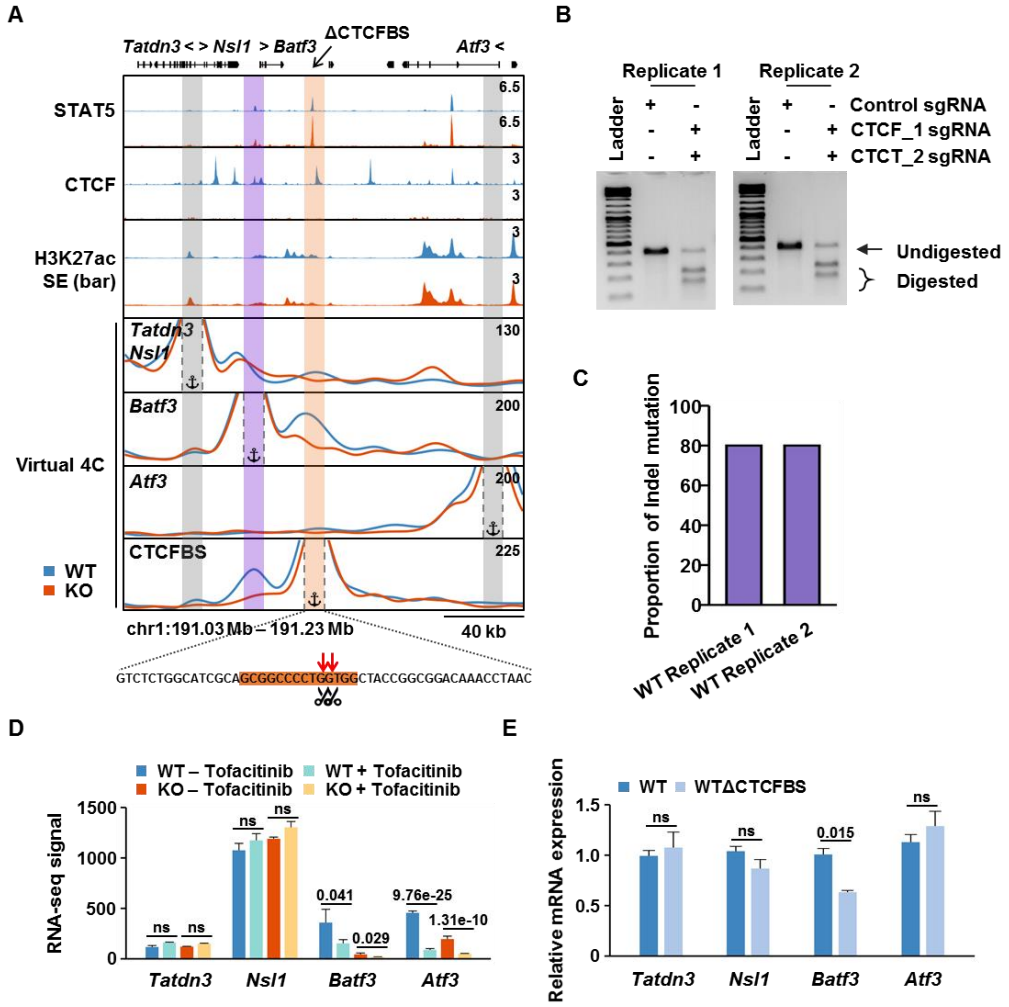


Figure 21. The chromatin interaction between the super-enhancer bound by STAT5 and the *Batf3* promoter is perturbed following CTCF depletion

(A) Snapshot showing ChIP-seq signal tracks and virtual 4C plot at the *Batf3* locus. Blue color represents WT and red color represents KO. ChIP-seq signal tracks show STAT5, CTCF, H3K27Ac, and super-enhancer region information. Purple vertical bar highlights the location of *Batf3* promoter, green vertical bar highlights the location of CTCF binding site of enhancer, and gray vertical bar highlights the location of other genes' promoter used as viewpoints. (B) Results of the T7E1 mismatch detection assay for the CRISPR experiment targeting the CTCF binding site of the enhancer connected to *Batf3*. (C) Distribution plot that summarizes the level of mutation in the target site from the results of the CRISPR experiment, based on sequencing results from at least 18 samples or more. (D) Graph showing the expression of *Batf3* and surrounding genes in DESeq2 normalized count, based on RNA-seq data treated with tofacitinib. The statistical significance of differences between measurements was determined by two-side Wald test by the `nbinomWaldTest` function in DESeq2. (E) qRT-PCR results were obtained with the target CTCF binding site edited in both WT and KO. The statistical significance of differences between measurements was determined by a one-sided Wilcoxon rank-sum test.

IV. DISCUSSION

Enhancers, activating genes over long genomic distances, are frequently situated close to their target genes in the 3D chromatin¹¹⁰. This proximity suggests enhancer looping, where enhancers physically interact with promoters, establishing loops that skip intervening regions. The organization of interphase chromosomes plays a crucial role in governing gene expression and maintaining the genome¹¹¹. Recent studies on enhancer establishment have uncovered that DNA often facilitates cooperativity between TFs, even in the absence of direct contact between the TF proteins. For instance, GATA1¹¹² and TAL1¹¹³ play crucial roles as transcription factors in the processes of hematopoiesis and erythropoiesis. Moreover, there are TF families in humans, such as AP-1, NF-Y, and E2F family, which form protein-level dimers in solution¹¹⁴. Phosphorylation of STAT proteins is required for the formation of their respective dimeric forms that bind to DNA¹¹⁵.

Various types of factors are known to establish and regulate the 3D genome structure between enhancer complexes and target genes. YY1, a zinc-finger family transcription factor, has the capability to either activate or suppress a diverse range of genes. YY1 engages with active enhancers and elements proximal to promoters, creating dimers that enhance the interaction between these DNA elements¹¹⁶. YY1 knockdown resulted in decreased intra-chromosomal interactions between the Th2 LCR and the IL4 promoter, indicating the involvement of YY1 in this regulatory process¹¹⁷. SATB1 showed considerable similarity to the widely expressed factor YY1. Regulatory chromatin loops controlled by SATB1 constitute a finer level of genome organization established on a higher-order scaffold facilitated by CTCF and other factors¹¹⁸.

It is well-known that CTCF is important as a TAD boundary. However, recent studies suggest that even in the absence of CTCF, there may not be significant changes in the overall gene expression pattern of the cell⁵³. In other words, there are arguments suggesting that CTCF, especially from the perspective of E-P interactions, does not have

a major impact on target gene expression. Depleting conventional genome organizers like CTCF or cohesin led to significant deregulation of TADs without causing a substantial alteration in gene expression¹¹⁹. In contrast, depleting SATB1 did not result in significant changes in higher-order chromatin organization, but a notable shift in the transcription profile was observed within the unaffected TADs, specifically in promoter-enhancer interactions¹¹⁸.

Furthermore, even enhancers with strong activity may behave as if they are not affected by CTCF insulation¹²⁰. However, conflicting studies, particularly emphasizing the significance of CTCF in the vicinity of promoters, are present^{85,121,122}. These differing viewpoints suggest that the mechanisms related to CTCF are not straightforward and require further clarification.

Through experiments involving CTCF depletion in CD4⁺ T cells, it was confirmed that approximately half of the loops exist in the absence of CTCF, represented by H3K27ac HiChIP (**Figure 5D**). In CTCF-independent anchors, STAT5, the master regulator of T cells, was identified and proposed to play a role in maintaining enhancer loops (**Figure 12A**), contrary to the previously suggested TF affinity model⁵³. However, as reported earlier, CTCF-mediated chromatin looping serves as a crucial prerequisite for the formation of phase-separated transcriptional condensates¹²³. From this perspective, comprehensive investigation into the approximately half of the loops that decrease with CTCF knockout is imperative (**Figure 5A**). These findings suggest that CTCF, beyond its boundary function, may also participate in looping mechanisms that impact gene expression.

Enhancer activity is closely related to target gene expression, and it has been reported that the pausing index of genes connected to super-enhancers tends to decrease more than those connected to typical enhancers⁹³. In other words, as enhancer activity increases, there is a tendency for the release of pol II at the target gene to be more effective. Furthermore, super-enhancers are known to have stronger loop strength

compared to typical enhancers¹²⁴ and are crucial for late-point loop formation¹²⁵. Our experimental results align with previous research findings, indicating that the loops mediated by super-enhancers tend to be maintained even in the absence of cohesin, and our experiments confirm that CTCF depletion does not impact super-enhancer activity (**Figure 7B, E**), consistent with existing studies that suggest cohesin-independent loops have a low CTCF component¹¹⁹.

Transcription is an intricate process, not a straightforward event, encompassing a variety of transcription factors focused on Pol II. Delving into the basics, a comprehensive understanding of transcription begins by exploring the pre-initiation complex (PIC), a crucial point in eukaryotic transcription regulation. The formation of PIC represents a major bottleneck in transcriptional activation and hinges on a group of general transcription factors (GTFs) essential for Pol II's initiation of promoter-specific transcription¹²⁶. Chromatin remodeling is essential for both preinitiation complex assembly and transcription initiation and elongation¹²⁷, with predicted factor contacts from the stepwise model confirmed through structural studies¹²⁸. At the extreme end of the model spectrum, co-immunoprecipitation studies in yeast and mammals suggest the arrival of an RNA Pol II "holoenzyme", including multiple GTFs, Mediator, and often other co-activators, at the promoter as a pre-assembled complex¹²⁹. A recent hypothesis of branched pathways proposes that Pol II and basal transcription factors TFIIF and TFIIE preassemble on UAS/enhancer-bound activators, ready for loading into initiation complexes, with TFIIF at the core promoter¹³⁰. Transcription activators kinetically enhance factor recruitment, forming a localized cluster of polymerases at the UAS/enhancer. Loops are believed to play a crucial role in transferring this PIC complex.

Even if this hypothesis suggests another plausible mechanism independent of phase separation, the significance of the super-loop proposed in this paper remains unchanged. This is because, even though the CTCF depletion does not alter the super-enhancer repertoire, the super-loop undergoes significant changes. Interestingly, a higher

proportion of super-loops was affected by CTCF depletion compared to typical loops. (**Figure 14E, 16A**). Considering the research suggesting that intragenic interaction affects target gene elongation¹³¹, we anticipated that changes in loop strength due to CTCF could sufficiently alter the pausing pattern of target genes, and indeed, we observed a corresponding change in the pausing index (**Figure 16D**). Particularly, these results were centered around the crucial STAT5-mediated function, one of the most important signaling pathways in CD4⁺ T cells, highlighting that CTCF deletion can impact even immunologically significant genes (**Figure 18A-D**). These findings suggest that the super-loop supervises the impact of enhancer activity on the promoter and the control of Pol II pause-release (**Figure 22**).

Emphasizing the significance, disruptions in transcriptional regulation within lymphocytes can have adverse effects on the development of immune cells, as observed in conditions like cancers, immune-deficiencies, and autoimmune disorders¹³². Moreover, the previously recognized 3D genome folding influences immune cell activation, differentiation, and dysfunction through the regulation of gene expression¹³³. In particular, the widely recognized V (D) J recombination commences with the formation of a protein complex involving the recombination activating gene 1 (RAG1) and recombination activating gene 2 (RAG2) within recombination centers, where gene segments become available to the complex¹³⁴. The orientation of CTCF binding sites in the V region is forward, while reverse-oriented CTCF binding sites surround the recombination center. The compacted structure, facilitated by cohesin-mediated loop extrusion constrained by convergent CTCF sites, is expected to enhance the interaction of D/J recombination signal sequences (RSSs) bound to RAG¹³⁵. The requirement for cohesin–CTCF-dependent loop extrusion in V(D)J recombination is demonstrated by the observed elimination of V(D)J recombination in a pro-B cell model upon cohesin inactivation¹³⁶. Besides, research on factors that can contribute to regulating the structural functions of CTCF in immune cells is also noteworthy. The essential

transcription factor, basic leucine zipper TF activating transcription factor-like (BATF), required for the development of Th17 and follicular helper T cell (Tfh) cells, engages CTCF in the establishment of chromatin loops at lineage-specifying gene loci¹³⁷. This process contributes to the transcriptional programming of diverse effector T cells.

As a result, the importance of approaching the responsiveness of target cells to drugs from the perspective of the 3D genome has also been emphasized¹³⁸⁻¹⁴⁰. Immune disorders often involve disturbances in gene expression resulting from changes in 3D architecture¹³³, which can manifest in several scenarios. The alteration of non-coding sequences obstructs the binding of transcription factors or loop extrusion proteins, leading to changes in the conformation of the 3D genome and disruptions of transcriptional regulation. A case in point is the presence of single nucleotide polymorphisms (SNPs) in non-coding regions that interact with tumor necrosis factor alpha-induced protein 3 (TNFAIP3), which hinders transcription factor binding and disturbs 3D chromatin structure in human CD4⁺ T cells¹⁴¹. Meanwhile, alterations in genes encoding chromatin modifiers can modify their function and disrupt the organization of the 3D genome. For instance, SATB1, linked to T-cell development, exhibits deficiency-related autoimmune and inflammatory phenotypes. This deficiency alters the landscape of super-enhancers, and the impeded promoter–enhancer loops lead to the downregulation of genes encoding master regulators, such as Bcl6 and Ets2¹⁴². Identifying genes enriched for disease-relevant pathways through enhancer–promoter interactions with disease-associated SNPs in certain inflammatory skin diseases can pave the way for repurposing and developing drugs to target these pathways. In particular, there was an enrichment of CTCF binding within differentially methylated positions (DMPs) in CD4⁺ cells obtained from individuals with SSc, possibly arising from an abnormal increase in CTCF gene expression¹⁴³.

Recently, therapies targeting immune cells have gained attention for the treatment of various diseases, with a focus on cancer¹⁴⁴. Given that STAT5 plays a crucial role in

various malignant characteristics of AML cells, precise targeting of STAT5 holds substantial clinical importance¹⁴⁵. Increased STAT5 activity levels have been associated with an adverse prognosis in myeloid malignancies¹⁴⁶ and have shown correlation with resistance to tyrosine kinase inhibitors (TKIs)¹⁴⁷. The conventional conclusion regarding signaling therapy has focused on the aspect of "resistance." Identifying the causes of resistance and discovering new drugs or alternative treatment approaches, such as chimeric antigen receptor (CAR)-T cells¹⁴⁸, that can bypass it, are important research tasks.

However, our results demonstrate that even if STAT5 signaling is functioning normally, the responsiveness of CD4⁺ T cells to JAK inhibitors can vary significantly depending on the presence or absence of CTCF. Notably, central to the adaptive immune system, CD4⁺ T cells play a pivotal role, and the activation of T cells constitutes a crucial pathogenic pathway in numerous autoimmune disorders. We anticipate that our results can serve as crucial evidence spotlighting the necessity of considering 3D chromatin when applying chemical substances that affect major signaling pathways in CD4⁺ T cells for therapeutic purposes targeting various diseases, including cancer.

Nevertheless, there are still issues that need to be addressed in the future. Powerful tools based on 3C techniques for uncovering 3D chromatin structure and functions exhibit limitations in tracking weak interactions or rapidly changing loops in real-time. Additionally, aligning 3D genome data with spatial conformation is an evolving field that demands further advancements. To overcome this, integrated research is required, focusing on epigenetics and utilizing various technologies such as imaging, biochemistry, genetic engineering, biophysics, computational biology, and mathematical approaches³⁵.

In the clinical application, there are still some remaining challenges. For example, addressing how to modify chromatin structure or manipulate genetic loci to explore their influence on the disease process remains an ongoing issue. Drugs interfering with CTCF

binding have been reported¹⁴⁹, and alternative approaches using proteins such as dCas9 that can block loop extrusion are also worth considering¹⁵⁰. Developing chemical compounds targeting non-protein factors, like Jpx RNA¹⁵¹, which regulates CTCF anchor site selection, is anticipated to be a positive therapeutic strategy.

This study focused on CD4⁺ T cells and confirmed the orchestration of CTCF and associating key factors in immune cells. However, these results are not necessarily limited to CD4⁺ T cells, and it is anticipated that similar conclusions may arise from other immune cells, such as NK cells¹⁵², or even cells in different tissues such as the liver¹⁵³ or brain¹⁵⁴. For instance, considering the variation in CTCF levels during brain development, where the highest expression occurs in the embryonic brain and decreases from birth to adulthood¹⁵⁵, exploring this phenomenon from the perspective of pause-release mediated by super-loops that regulate master regulators would be a meaningful avenue of research. Finally, there is an expectation for engaging in a discussion on the presence of additional factors specific to certain tissues or cell types. These factors could potentially enhance the overall complexity and direct regulatory capacity of the 3D chromatin architecture.

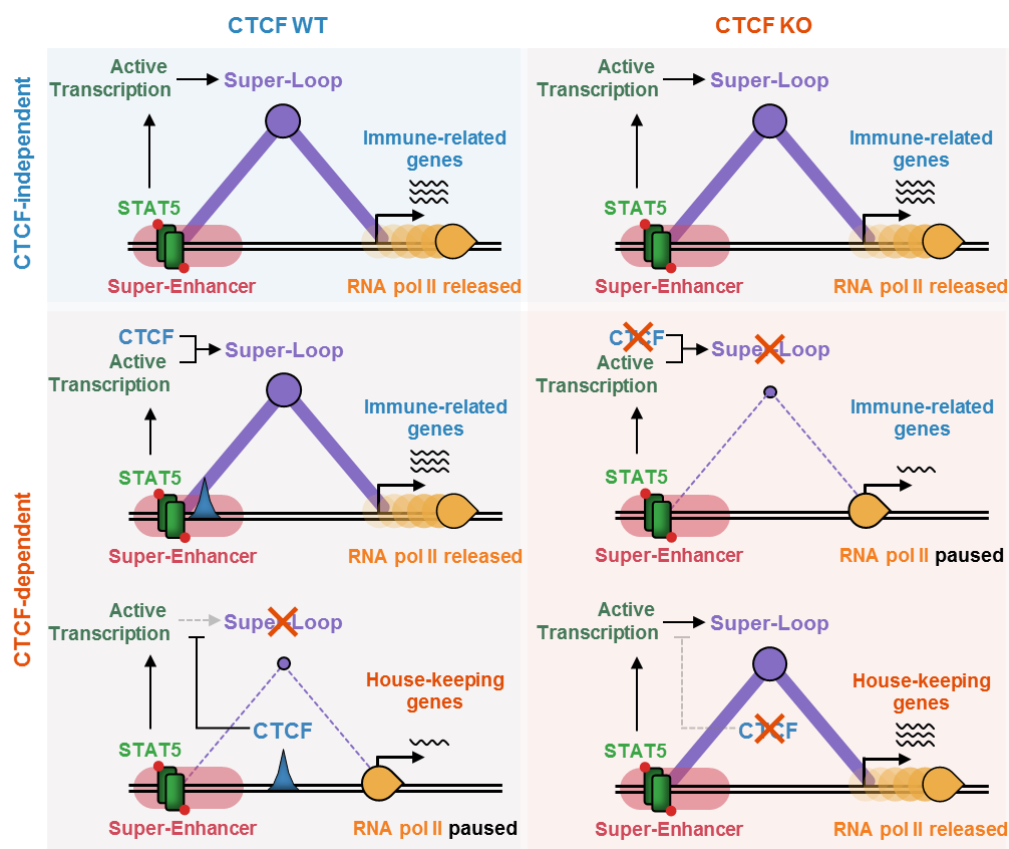


Figure 22. Super-loop oversees the influence of enhancer activity to the promoter and the regulation of Pol II pause-release

Super-loops in CD4⁺ T cells are established through active transcription, utilizing both CTCF-independent and CTCF-dependent mechanisms. They facilitate robust chromatin interactions between STAT5-bound super-enhancers and immune-related genes, leading to increased RNA expression and the release of RNA Pol II pausing. CTCF depletion is dispensable for the formation of CTCF-independent super-loops and the expression of their target genes (top), while it disrupts the formation of CTCF-dependent super-loops, reducing the expression of their target genes (middle). The chromatin interaction between STAT5-bound super-enhancer and housekeeping genes can be hindered by the intervening insulator CTCF. CTCF depletion can rewire STAT5-bound super-enhancers to unrelated housekeeping genes, resulting in their elevated RNA expression and the release of RNA Pol II pausing (bottom).

V. CONCLUSION

Here, I illuminated the role of CTCF in enhancer-promoter interactions in CD4⁺ T cells. In this study, CD4⁺ T cells with complete CTCF depletion were obtained using the CreER system. CTCF is dispensable for compartment organization but essential for TAD insulation. Interestingly, high transcription activity was observed not only in CTCF-depleted anchors but also in anchors where CTCF was absent.

To investigate the reasons behind this, the study classified super-loops and typical loops based on statistical significance, ranking loop strength. Super-loops showed a high correlation with super-enhancers, confirming that the essential master regulator in CD4⁺ cells, STAT5, played a role in maintaining loops in the absence of CTCF. Additionally, genes targeted by super-enhancers exhibited higher RNA expression and lower pausing index compared to non-targeted genes.

Although super-enhancers remained largely unchanged in the absence of CTCF, loop strength alterations were observed. Approximately half of strong super-loops lost their strength in CTCF knockout. Target genes of weakened super-loops still proved to be important cell-identity-related genes, and their pause-release patterns were observed to be affected. This implies that CTCF plays a pivotal role in ensuring the proper interaction between enhancers and target genes. To further understand the impact of CTCF on STAT5 target genes, especially those responsive to JAK inhibitors, experiments were conducted using CRISPR KO to inhibit STAT5 and CTCF binding. The results validated the role of CTCF as an insulator and facilitator in CD4⁺ T cells.

As CD4⁺ T cells play a vital role in adaptive immunity, being the target cells of immunotherapy, the study's focus on the 3D genome structure is significant. This research is expected to have implications in clinical medical fields, particularly in drug therapies targeting the signaling pathways of immune cells.

REFERENCES

1. Barabasi AL, Oltvai ZN. Network biology: understanding the cell's functional organization. *Nat Rev Genet* 2004;5:101-13.
2. Song N, Sengupta S, Khoruzhenko S, Welsh RA, Kim A, Kumar MR, et al. Multiple genetic programs contribute to CD4 T cell memory differentiation and longevity by maintaining T cell quiescence. *Cell Immunol* 2020;357:104210.
3. Mirmohammadsadegh A, Hassan M, Bardenheuer W, Marini A, Gustrau A, Nambiar S, et al. STAT5 phosphorylation in malignant melanoma is important for survival and is mediated through SRC and JAK1 kinases. *J Invest Dermatol* 2006;126:2272-80.
4. Hu X, Li J, Fu M, Zhao X, Wang W. The JAK/STAT signaling pathway: from bench to clinic. *Signal Transduct Target Ther* 2021;6:402.
5. Luckheeram RV, Zhou R, Verma AD, Xia B. CD4(+)T cells: differentiation and functions. *Clin Dev Immunol* 2012;2012:925135.
6. Morou A, Brunet-Ratnasingham E, Dube M, Charlebois R, Mercier E, Darko S, et al. Altered differentiation is central to HIV-specific CD4(+) T cell dysfunction in progressive disease. *Nat Immunol* 2019;20:1059-70.
7. Jones N, Vincent EE, Cronin JG, Panetti S, Chambers M, Holm SR, et al. Akt and STAT5 mediate naive human CD4+ T-cell early metabolic response to TCR stimulation. *Nat Commun* 2019;10:2042.
8. Li P, Mitra S, Spolski R, Oh J, Liao W, Tang Z, et al. STAT5-mediated chromatin interactions in superenhancers activate IL-2 highly inducible genes: Functional dissection of the *Il2ra* gene locus. *Proc Natl Acad Sci U S A* 2017;114:12111-9.
9. Hirahara K, Nakayama T. CD4+ T-cell subsets in inflammatory diseases: beyond the Th1/Th2 paradigm. *Int Immunol* 2016;28:163-71.
10. Golubovskaya V, Wu L. Different Subsets of T Cells, Memory, Effector Functions, and CAR-T Immunotherapy. *Cancers (Basel)* 2016;8.
11. Sharpe M, Mount N. Genetically modified T cells in cancer therapy: opportunities and challenges. *Dis Model Mech* 2015;8:337-50.
12. Heath H, Ribeiro de Almeida C, Sleutels F, Dingjan G, van de Nobelen S, Jonkers I, et al. CTCF regulates cell cycle progression of alphabeta T cells in the thymus. *EMBO J* 2008;27:2839-50.
13. Hnisz D, Weintraub AS, Day DS, Valton AL, Bak RO, Li CH, et al. Activation

- of proto-oncogenes by disruption of chromosome neighborhoods. *Science* 2016;351:1454-8.
14. Perez-Garcia A, Marina-Zarate E, Alvarez-Prado AF, Ligos JM, Galjart N, Ramiro AR. CTCF orchestrates the germinal centre transcriptional program and prevents premature plasma cell differentiation. *Nat Commun* 2017;8:16067.
 15. Luger K, Dechassa ML, Tremethick DJ. New insights into nucleosome and chromatin structure: an ordered state or a disordered affair? *Nat Rev Mol Cell Biol* 2012;13:436-47.
 16. Berger SL. The complex language of chromatin regulation during transcription. *Nature* 2007;447:407-12.
 17. Hargreaves DC, Horng T, Medzhitov R. Control of inducible gene expression by signal-dependent transcriptional elongation. *Cell* 2009;138:129-45.
 18. Bannister AJ, Kouzarides T. Regulation of chromatin by histone modifications. *Cell Res* 2011;21:381-95.
 19. Long HK, Prescott SL, Wysocka J. Ever-Changing Landscapes: Transcriptional Enhancers in Development and Evolution. *Cell* 2016;167:1170-87.
 20. Furlong EEM, Levine M. Developmental enhancers and chromosome topology. *Science* 2018;361:1341-5.
 21. Shlyueva D, Stampfel G, Stark A. Transcriptional enhancers: from properties to genome-wide predictions. *Nat Rev Genet* 2014;15:272-86.
 22. Hnisz D, Abraham BJ, Lee TI, Lau A, Saint-Andre V, Sigova AA, et al. Super-enhancers in the control of cell identity and disease. *Cell* 2013;155:934-47.
 23. Whyte WA, Orlando DA, Hnisz D, Abraham BJ, Lin CY, Kagey MH, et al. Master transcription factors and mediator establish super-enhancers at key cell identity genes. *Cell* 2013;153:307-19.
 24. Bernstein BE, Kamal M, Lindblad-Toh K, Bekiranov S, Bailey DK, Huebert DJ, et al. Genomic maps and comparative analysis of histone modifications in human and mouse. *Cell* 2005;120:169-81.
 25. Rando OJ. Combinatorial complexity in chromatin structure and function: revisiting the histone code. *Curr Opin Genet Dev* 2012;22:148-55.
 26. Wang Q, Xiao Y, Shi Y, Luo Y, Li Y, Zhao M, et al. Overexpression of JMJD3 may contribute to demethylation of H3K27me3 in CD4+ T cells from patients with systemic sclerosis. *Clin Immunol* 2015;161:396-9.
 27. Liu Y, Liao J, Zhao M, Wu H, Yung S, Chan TM, et al. Increased expression of TLR2 in CD4(+) T cells from SLE patients enhances immune reactivity and promotes IL-17 expression through histone modifications. *Eur J Immunol*

- 2015;45:2683-93.
28. Bettini ML, Pan F, Bettini M, Finkelstein D, Rehg JE, Floess S, et al. Loss of epigenetic modification driven by the Foxp3 transcription factor leads to regulatory T cell insufficiency. *Immunity* 2012;36:717-30.
 29. Durek P, Nordstrom K, Gasparoni G, Salhab A, Kressler C, de Almeida M, et al. Epigenomic Profiling of Human CD4(+) T Cells Supports a Linear Differentiation Model and Highlights Molecular Regulators of Memory Development. *Immunity* 2016;45:1148-61.
 30. Rowley MJ, Corces VG. Organizational principles of 3D genome architecture. *Nat Rev Genet* 2018;19:789-800.
 31. Puceat M. Capturing Chromosome Conformation. *Methods Mol Biol* 2021;2157:1-7.
 32. Fraser J, Williamson I, Bickmore WA, Dostie J. An Overview of Genome Organization and How We Got There: from FISH to Hi-C. *Microbiol Mol Biol Rev* 2015;79:347-72.
 33. Rao SS, Huntley MH, Durand NC, Stamenova EK, Bochkov ID, Robinson JT, et al. A 3D map of the human genome at kilobase resolution reveals principles of chromatin looping. *Cell* 2014;159:1665-80.
 34. Schoenfelder S, Fraser P. Long-range enhancer-promoter contacts in gene expression control. *Nat Rev Genet* 2019;20:437-55.
 35. Dekker J, Belmont AS, Guttman M, Leshyk VO, Lis JT, Lomvardas S, et al. The 4D nucleome project. *Nature* 2017;549:219-26.
 36. Merkenschlager M, Nora EP. CTCF and Cohesin in Genome Folding and Transcriptional Gene Regulation. *Annu Rev Genomics Hum Genet* 2016;17:17-43.
 37. Kim TH, Abdullaev ZK, Smith AD, Ching KA, Loukinov DI, Green RD, et al. Analysis of the vertebrate insulator protein CTCF-binding sites in the human genome. *Cell* 2007;128:1231-45.
 38. Rotondo JC, Selvatici R, Di Domenico M, Marci R, Vesce F, Tognon M, et al. Methylation loss at H19 imprinted gene correlates with methylenetetrahydrofolate reductase gene promoter hypermethylation in semen samples from infertile males. *Epigenetics* 2013;8:990-7.
 39. Filippova GN, Fagerlie S, Klenova EM, Myers C, Dehner Y, Goodwin G, et al. An exceptionally conserved transcriptional repressor, CTCF, employs different combinations of zinc fingers to bind diverged promoter sequences of avian and mammalian c-myc oncogenes. *Mol Cell Biol* 1996;16:2802-13.

40. Ong CT, Corces VG. CTCF: an architectural protein bridging genome topology and function. *Nat Rev Genet* 2014;15:234-46.
41. Bell AC, Felsenfeld G. Methylation of a CTCF-dependent boundary controls imprinted expression of the *Igf2* gene. *Nature* 2000;405:482-5.
42. Lobanenko VV, Nicolas RH, Adler VV, Paterson H, Klenova EM, Polotskaja AV, et al. A novel sequence-specific DNA binding protein which interacts with three regularly spaced direct repeats of the CCCTC-motif in the 5'-flanking sequence of the chicken *c-myc* gene. *Oncogene* 1990;5:1743-53.
43. Zheng H, Xie W. The role of 3D genome organization in development and cell differentiation. *Nat Rev Mol Cell Biol* 2019;20:535-50.
44. Narendra V, Rocha PP, An D, Raviram R, Skok JA, Mazzoni EO, et al. CTCF establishes discrete functional chromatin domains at the Hox clusters during differentiation. *Science* 2015;347:1017-21.
45. Flavahan WA, Drier Y, Liao BB, Gillespie SM, Venteicher AS, Stemmer-Rachamimov AO, et al. Insulator dysfunction and oncogene activation in IDH mutant gliomas. *Nature* 2016;529:110-4.
46. Katainen R, Dave K, Pitkanen E, Palin K, Kivioja T, Valimaki N, et al. CTCF/cohesin-binding sites are frequently mutated in cancer. *Nat Genet* 2015;47:818-21.
47. Ohlsson R, Renkawitz R, Lobanenko V. CTCF is a uniquely versatile transcription regulator linked to epigenetics and disease. *Trends Genet* 2001;17:520-7.
48. Lupianez DG, Kraft K, Heinrich V, Krawitz P, Brancati F, Klopocki E, et al. Disruptions of topological chromatin domains cause pathogenic rewiring of gene-enhancer interactions. *Cell* 2015;161:1012-25.
49. Shukla S, Kavak E, Gregory M, Imashimizu M, Shutinoski B, Kashlev M, et al. CTCF-promoted RNA polymerase II pausing links DNA methylation to splicing. *Nature* 2011;479:74-9.
50. Guo Y, Xu Q, Canzio D, Shou J, Li J, Gorkin DU, et al. CRISPR Inversion of CTCF Sites Alters Genome Topology and Enhancer/Promoter Function. *Cell* 2015;162:900-10.
51. Guo Y, Monahan K, Wu H, Gertz J, Varley KE, Li W, et al. CTCF/cohesin-mediated DNA looping is required for protocadherin alpha promoter choice. *Proc Natl Acad Sci U S A* 2012;109:21081-6.
52. Oh S, Shao J, Mitra J, Xiong F, D'Antonio M, Wang R, et al. Enhancer release and retargeting activates disease-susceptibility genes. *Nature* 2021;595:735-40.

53. Hsieh TS, Cattoglio C, Slobodyanyuk E, Hansen AS, Darzacq X, Tjian R. Enhancer-promoter interactions and transcription are largely maintained upon acute loss of CTCF, cohesin, WAPL or YY1. *Nat Genet* 2022;54:1919-32.
54. Mahat DB, Kwak H, Booth GT, Jonkers IH, Danko CG, Patel RK, et al. Base-pair-resolution genome-wide mapping of active RNA polymerases using precision nuclear run-on (PRO-seq). *Nat Protoc* 2016;11:1455-76.
55. Corces MR, Trevino AE, Hamilton EG, Greenside PG, Sinnott-Armstrong NA, Vesuna S, et al. An improved ATAC-seq protocol reduces background and enables interrogation of frozen tissues. *Nat Methods* 2017;14:959-62.
56. Schmidl C, Rendeiro AF, Sheffield NC, Bock C. ChIPmentation: fast, robust, low-input ChIP-seq for histones and transcription factors. *Nat Methods* 2015;12:963-5.
57. Mumbach MR, Rubin AJ, Flynn RA, Dai C, Khavari PA, Greenleaf WJ, et al. HiChIP: efficient and sensitive analysis of protein-directed genome architecture. *Nat Methods* 2016;13:919-22.
58. Dobin A, Davis CA, Schlesinger F, Drenkow J, Zaleski C, Jha S, et al. STAR: ultrafast universal RNA-seq aligner. *Bioinformatics* 2013;29:15-21.
59. Li B, Dewey CN. RSEM: accurate transcript quantification from RNA-Seq data with or without a reference genome. *BMC Bioinformatics* 2011;12:323.
60. Love MI, Huber W, Anders S. Moderated estimation of fold change and dispersion for RNA-seq data with DESeq2. *Genome Biol* 2014;15:550.
61. Yu G, Wang LG, Han Y, He QY. clusterProfiler: an R package for comparing biological themes among gene clusters. *OMICS* 2012;16:284-7.
62. Li H, Handsaker B, Wysoker A, Fennell T, Ruan J, Homer N, et al. The Sequence Alignment/Map format and SAMtools. *Bioinformatics* 2009;25:2078-9.
63. Ramirez F, Dundar F, Diehl S, Gruning BA, Manke T. deepTools: a flexible platform for exploring deep-sequencing data. *Nucleic Acids Res* 2014;42:W187-91.
64. Li H, Durbin R. Fast and accurate short read alignment with Burrows-Wheeler transform. *Bioinformatics* 2009;25:1754-60.
65. Zhang Y, Liu T, Meyer CA, Eeckhoute J, Johnson DS, Bernstein BE, et al. Model-based analysis of ChIP-Seq (MACS). *Genome Biol* 2008;9:R137.
66. Langmead B, Salzberg SL. Fast gapped-read alignment with Bowtie 2. *Nat Methods* 2012;9:357-9.
67. Heinz S, Benner C, Spann N, Bertolino E, Lin YC, Laslo P, et al. Simple

- combinations of lineage-determining transcription factors prime cis-regulatory elements required for macrophage and B cell identities. *Mol Cell* 2010;38:576-89.
68. Servant N, Varoquaux N, Lajoie BR, Viara E, Chen CJ, Vert JP, et al. HiC-Pro: an optimized and flexible pipeline for Hi-C data processing. *Genome Biol* 2015;16:259.
 69. Yan KK, Yardimci GG, Yan C, Noble WS, Gerstein M. HiC-spector: a matrix library for spectral and reproducibility analysis of Hi-C contact maps. *Bioinformatics* 2017;33:2199-201.
 70. Durand NC, Shamim MS, Machol I, Rao SS, Huntley MH, Lander ES, et al. Juicer Provides a One-Click System for Analyzing Loop-Resolution Hi-C Experiments. *Cell Syst* 2016;3:95-8.
 71. Open2C, Nezar A, Sameer A, Geoffrey F, Ilya MF, Aleksandra AG, et al. Cooltools: enabling high-resolution Hi-C analysis in Python. *bioRxiv* 2022:2022.10.31.514564.
 72. Crane E, Bian Q, McCord RP, Lajoie BR, Wheeler BS, Ralston EJ, et al. Condensin-driven remodelling of X chromosome topology during dosage compensation. *Nature* 2015;523:240-4.
 73. Kruse K, Hug CB, Vaquerizas JM. FAN-C: a feature-rich framework for the analysis and visualisation of chromosome conformation capture data. *Genome Biol* 2020;21:303.
 74. Bhattacharyya S, Chandra V, Vijayanand P, Ay F. Identification of significant chromatin contacts from HiChIP data by FitHiChIP. *Nat Commun* 2019;10:4221.
 75. Quinlan AR, Hall IM. BEDTools: a flexible suite of utilities for comparing genomic features. *Bioinformatics* 2010;26:841-2.
 76. Nagraj VP, Magee NE, Sheffield NC. LOLAweb: a containerized web server for interactive genomic locus overlap enrichment analysis. *Nucleic Acids Res* 2018;46:W194-W9.
 77. Ramirez F, Bhardwaj V, Arrigoni L, Lam KC, Gruning BA, Villaveces J, et al. High-resolution TADs reveal DNA sequences underlying genome organization in flies. *Nat Commun* 2018;9:189.
 78. Lopez-Delisle L, Rabbani L, Wolff J, Bhardwaj V, Backofen R, Gruning B, et al. pyGenomeTracks: reproducible plots for multivariate genomic datasets. *Bioinformatics* 2021;37:422-3.
 79. Moore JM, Rabaia NA, Smith LE, Fagerlie S, Gurley K, Loukinov D, et al.

- Loss of maternal CTCF is associated with peri-implantation lethality of *Ctcf* null embryos. *PLoS One* 2012;7:e34915.
80. Metzger D, Clifford J, Chiba H, Chambon P. Conditional site-specific recombination in mammalian cells using a ligand-dependent chimeric Cre recombinase. *Proc Natl Acad Sci U S A* 1995;92:6991-5.
 81. Indra AK, Warot X, Brocard J, Bornert JM, Xiao JH, Chambon P, et al. Temporally-controlled site-specific mutagenesis in the basal layer of the epidermis: comparison of the recombinase activity of the tamoxifen-inducible Cre-ER(T) and Cre-ER(T2) recombinases. *Nucleic Acids Res* 1999;27:4324-7.
 82. Nora EP, Goloborodko A, Valton AL, Gibcus JH, Uebersohn A, Abdennur N, et al. Targeted Degradation of CTCF Decouples Local Insulation of Chromosome Domains from Genomic Compartmentalization. *Cell* 2017;169:930-44 e22.
 83. Yatskevich S, Rhodes J, Nasmyth K. Organization of Chromosomal DNA by SMC Complexes. *Annu Rev Genet* 2019;53:445-82.
 84. Li Y, Haarhuis JHI, Sedeno Cacciatore A, Oldenkamp R, van Ruiten MS, Willems L, et al. The structural basis for cohesin-CTCF-anchored loops. *Nature* 2020;578:472-6.
 85. Kubo N, Ishii H, Xiong X, Bianco S, Meitinger F, Hu R, et al. Promoter-proximal CTCF binding promotes distal enhancer-dependent gene activation. *Nat Struct Mol Biol* 2021;28:152-61.
 86. Xie L, Dong P, Chen X, Hsieh TS, Banala S, De Marzio M, et al. 3D ATAC-PALM: super-resolution imaging of the accessible genome. *Nat Methods* 2020;17:430-6.
 87. Pott S, Lieb JD. What are super-enhancers? *Nat Genet* 2015;47:8-12.
 88. Hsieh TS, Cattoglio C, Slobodyanyuk E, Hansen AS, Rando OJ, Tjian R, et al. Resolving the 3D Landscape of Transcription-Linked Mammalian Chromatin Folding. *Mol Cell* 2020;78:539-53 e8.
 89. Ren G, Jin W, Cui K, Rodrigez J, Hu G, Zhang Z, et al. CTCF-Mediated Enhancer-Promoter Interaction Is a Critical Regulator of Cell-to-Cell Variation of Gene Expression. *Mol Cell* 2017;67:1049-58 e6.
 90. Sexton T, Yaffe E, Kenigsberg E, Bantignies F, Leblanc B, Hoichman M, et al. Three-dimensional folding and functional organization principles of the *Drosophila* genome. *Cell* 2012;148:458-72.
 91. Loven J, Hoke HA, Lin CY, Lau A, Orlando DA, Vakoc CR, et al. Selective inhibition of tumor oncogenes by disruption of super-enhancers. *Cell*

- 2013;153:320-34.
92. Parker SC, Stitzel ML, Taylor DL, Orozco JM, Erdos MR, Akiyama JA, et al. Chromatin stretch enhancer states drive cell-specific gene regulation and harbor human disease risk variants. *Proc Natl Acad Sci U S A* 2013;110:17921-6.
 93. Henriques T, Scruggs BS, Inouye MO, Muse GW, Williams LH, Burkholder AB, et al. Widespread transcriptional pausing and elongation control at enhancers. *Genes & Development* 2018;32:26-41.
 94. Dollinger R, Gilmour DS. Regulation of Promoter Proximal Pausing of RNA Polymerase II in Metazoans. *J Mol Biol* 2021;433:166897.
 95. Phatnani HP, Greenleaf AL. Phosphorylation and functions of the RNA polymerase II CTD. *Genes Dev* 2006;20:2922-36.
 96. Zhu J, Liu M, Liu X, Dong Z. RNA polymerase II activity revealed by GRO-seq and pNET-seq in Arabidopsis. *Nat Plants* 2018;4:1112-23.
 97. Williams LH, Fromm G, Gokey NG, Henriques T, Muse GW, Burkholder A, et al. Pausing of RNA polymerase II regulates mammalian developmental potential through control of signaling networks. *Mol Cell* 2015;58:311-22.
 98. Gorbovytska V, Kim SK, Kuybu F, Gotze M, Um D, Kang K, et al. Enhancer RNAs stimulate Pol II pause release by harnessing multivalent interactions to NELF. *Nat Commun* 2022;13:2429.
 99. Wang H, Fan Z, Shliaha PV, Miele M, Hendrickson RC, Jiang X, et al. H3K4me3 regulates RNA polymerase II promoter-proximal pause-release. *Nature* 2023;615:339-48.
 100. Owen DL, Farrar MA. STAT5 and CD4 (+) T Cell Immunity. *F1000Res* 2017;6:32.
 101. Gladman D, Rigby W, Azevedo VF, Behrens F, Blanco R, Kaszuba A, et al. Tofacitinib for Psoriatic Arthritis in Patients with an Inadequate Response to TNF Inhibitors. *N Engl J Med* 2017;377:1525-36.
 102. Dhillon S. Tofacitinib: A Review in Rheumatoid Arthritis. *Drugs* 2017;77:1987-2001.
 103. D'Amico F, Parigi TL, Fiorino G, Peyrin-Biroulet L, Danese S. Tofacitinib in the treatment of ulcerative colitis: efficacy and safety from clinical trials to real-world experience. *Therap Adv Gastroenterol* 2019;12:1756284819848631.
 104. Vahedi G, Kanno Y, Furumoto Y, Jiang K, Parker SC, Erdos MR, et al. Super-enhancers delineate disease-associated regulatory nodes in T cells. *Nature* 2015;520:558-62.
 105. Dos Santos RS, Marroqui L, Velayos T, Olazagoitia-Garmendia A, Jauregi-

- Miguel A, Castellanos-Rubio A, et al. DEXI, a candidate gene for type 1 diabetes, modulates rat and human pancreatic beta cell inflammation via regulation of the type I IFN/STAT signalling pathway. *Diabetologia* 2019;62:459-72.
106. Pang H, Luo S, Huang G, Xia Y, Xie Z, Zhou Z. Advances in Knowledge of Candidate Genes Acting at the Beta-Cell Level in the Pathogenesis of T1DM. *Front Endocrinol (Lausanne)* 2020;11:119.
 107. Gingerich MA, Sidarala V, Soleimanpour SA. Clarifying the function of genes at the chromosome 16p13 locus in type 1 diabetes: CLEC16A and DEXI. *Genes Immun* 2020;21:79-82.
 108. Decker T, Kovarik P, Meinke A. GAS elements: a few nucleotides with a major impact on cytokine-induced gene expression. *J Interferon Cytokine Res* 1997;17:121-34.
 109. Sentmanat MF, Peters ST, Florian CP, Connelly JP, Pruett-Miller SM. A Survey of Validation Strategies for CRISPR-Cas9 Editing. *Sci Rep* 2018;8:888.
 110. Kim YW, Kang J, Kim A. Hematopoietic/erythroid enhancers activate nearby target genes by extending histone H3K27ac and transcribing intergenic RNA. *FASEB J* 2023;37:e22870.
 111. Bickmore WA, van Steensel B. Genome architecture: domain organization of interphase chromosomes. *Cell* 2013;152:1270-84.
 112. Pevny L, Simon MC, Robertson E, Klein WH, Tsai SF, D'Agati V, et al. Erythroid differentiation in chimaeric mice blocked by a targeted mutation in the gene for transcription factor GATA-1. *Nature* 1991;349:257-60.
 113. Robb L, Lyons I, Li R, Hartley L, Kontgen F, Harvey RP, et al. Absence of yolk sac hematopoiesis from mice with a targeted disruption of the scl gene. *Proc Natl Acad Sci U S A* 1995;92:7075-9.
 114. Morgunova E, Taipale J. Structural perspective of cooperative transcription factor binding. *Curr Opin Struct Biol* 2017;47:1-8.
 115. Wentz N, Strauss H, Meyer S, Vinkemeier U. Tyrosine phosphorylation regulates the partitioning of STAT1 between different dimer conformations. *Proc Natl Acad Sci U S A* 2008;105:9238-43.
 116. Weintraub AS, Li CH, Zamudio AV, Sigova AA, Hannett NM, Day DS, et al. YY1 Is a Structural Regulator of Enhancer-Promoter Loops. *Cell* 2017;171:1573-88 e28.
 117. Hwang SS, Kim YU, Lee S, Jang SW, Kim MK, Koh BH, et al. Transcription factor YY1 is essential for regulation of the Th2 cytokine locus and for Th2 cell

- differentiation. *Proc Natl Acad Sci U S A* 2013;110:276-81.
118. Zelenka T, Klonizakis A, Tsoukatou D, Papamatheakis DA, Franzenburg S, Tzerpos P, et al. The 3D enhancer network of the developing T cell genome is shaped by SATB1. *Nat Commun* 2022;13:6954.
 119. Rao SSP, Huang SC, St Hilaire BG, Engreitz JM, Perez EM, Kieffer-Kwon KR, et al. Cohesin Loss Eliminates All Loop Domains. *Cell* 2017;171:305-+.
 120. Chakraborty S, Kopitchinski N, Zuo ZY, Eraso A, Awasthi P, Chari R, et al. Enhancer-promoter interactions can bypass CTCF-mediated boundaries and contribute to phenotypic robustness. *Nature Genetics* 2023;55:280-+.
 121. Xu BS, Wang H, Wright S, Hyle J, Zhang Y, Shao Y, et al. Acute depletion of CTCF rewires genome-wide chromatin accessibility. *Genome Biology* 2021;22.
 122. Yang BB, Kim S, Jung WJ, Kim K, Kim S, Kim YJ, et al. CTCF controls three-dimensional enhancer network underlying the inflammatory response of bone marrow-derived dendritic cells. *Nature Communications* 2023;14.
 123. Lee R, Kang MK, Kim YJ, Yang B, Shim H, Kim S, et al. CTCF-mediated chromatin looping provides a topological framework for the formation of phase-separated transcriptional condensates. *Nucleic Acids Research* 2022;50:207-26.
 124. Huang J, Li K, Cai W, Liu X, Zhang Y, Orkin SH, et al. Dissecting super-enhancer hierarchy based on chromatin interactions. *Nat Commun* 2018;9:943.
 125. Ryu J, Kim H, Yang D, Lee AJ, Jung I. A new class of constitutively active super-enhancers is associated with fast recovery of 3D chromatin loops. *Bmc Bioinformatics* 2019;20.
 126. Malik S, Roeder RG. Regulation of the RNA polymerase II pre-initiation complex by its associated coactivators. *Nat Rev Genet* 2023;24:767-82.
 127. Gottesfeld JM. Milestones in transcription and chromatin published in the *Journal of Biological Chemistry*. *J Biol Chem* 2019;294:1652-60.
 128. He Y, Fang J, Taatjes DJ, Nogales E. Structural visualization of key steps in human transcription initiation. *Nature* 2013;495:481-6.
 129. Kim YJ, Bjorklund S, Li Y, Sayre MH, Kornberg RD. A multiprotein mediator of transcriptional activation and its interaction with the C-terminal repeat domain of RNA polymerase II. *Cell* 1994;77:599-608.
 130. Baek I, Friedman LJ, Gelles J, Buratowski S. Single-molecule studies reveal branched pathways for activator-dependent assembly of RNA polymerase II pre-initiation complexes. *Mol Cell* 2021;81:3576-88 e6.
 131. Rowley MJ, Lyu XW, Rana V, Ando-Kuri M, Karns R, Bosco G, et al.

- Condensin II Counteracts Cohesin and RNA Polymerase II in the Establishment of 3D Chromatin Organization. *Cell Reports* 2019;26:2890-+.
132. Smale ST, Natoli G. Transcriptional control of inflammatory responses. *Cold Spring Harb Perspect Biol* 2014;6:a016261.
 133. Cuartero S, Stik G, Stadhouders R. Three-dimensional genome organization in immune cell fate and function. *Nature Reviews Immunology* 2023;23:206-21.
 134. Schatz DG, Ji Y. Recombination centres and the orchestration of V(D)J recombination. *Nat Rev Immunol* 2011;11:251-63.
 135. Davidson IF, Peters JM. Genome folding through loop extrusion by SMC complexes. *Nat Rev Mol Cell Biol* 2021;22:445-64.
 136. Ba Z, Lou J, Ye AY, Dai HQ, Dring EW, Lin SG, et al. CTCF orchestrates long-range cohesin-driven V(D)J recombinational scanning. *Nature* 2020;586:305-10.
 137. Pham D, Moseley CE, Gao M, Savic D, Winstead CJ, Sun M, et al. Batf1 Pioneer the Reorganization of Chromatin in Developing Effector T Cells via Ets1-Dependent Recruitment of Ctcf. *Cell Rep* 2019;29:1203-20 e7.
 138. Qiu YQ, Feng DL, Jiang WJ, Zhang TT, Lu QJ, Zhao M. 3D genome organization and epigenetic regulation in autoimmune diseases. *Frontiers in Immunology* 2023;14.
 139. Burren OS, García AR, Javierre BM, Rainbow DB, Cairns J, Cooper NJ, et al. Chromosome contacts in activated T cells identify autoimmune disease candidate genes. *Genome Biology* 2017;18.
 140. Shi CF, Ray-Jones H, Ding J, Duffus K, Fu Y, Gaddi VP, et al. Chromatin Looping Links Target Genes with Genetic Risk Loci for Dermatological Traits. *Journal of Investigative Dermatology* 2021;141:1975-84.
 141. Bourges C, Groff AF, Burren OS, Gerhardinger C, Mattioli K, Hutchinson A, et al. Resolving mechanisms of immune-mediated disease in primary CD4 T cells. *EMBO Mol Med* 2020;12:e12112.
 142. Feng D, Chen Y, Dai R, Bian S, Xue W, Zhu Y, et al. Chromatin organizer SATB1 controls the cell identity of CD4(+) CD8(+) double-positive thymocytes by regulating the activity of super-enhancers. *Nat Commun* 2022;13:5554.
 143. Li T, Ortiz-Fernandez L, Andres-Leon E, Ciudad L, Javierre BM, Lopez-Isac E, et al. Epigenomics and transcriptomics of systemic sclerosis CD4+ T cells reveal long-range dysregulation of key inflammatory pathways mediated by disease-associated susceptibility loci. *Genome Med* 2020;12:81.

144. Verdeil G, Lawrence T, Schmitt-Verhulst AM, Auphan-Anezin N. Targeting STAT3 and STAT5 in Tumor-Associated Immune Cells to Improve Immunotherapy. *Cancers (Basel)* 2019;11.
145. Wingelhofer B, Maurer B, Heyes EC, Cumaraswamy AA, Berger-Becvar A, de Araujo ED, et al. Pharmacologic inhibition of STAT5 in acute myeloid leukemia. *Leukemia* 2018;32:1135-46.
146. Kotecha N, Flores NJ, Irish JM, Simonds EF, Sakai DS, Archambeault S, et al. Single-cell profiling identifies aberrant STAT5 activation in myeloid malignancies with specific clinical and biologic correlates. *Cancer Cell* 2008;14:335-43.
147. Warsch W, Kollmann K, Eckelhart E, Fajmann S, Cerny-Reiterer S, Holbl A, et al. High STAT5 levels mediate imatinib resistance and indicate disease progression in chronic myeloid leukemia. *Blood* 2011;117:3409-20.
148. Sterner RC, Sterner RM. CAR-T cell therapy: current limitations and potential strategies. *Blood Cancer J* 2021;11:69.
149. Kantidze OL, Luzhin AV, Nizovtseva EV, Safina A, Valieva ME, Golov AK, et al. The anti-cancer drugs curaxins target spatial genome organization. *Nat Commun* 2019;10:1441.
150. Zhang H, Shi Z, Banigan EJ, Kim Y, Yu H, Bai XC, et al. CTCF and R-loops are boundaries of cohesin-mediated DNA looping. *Mol Cell* 2023;83:2856-71 e8.
151. Oh HJ, Aguilar R, Kesner B, Lee HG, Kriz AJ, Chu HP, et al. Jpx RNA regulates CTCF anchor site selection and formation of chromosome loops. *Cell* 2021;184:6157-73 e24.
152. Lee EC, Kim K, Jung WJ, Kim HP. Vorinostat-induced acetylation of RUNX3 reshapes transcriptional profile through long-range enhancer-promoter interactions in natural killer cells. *Bmb Reports* 2023;56:398-+.
153. Choi Y, Song MJ, Jung WJ, Jeong H, Park S, Yang B, et al. Liver-Specific Deletion of Mouse CTCF Leads to Hepatic Steatosis via Augmented PPARgamma Signaling. *Cell Mol Gastroenterol Hepatol* 2021;12:1761-87.
154. Prickett AR, Barkas N, McCole RB, Hughes S, Amante SM, Schulz R, et al. Genome-wide and parental allele-specific analysis of CTCF and cohesin DNA binding in mouse brain reveals a tissue-specific binding pattern and an association with imprinted differentially methylated regions. *Genome Res* 2013;23:1624-35.
155. Beagan JA, Duong MT, Titus KR, Zhou L, Cao Z, Ma J, et al. YY1 and CTCF

orchestrate a 3D chromatin looping switch during early neural lineage commitment. *Genome Res* 2017;27:1139-52.

ABSTRACT(IN KOREAN)

CD4 T세포에서 STAT5가 매개하는 유전자의 적절한 전사 조절을 제어하는 CTCF 의존적 크로마틴 3차구조의 역할

<지도교수 김 형 표>

연세대학교 대학원 의학과

이 은 총

세포가 정상적으로 기능하는 데 있어서 적절한 유전자 발현을 보장하기 위해서는 프로모터에서 작용하는 단백질뿐만 아니라, 장거리 상호작용을 통해 유전자 발현에 영향을 주는 인핸서의 역할이 중요하다. CCCTC-binding factor (CTCF)는 3차원 크로마틴 구조에서 핵심적인 역할을 하는 단백질로 잘 알려져 있다. 그러나 CTCF가 유전자 발현을 어떻게 조절하는지에 대한 메커니즘과 그 중요성에 대해서는 여전히 논란이 존재한다. 여기서 나는 CTCF가 CD4 T 세포에서 인핸서-프로모터 상호작용을 통해 표적유전자의 전사를 조절하는 능력을 가지고 있다는 것을 보였다. 특히, CTCF의 감소를 통해 CD4 T 세포의 특성을 대표하는 전사인자인 STAT5의 기능적 중요성이 조명되었다. STAT5가 관여한 슈퍼

인헨서는 CTCF에 독립적으로 인헨서 고리를 견고하게 유지하는 데 기여한다. 또한, 인헨서 고리 형성이 리보핵산 중합효소의 전사 정지-해제에 깊게 관여하는 것이 관찰되었다. 그러나 CTCF에 의해 변화한 인헨서 고리 구조는 세포 정체성을 정의하는 유전자의 발현까지도 영향을 미칠 수 있다. CTCF는 인헨서 고리의 강도에 영향을 주며, 더 나아가 표적유전자의 프로모터에서 일어나는 전사과정에서 리보핵산 중합효소의 전사 정지 기작을 조절하는 중요한 요소가 된다. 정리하면, 본 연구는 활성화된 CD4 T 세포에서 세포 특이적인 JAK/STAT 신호전달 경로가 유지되는 방식과, 이러한 상황에서도 CTCF가 인헨서 네트워크를 재구성하여 세포 정체성 유전자에 미칠 수 있는 영향에 대한 통찰력을 제공한다. 또한 이 결과는 면역 세포에서 적절한 유전자 발현을 촉진하는 과정에서 고려해야 하는 CTCF의 복잡한 기능에 대한 종합적인 관점을 제공하는데 의의가 있다.

핵심되는 말 : CD4 T 세포, CTCF, STAT5, 리보핵산 중합효소 일시정지, 3차원 염색질 구조

PUBLICATION LIST

1. Lee EC, Kim K, Jung WJ, Kim HP. Vorinostat-induced acetylation of RUNX3 reshapes transcriptional profile through long-range enhancer-promoter interactions in natural killer cells. *Bmb Reports* 2023;56:398-+.
2. Yang BB, Kim S, Jung WJ, Kim K, Kim S, Kim YJ, Kim TG, Lee EC et al. CTCF controls three-dimensional enhancer network underlying the inflammatory response of bone marrow-derived dendritic cells. *Nature Communications* 2023;14.
3. Lee R, Kang MK, Kim YJ, Yang B, Shim H, Kim S, Kim K, Yang CM, Min B, Jung WJ, Lee EC et al. CTCF-mediated chromatin looping provides a topological framework for the formation of phase-separated transcriptional condensates. *Nucleic Acids Research* 2022;50:207-26.
4. Choi Y, Song MJ, Jung WJ, Jeong H, Park S, Yang B, Lee EC et al. Liver-Specific Deletion of Mouse CTCF Leads to Hepatic Steatosis via Augmented PPAR γ Signaling. *Cellular and Molecular Gastroenterology and Hepatology* 2021;12:1761-87.